technische universität
dortmund

Spatial unification of coupling interactions between EGFR and PTPs establishes a growth factor sensing network

Angel Stanoev

Fakultät für Chemie und Chemische Biologie
Technische Universität, Dortmund

Zur Erlangung des akademischen Grades eines
Doktors der Naturwissenschaften (Dr. rer. nat.)

Juni 2018

Vorgelegt im Juni 2018
von Angel Stanoev

Gutachter:
Priv. Doz. Dr. Aneta Koseska
Prof. Dr. Philippe Bastiaens

The work presented in this dissertation was performed in the group of PD Dr. Aneta Koseska at the Department of Systemic Cell Biology, Max Planck Institute of Molecular Physiology, Dortmund, Germany.

Angel Stanoev was affiliated to the International Max Planck Research School in Chemical and Molecular Biology, Dortmund, Germany.

The work described in this thesis partly has been included in the following publications:

Angel Stanoev, Amit Mhamane, Klaus C Schuermann, Hernán E Grecco, Wayne Stallaert, Martin Baumdick, Yannick Brüggemann, Maitreyi S Joshi, Pedro Roda-Navarro, Sven Fengler, Rabea Stockert, Lisaweta Roßmannek, Jutta Luig, Aneta Koseska, and Philippe IH Bastiaens. Interdependence of EGFR with PTPs on juxtaposed membranes generates a growth factor sensing and responding network. *Cell Systems*, 2018. In press

Angel Stanoev, Akhilesh Nandan, and Aneta Koseska. Spatially distributed EGFR-PTP network optimizes growth factor sensing at criticality. In preparation

Abstract

Cells continuously sense and respond to stimuli from the non-stationary environment. For this, they optimise processing of the perceived signals while maintaining continuous responsiveness. Cell surface receptors, such as the receptor tyrosine kinases, comprise the first layer of sensing. They translate the extracellular signal into internal activity using the protein interaction networks in which they are embedded.

The proto-oncogenic epidermal growth factor receptor (EGFR) is a receptor tyrosine kinase whose sensitivity to epidermal growth factor (EGF) and signalling duration determines cellular behaviour. In the canonical view, signal processing occurs through the ligand-induced dimer formation mechanism and subsequent trans-phosphorylation. However, it has been also established recently that signal amplification via the unliganded EGFR monomers through an autocatalytic mechanism enhances the phosphorylation response of EGFR.

In this thesis, I demonstrate how autocatalytic phosphorylation of EGFR in concert with the coupling interactions with the protein tyrosine phosphatases (PTPs) shape the response dynamics of EGFR. Single cell dose-response analysis revealed that a toggle switch between autocatalytically activated monomeric EGFR and the tumour suppressor PTPRG at the plasma membrane (PM) shapes the sensitivity of EGFR to EGF dose. As the system exhibits switch-like activation due to the bistable regime of operation, irreversible activation occurs as an adversary side effect. To ensure continuous growth factor sensing, the system is positioned outside of the bistable regime by the PM-localised PTPRJ, which negatively regulates EGFR phosphorylation. On the other hand, a spatially-distributed negative feedback with the ER-bound PTPN2 that is established by vesicular trafficking resets the phosphorylation state of monomeric EGFR on the plasma membrane. The distinct recycling route of the unliganded receptor, as opposed to the unidirectional degradation route towards the perinuclear area of the liganded receptor, enables it to repopulate the plasma membrane and thus maintain sensitivity to upcoming stimuli.

In this manner, the coupling interactions between EGFR and the PTPs on different membranes are spatially unified in a network that enables sensing of time-varying EGF signals. The signal processing capabilities of this network are optimised by the system organisation, as its parameters are poised at the criticality point, just outside the bistable regime of operation. In this region, the EGFR response is characterised by prolonged but reversible phosphorylation, enabling the cell to maintain a balance between preserving a transient memory of previous EGF stimulations, while still remaining responsive to upcoming stimuli.

Zusammenfassung

Zellen erfassen kontinuierlich und reagieren auf Stimuli aus der nichtstationären Umgebung. Dazu müssen sie die Verarbeitung der wahrgenommenen Signale optimieren und gelichzeitig für eine kontinuierliche Wirkungsfähigkeit sorgen. Zelloberflächenrezeptoren, wie die Rezeptortyrosinkinasen, umfassen die erste Stufe der Wahrnehmung. Sie übertragen das extrazelluläre Signal in interne Aktivität unter Verwendung der Proteinwechselwirkungsnetzwerke, in die sie eingebettet sind.

Der proto-onkogene epidermale Wachstumsfaktorrezeptor (EGFR) ist eine Rezeptortyrosinkinase, deren Empfindlichkeit gegenüber dem epidermalen Wachstumsfaktor (EGF) und der Signaldauer das zelluläre Verhalten bestimmt. Das kanonische Modell der EGFR-Signalgebung interpretiert ihre Signalverarbeitung durch den ligandeninduzierten Dimerbildungsmechanismus und die anschließende Trans-Phosphorylierung. Es wurde jedoch kürzlich auch festgestellt, dass die Signalamplifikation über die nichtligierten EGFR-Monomere durch einen autokatalytischen Mechanismus die Phosphorylierungsantwort von EGFR verstärkt.

In dieser Arbeit zeige ich, wie die autokatalytische Phosphorylierung von EGFR zusammen mit den Kopplungswechselwirkungen mit Protein Tyrosin Phosphatasen (PTPs) die Wirkungsdynamik von EGFR prägt. Die Einzelzelle-Dosis-Wirkungs-Analyse zeigte, dass ein Kippschalter zwischen autokatalytisch aktiviertem monomerem EGFR und dem Tumorsuppressor PTPRG an der Plasmamembran (PM) die Empfindlichkeit des EGFR gegenüber der EGF-Dosis formt. Da das System eine schalterartige Aktivierung aufgrund des bistabilen Betriebsmodus zeigt, tritt eine irreversible Aktivierung als ein gegenteiliger Nebeneffekt auf. Um eine kontinuierliche Wahrnehmung des Wachstumsfaktors sicherzustellen, wird das System durch das PM-lokalisierte PTPRJ, das die EGFR-Phosphorylierung negativ reguliert, außerhalb des bistabilen Systems positioniert. Auf der anderen Seite setzt eine räumlich verteilte negative Rückkopplung mit dem ER-gebundenen PTPN2, die durch vesikulären Transport hergestellt wird, den Phosphorylierungszustand vom monomeren EGFR auf der Plasmamembran zurück. Die ausgeprägte Recycling-Route des nichtligierten-Rezeptors im Gegensatz zu dem unidirektionalen Abbauweg in Richtung des perinukleären Bereichs des ligandierten-Rezeptors macht es möglich, die Plasmamembran neu zu bevölkern und somit die Wahrnehmung von bevorstehenden Stimuli aufrechtzuerhalten.

Auf diese Weise sind die Kopplungswechselwirkungen zwischen EGFR und den PTPs auf verschiedenen Membranen räumlich in einem Netzwerk vereinigt, dass die Wahrnehmung zeitvariabler EGF-Signale ermöglicht. Die Signalverarbeitungsfähigkeiten dieses Netzwerks

werden durch die Systemorganisation optimiert, da seine Parameter am kritischen Punkt gerade außerhalb des bistabilen Betriebsmodus liegen. Länger andauernde, aber reversible Phosphorylierung charakterisiert das System dort und versorgt die Zelle mit Wahrnehmungs- und Wirkungsfähigkeiten für zeitveränderliche Wachstumsfaktorsignale.

Contents

List of Figures

List of Tables

Nomenclature

Acronyms / Abbreviations

ATP Adenosine triphosphate

CCP Clathrin-coated pit

CCV Clathrin-coated vesicle

CIE Clathrin-independent endocytosis

CME Clathrin-mediated endocytosis

EE Early endosome

MVB Multivesicular body

EGF Epidermal growth factor

EGFR Epidermal growth factor receptor

ERK Extracellular signal-regulated kinase

LE Late endosome

MAPK Mitogen-activated protein kinase

MCMC Monte Carlo Markov Chain

NGF Neural growth factor

PI3K Phosphoinositide 3-kinase

PTP Protein tyrosine phosphatase

RE Recycling endosome

RTK Receptor tyrosine kinase

Introduction

One of the principle goals in cell signalling biology is to understand how the cells process information from a continuously changing environment in order to respond and readily adapt to the perceived changes. Traditional biology studies have had great success in discovering and describing the prominent molecular components involved in many of the signalling processes. Starting from the early endocrinology discoveries of the major hormones and growth factors, through the developments in molecular biology that advanced the classification of ligands and receptors, to the proteomic tools for characterising proteins and intracellular protein-protein interactions, the biology of cell signalling has progressed remarkably in understanding and appreciating the dynamical cellular responses to environmental stimuli [1]. Knowing the components of a biological system is however not sufficient for understanding its functioning as a system, its dynamics and flow of information. The need for a systemic level of description of the collective molecular behaviour and emergent dynamical properties as functional outcomes has brought about the rise of systems biology in the past decades [2]. Grounded on the continuously increasing molecular level knowledge, modern systems biology approaches have the potential to span the understanding of biological signal processing systems across multiple levels.

The famous hypothesis of Marr and Poggio postulates that information processing systems in general should be studied at three distinct, but complementary levels of description/analysis [3, 4]: computational - or what is the function of the system (the "why" of cognition); algorithmic/representational - or which representations does the system use and what kind of processes it employs; and implementational - or how do the actual components operate in the process. When applying this view on a signal processing system, the computational goal would translate to perceiving the changes in the environment, while the algorithmic level would capture the dynamical properties of the molecular system. Determining the physical protein interaction mechanisms would comprise the implementational level. Studying this multi-level interplay by combining experimental with theoretical approaches is thus necessary

for understanding the underlying organisational principles behind growth factor cellular sensing.

Cellular signal processing systems have undergone a transition from being viewed as mere signal transport pathways, operating in a linear pipeline fashion from the input ligand to the output gene, to being treated as complex systems of molecules, composed of feedback and feedforward loops, sharing components and being spatially organised [5]. It is well established that cells can process different signals to generate distinct outcomes using the same components. This renders the signalling function of a system context-dependent - two systems with overlapping components can generate their respective specific outcome within their own context (e.g. growth factor input). In one of the landmark examples of context-dependent signalling it was observed that the duration of extracellular signal-regulated kinase (ERK) activity was responsible for the functional outcome in PC-12 cells. Epidermal growth factor (EGF) induced transient ERK activation led to cell proliferation, whereas sustained ERK activation by the nerve growth factor (NGF) induced cellular differentiation [6]. It was demonstrated later that this temporal distinction arises from the context-dependency: stimulation by NGF activates a positive feedback from ERK to RAF, thereby sustaining high activity level, whereas stimulation by EGF attenuates ERK activity as a result of the presence of negative feedback to Raf in this context [7].

Spatial regulation is another layer of complexity in the organisation of the signal processing systems. The same system in different spatial locations can generate distinct signalling profiles as a result of local enrichment or depletion of its components. This can be conceived more easily for systems localised in discrete spatial compartments, but it applies as well to systems with gradual spatial changes. Such organisation is exemplified by the EGFR-PTP1B interaction where the increasing concentration of PTP1B towards the perinuclear area translates into decreasing EGFR activity gradient [8]. Furthermore, even a system of uniformly distributed components can result in heterogeneous activity outcomes under special conditions. This symmetry breaking process thus gives rise to formation of a specific non-homogeneous spatial activity arrangements, famously known as Turing patterns [9].

These examples thus indicate that the cells can respond and distinguish complex environmental signals by regulating and distributing the information processing in space and time.

1.1 How cells sense the environment

In multicellular organisms cells communicate with one another using signalling molecules. Typically secreted into the extracellular space from the signalling cells or presented on their

surface, they are recognised by the cognate receptors located on the surface of the target cells. By recognising these cues the cells sense their environment, alter their internal state and respond accordingly (Fig. 1.1a). Interpreting the continuously changing complex signals from the environment requires fine-tuned intrinsic sensing capabilities.

Sensitivity to external cues has been studied extensively in the literature, a field pioneered by Berg and Purcell who underlined the importance of understanding the fundamental physical limits of biological systems in detecting single molecule binding events [10]. It has been shown that noise, arising from inherent stochastic processes such as ligand diffusion, ligand-receptor binding reactions, receptor diffusion and the internal thermal fluctuations, is what gives an upper bound to the sensing precision of the system [10]. Moreover, trade-offs in resource allocation for sensing further constrain the processing capabilities [11]. To reduce the variability from the single noisy readouts the cells obtain independent measurements from multiple receptors and average out the results [12]. Integration over time can further decrease the noise sensitivity [12–14]. However, these works are generally based on information processing in a stationary environment by linear signalling networks. Nonetheless, the cells operate in continuously changing environments, where the levels of the spatial cues vary readily. Additionally, the rates of the ligand binding/unbinding kinetics relative to the rate of change of the ligand concentration in the extracellular domain might become a kinetic bottleneck. Further, the receptors undergo vesicular trafficking, thus the plasma membrane population is constantly exchanged. Active sensing strategies are thus necessary to extend these concepts to non-equilibrium assumptions and more realistic scenarios. Especially it is important to study how the dynamical properties of cell surface receptors arises from the networks in which they are embedded.

Cell signalling by receptor tyrosine kinases

The first layer that perceives the environment are the cell surface receptors. Receptor tyrosine kinases (RTKs) are one of the most prominent families of receptors that recognise growth factors and act as enzymes upon activation. There are 58 known RTKs in the human proteome, grouped into 20 subfamilies based on their kinase domain sequences [15].Typical structural organisation of an RTK consists of an extracellular ligand-binding domain, a transmembrane region followed by a cytosolic juxtamembrane domain, a kinase domain and a C-terminal tail. Their activation mechanisms and downstream signalling interaction partners are evolutionary conserved, in line with their pivotal roles in many cell-cell communication responses [16]. These include differentiation, proliferation, adhesion, immune defense and hormone responses.

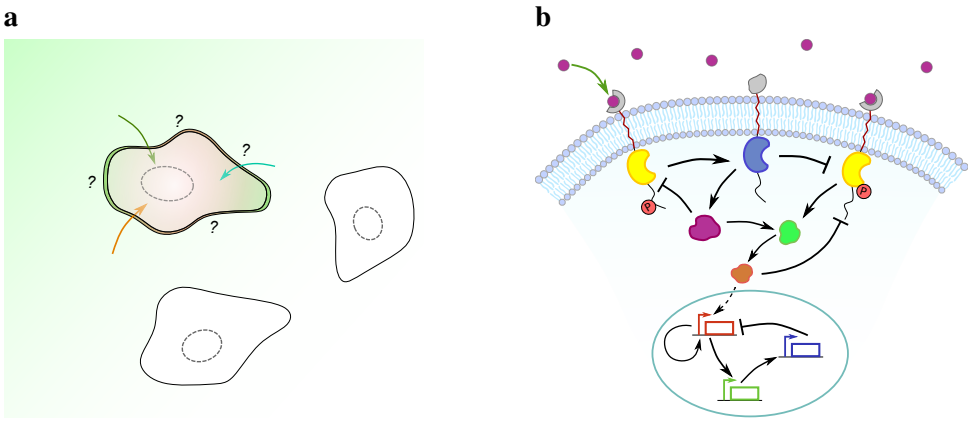

Figure 1.1 Cellular sensing. a) Cells perceive their dynamic environment by sensing the extracellular stimuli, processing the information and responding by updating the internal state. b) Surface receptors transduce the extracellular signal into internal activity pattern, using the dynamics of the protein interaction networks.

RTKs trigger these responses upon activation by growth factors by interacting with effector proteins which further propagate the signal intracellularly. Typically, an activated kinase domain phosphorylates its substrate, a tyrosine residue of another protein of interest (POI), by transferring a phosphate group using a high-energy adenosine triphosphate (ATP) molecule as a donor (Fig. 1.2). Very often phosphorylation occurs within a homo-dimer, hence the substrate is a protein of the same type. SH2- or PTB-containing signal transducing proteins recognise these post-translational modifications of the protein and propagate the activity further in the cytoplasm [17].

Hydrolysis of the phosphorylated tyrosine residue, catalysed by a protein tyrosine phosphatase (PTP), removes the phosphate group, causing transition to the inactive state of the substrate protein, thus counterbalancing the RTK activity.

1.2 Epidermal growth factor receptor (EGFR) as a sensing entity

EGFR is one of the most studied proteins in cell biology due to its involvement in multitude of physiological processes such as wound healing, embryonic development and tissue homeostasis [18, 19]. The role of EGFR in regulation of epithelial proliferation and differentiation has been widely established. For example, EGFR-deficient mutant mice fetuses exhibit growth and development impairment phenotype and embryonic lethality [20, 21]. Notably, the EGF-EGFR ligand-receptor pair was one of the first discovered growth factor pairs [22].

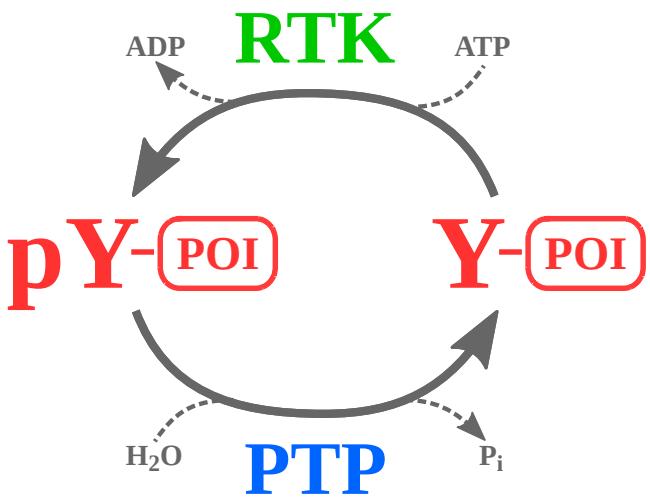

Figure 1.2 Phosphorylation/dephosphorylation transition cycle of a tyrosine residue-containing protein. Phosphorylation is carried out by the RTKs by using a phosphate group from an ATP molecule. Dephosphorylation by hydrolysis is carried out by the PTPs. POI: Protein of interest/study.

EGFR (ErbB1 or HER1) belongs to the ErbB family of receptor tyrosine kinases (RTKs), along with three other members (ErbB2-4/HER2-4) - it is localised at the PM and with its enzymatic activity it is typically targeting the tyrosine residues of its substrates for phosphorylation, as means for signal transduction. Phosphorylated tyrosine residues of EGFR and its substrates act as binding sites for effector proteins that initiate intracellular signalling, such as Grb2, PI3K, Shc, Src and PLCγ [17]. The Ras-MAPK network is a major signalling route for the ErbB family, as is the PI3K-Akt-mTOR network, both of which lead to increased cell proliferation and inhibition of apoptosis [23]. The PI3K-Rac-RhoGTP network is another signalling target of EGFR by which it can engage the cytoskeletal network [24, 25]. Thus, EGFR has multiple distinctive signalling functions (Fig. 1.3) - whereas it is signalling for survival in cortical astrocytes in the brain, it negatively regulates premature differentiation of keratinocytes in the epidermis [20, 26, 27] and osteoblasts, chondrocytes in bone development [28, 29]. In contrast, EGFR activation favours differentiation of mesenchymal cells in semilunar valves in the heart and of type II pneumocytes in the lung [20, 28, 30]. EGFR can also trigger cell migration in human breast cancer cells and NIH3T3 fibroblasts [31].

Unsurprisingly, abnormal activity of EGFR has been found in many cancer types such as gliomas and non-small-cell lung carcinoma [32], it is a known proto-oncogene [33]. Its persistent activation results in unchecked cell division [34]. Overexpression and mutations

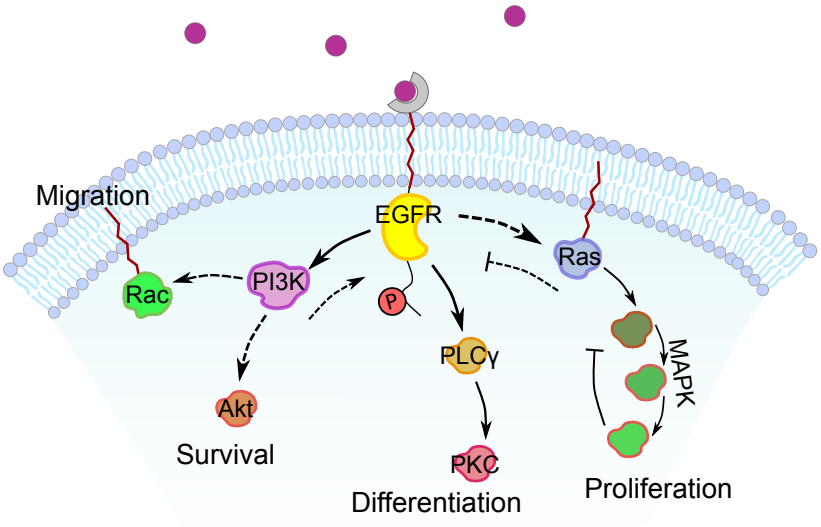

Figure 1.3 EGFR's context-dependent signalling. The signalling networks of EGFR are involved in multitude of cellular functions. Depending on the ligand stimulation and relative protein expression levels in different cell types and conditions, EGFR signalling can lead to different cellular outcomes.

of the tyrosine kinase domain are common causes of this abnormal activity, inducing cell transformation in carcinoma patients [35]. They are present in 40–50% of glioblastoma [36], sometimes in addition to a loss of tumour suppressor [37], and in one-third of epithelial cancers [38]. On the other hand, insufficient ErbB signalling in humans is associated with the development of neurodegenerative diseases, such as multiple sclerosis and Alzheimer's disease [39]. It is therefore of great importance to understand the principles of EGFR activation and regulation in both space and time, and how it leads to rich dynamical behaviours. Its systemic mechanisms for therapeutic targeting have spiked strong interest recently [40].

1.2.1 Activation mechanism of EGFR

EGFR is comprised of five major domains, in order from N- to C-terminal: extracellular domain, transmembrane domain, juxtramembrane domain, a kinase domain and a C-terminal tail (see Fig. 1.4, left). The extracellular domain consists of four subdomains, enumerated I to IV. Subdomains I and III comprise the EGF recognition pocket, whereas subdomains II and IV maintain tethered conformation by interacting with each other in the absence of a ligand [41]. Ligand binding inhibits this interaction allosterically, releasing the 'dimerisation arm' of subdomain II which induces association with other receptors [41, 42], while subdomain IV contributes to higher-order clustering [43]. These processes also result in allosteric conformational changes in the cytosolic part via the transmembrane domain and release of

the juxtamembrane segments from the PM, which confine the activity of EGFR by default [44].

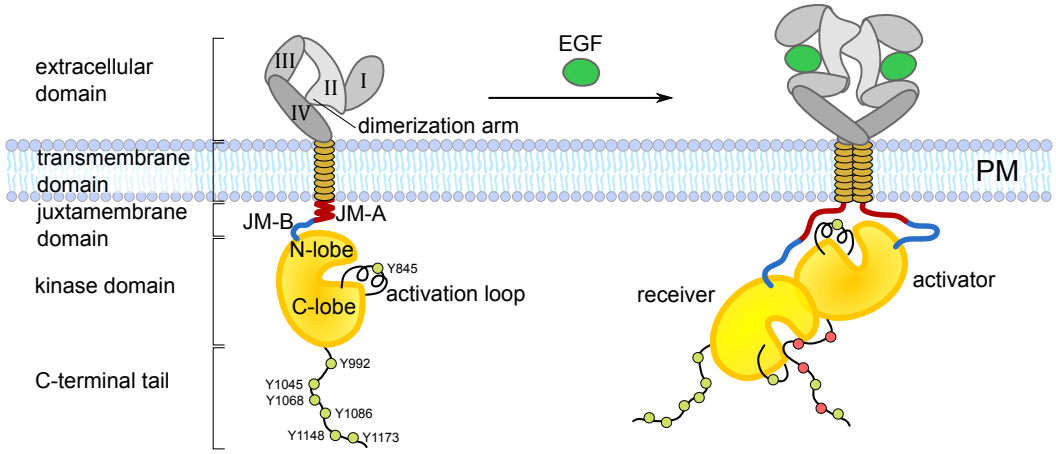

Figure 1.4 Structural organisation of EGFR and asymmetric dimer formation. Left: EGFR consists of the five denoted major domains, some of which contain notable subdomains. The unphosphorylated tyrosine residues are depicted with light green circles. Right: EGF binding induces asymmetric dimer formation where one of the receptors acts as 'activator', allosterically changing the position of the activation loop of the other receptor - the 'receiver', which can then trans-phosphorylate the tyrosine residues of the 'activator' in return, denoted here with red circles. Should they switch their roles dynamically then the 'receiver' receptor's tyrosines would also get phosphorylated.

The kinase domain of EGFR consists of two lobes: C-lobe and N-lobe. These two lobes have distinct roles in the trans-autophosphorylation process: the C-lobe of one protein acts as an activator, while the N-lobe of the binding partner acts as a receiver of activity. This forms the basis of the so-called asymmetric dimer model [44] (Fig. 1.4, right), where the allosteric activation mechanism alters the activation loop position, thus favouring the open conformation of the receiver molecule's kinase domain. Subsequently, the tyrosine residues of the C-terminal tail of the 'activator' receptor - Y992, Y1045, Y1068, Y1086, Y1148 and Y1173 among others, can get trans-phosphorylated. SH2- or PTB-containing signal transducing proteins are then recruited to these phosphorylated tyrosines, further propagating the signal in the cytoplasm [17]. One such protein is the E3-ligase Cbl, which binds to pY1045 and attaches a ubiquitin group at the kinase domain of EGFR, marking it for degradation [45].

In absence of a ligand the transition between open and closed conformation is biased towards the closed one by the auto-inhibitory mechanisms: the extracellular subdomain interactions, the juxtamembrane domain position and the activation loop position, counteracting the thermal conformational fluctuations of the molecule. However, despite the self-inhibition,

aberrant EGFR activation has been reported at high receptor concentrations [46], suggesting that there is an additional intermolecular ligand-independent activation mechanism. Recently, it has been shown that the phosphorylation of the Y845 residue within the activation loop of the kinase domain can enhance the activity of EGFR, shifting the conformational equilibrium towards the open conformation state [47, 8]. This provides a mechanism for a non-canonical activation of EGFR, where an unliganded molecule can obtain an active state and can also propagate that state to other EGFR molecules via transient interactions and phosphorylation. This non-linear self-amplification mechanism in effect constitutes the autocatalytic activation of EGFR, initially observed in [48]. In summary, these mechanisms can be represented using the simplified model shown in Fig. 1.5.

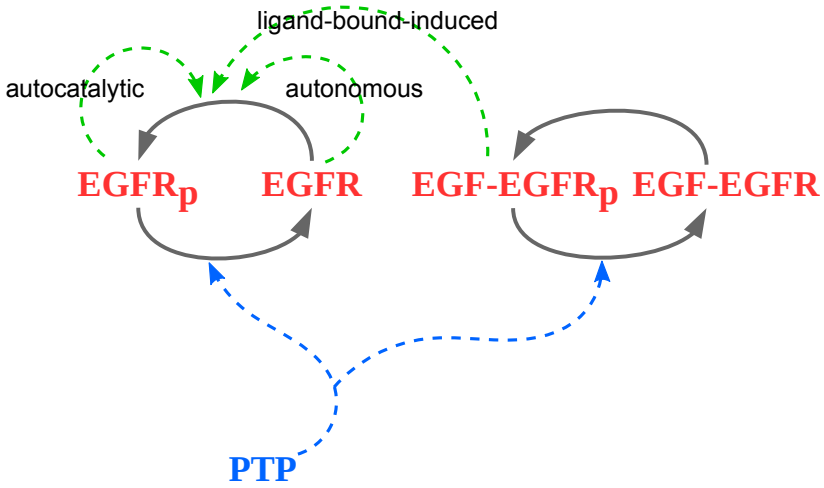

Figure 1.5 Diagram of EGFR activity regulation. State transitions between phosphorylated (p) and non-phosphorylated state are shown for the unliganded (EGFR) and liganded (EGF-EGFR) receptor. Self-association causes unliganded EGFR phosphorylation with different rates for autocatalytic, ligand-bound-induced and autonomous activation (green dashed arrows, left to right respectively). The PTPs cause dephosphorylation of both species.

1.2.2 Regulation of spatial-temporal distribution of EGFR by vesicular trafficking

Upon ligand-binding, activation and signal initiation, EGFR molecules undergo internalisation into plasma membrane-derived vesicles that traffic through the cytoplasm (Fig. 1.6). Typically this process starts by entry of activated EGFR molecules into Clathrin-coated pits (CCPs), a selection process moderated by the effector Grb2 and Clathrin adaptor AP-2 [49–51]. The curvature-inducing CCPs then promote membrane invagination, scission and internalisation into clathrin-coated vesicles (CCVs) of ~200 nm in diameter, constituting the

so-called clathrin-mediated endocytosis (CME) mechanism. At high EGF concentrations though, this mechanism is saturated and most of the receptors undergo clathrin-independent endocytosis (CIE) [52]. Alternatively, internalisation can occur via large macropinocytic structures - non-selective plasma membrane engulfments resulting from its EGF-induced dynamic ruffling [49, 53].

Ubiquitination of EGFR by the E3-ligase c-Cbl is an important mechanism that contributes to endocytosis [51]. Cbl binds to pY1045 of EGFR directly or cooperatively with Grb2 (which binds to pY1068 or pY1086) [54] and tags the kinase domain of the receptor with a small ubiquitin (Ub) molecule [55]. However, phosphotyrosine-binding recruitment of Cbl to EGFR alone is not sufficient for successful ubiquitination, as it can only be achieved through EGF-induced activation, possibly requiring stable EGFR dimers [8]. Hence, receptor ubiquitination is a direct readout for receptor occupancy.

Following internalisation, EGFR-loaded vesicles use motor proteins and microtubules as tracks to carry out long-range ATP-fuelled active endocytic transport towards the perinuclear areas [56, Chapter 13]. There they fuse into the sorting, or early endosome (EE), which acts as an intermediate endocytic hub from where the proteins are sorted and redistributed towards the different cellular compartments [57, 58]. The EE is composed of regions of thin tubular extensions and large vesicles [59], which have different sorting functions. Recycling proteins primarily cluster within the extending tubular membranes that would eventually pinch off [60], whereas the vesicular elements are usually involved in sorting to the degradative pathway [61], typically using the ubiquitin interacting motif (UIM)-containing proteins as a sorting unit that associates with ubiquitinated EGFR [62]. Thereupon, trafficking coordination is carried out by the family of small Rab GTPases, which regulate fission and fusion events of vesicles [63]. Re-routing of the sorted EGFR molecules from the Rab5-positive EE towards the Rab11-positive recycling endosome (RE) leads to recycling of the receptor to the PM. Early exit from the EE and recycling via Rab4-positive vesicles is the faster alternative. Concurrently, the EEs undergo Rab5-Rab7 maturation into late endosomes (LEs), further commit into multivesicular bodies (MVBs) and ultimately fuse into the lysosome, progressively decreasing their intravesicular pH value in the process. Non-recycled EGFR molecules that reach the MVBs and the lysosome are thus further internalised into intraluminal vesicles and eventually degraded. The vesicular dynamics of EGFR are summarised in Fig. 1.6.

Under which conditions the different trafficking routes of EGFR will be activated is an important question. Upon activation with high EGF doses the receptor internalises through CIE, while at low doses it does so through CME [52]. The sorting decision in the EE then primarily depends on the state of the receptor. It was shown recently that unliganded EGFR

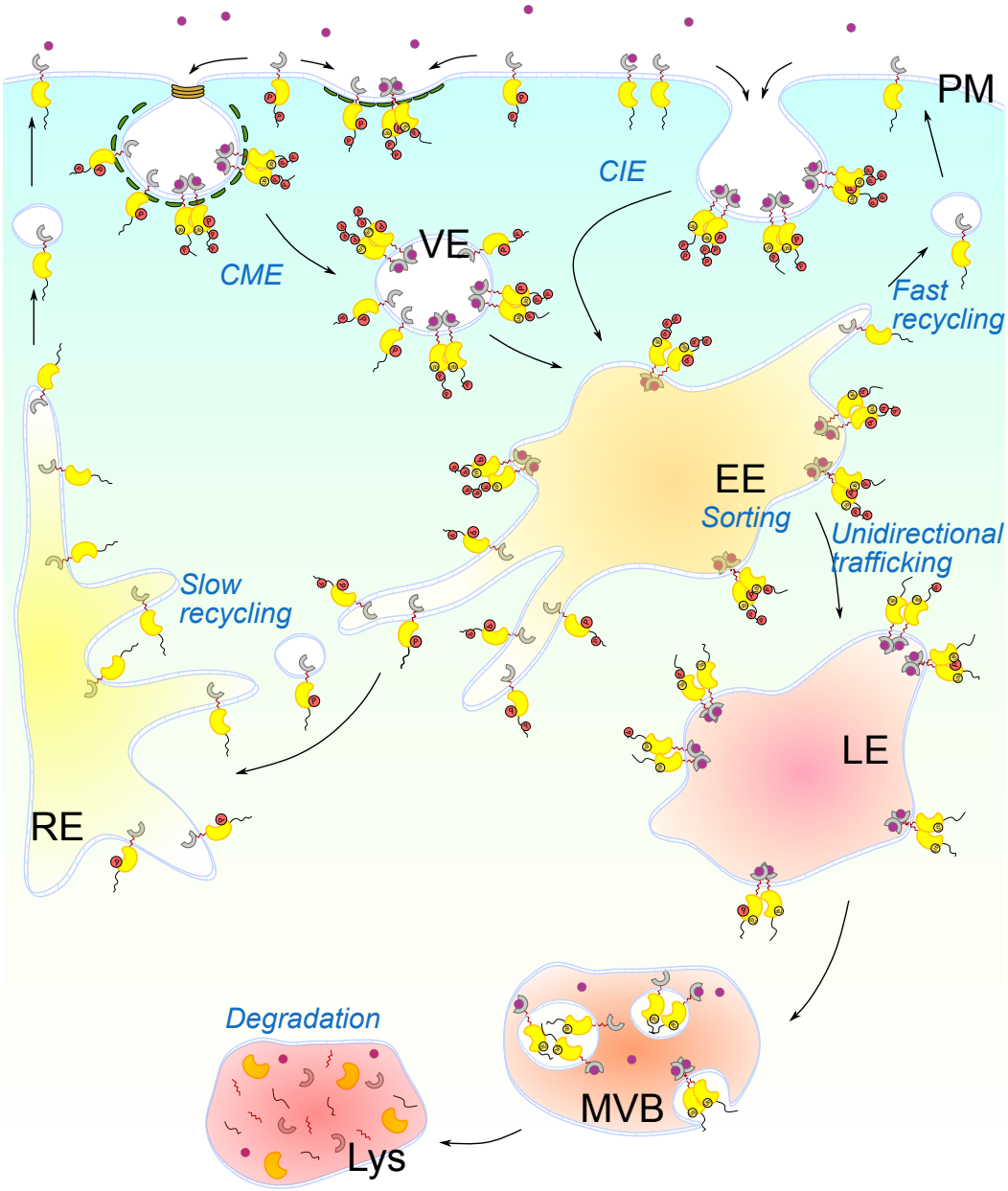

Figure 1.6 EGFR vesicular trafficking. Phosphorylated receptors are internalised via CME or CIM (PM, left and right respectively). Vesicular trafficking takes EGFR in the EE where critical routing sorting decision is made depending on the receptor state. Ubiquitinated ligand-bound receptors, typically in dimers, continue on the unidirectional route towards lysosomal degradation, whereas the unliganded receptors exit the EE and are recycled back to the PM via the RE-mediated- or fast-recycling route.

monomers recycle constantly in the absence of EGF through the RE in the perinuclear areas. There the abundance of PTP1B is high [64] and it dephosphorylates EGFR, safeguarding the system against spontaneous activation of EGFR [8]. However, once ubiquitinated EGFR

undertakes unidirectional trafficking towards lysosomal degradation, where it also interacts with PTP1B. Therefore, ubiquitination, being a readout for receptor occupancy, acts as a sorting cue which determines the fate of the receptor [8]. This indicates that vesicular dynamics plays an important role in determining the response of EGFR to growth factors, a feature that is also present in other RTKs [65].

Endocytic regulation of EGFR sensing and signalling is carried out on many levels. On the most obvious level, it attenuates PM signalling by internalising the ligand-bound receptors. However, EGFR can still potentially signal from the endosomes [66], so delivering more active molecules there will increase endosomal EGFR signalling [67, 68]. Depending on the local network of interaction partners, the strength and directionality of this signalling activity may defer from the ones at the PM. While MAPK activation persists from the endosomal compartments via scaffold proteins [69–72], Akt activation requires PI(3,4,5)P_3-enriched membrane domains which are only present at the PM [73]. Unsurprisingly, alterations in endocytotic distribution of EGFR is a frequent regulation evasion mechanism in cancer cells [74]. Therefore any spatial redistribution of EGFR will likely have an effect on its signalling outcome, and thus the study of phosphorylation regulation of EGFR must be in conjunction with its vesicular dynamics.

1.3 Protein tyrosine phosphatases

RTKs are positive regulators of their own signalling (Fig. 1.2). Using their kinase activity, EGFR molecules can phosphorylate other such receptors, thereby 'writing' information about the presence of a growth factor in the surrounding [75]. Thus, the PTPs have been viewed as simple 'erasers', dephosphorylating the tyrosines that were previously phosphorylated by EGFR. While the nature of the kinase activity itself allows for more complex non-linear dynamics, the negative regulation from the PTPs appears simply linear. However, causal coupling of a PTP with EGFR can generate a non-trivial interaction motif with complex response dynamics [76–80].

1.3.1 Signalling attenuation by the classical PTPs

The family of PTPs include member proteins with diverse localisations and activities [81]. They are divided into classical phosphotyrosine-specific PTPs and dual specificity phosphatases (DSPs). There are 37 known classical PTPs in the human genome [82], that can be further categorises according to their localisation motifs (See Fig. 1.7).

The transmembrane receptor-like PTPs (RPTPs) are PM localised and act primarily on the proteins sharing the same localisation domain. Their extracellular domains can display ligand recognition features, providing the potential for external regulation. These mostly include cell-cell and cell-matrix contact mediated mechanisms. On the intracellular region many of the RPTPs contain two tandem PTP catalytic domains - D1 (PM proximal) and D2. However, the D2 domain is typically a pseudo-PTP domain (with the exception of PTPRA), which possesses a proper PTP domain assembly but lacks activity. Nevertheless, they still play an important role for the stability and specific activity of the RPTP [83], as well as for promoting/demoting homo-dimerisation [84], by having higher/lower binding affinities between D1-D2 *cis*- and D2-D2 *trans*-interactions [85]. See Fig. 1.7 for more details.

The cytoplasmic PTPs on the other hand typically contain only one PTP domain. The cytosolic ones have non-catalytic sequences with which they can interact with their substrates, such as the SH2 domains of PTPN6 (SHP1) and PTPN11 (SHP2). Further, regulation is imposed by trans-interactions with some of these domains, as they can interact in cis and induce auto-inhibitory conformation by blocking the access of the PTP domain [86]. Localisation sequences are present on some of the cytoplasmic PTPs, targeting them to specific compartments in order to interact locally with their substrate partner. PTPN1 (PTP1B) and PTPN2 (TCPTP) are ER-bound PTPs and they interact with RTKs on the cytoplasmic face of the contact sides with the RTK rich vesicles [87, 88]. Sec14 domain-containing PTPN9 (MEG2) localises in the perinuclear area, bound to granules or secretory vesicles [89]. FERM domain-containing PTPN14 (PTPD1) and PTPN21 (PTPD2) have been shown to localise at actin cytoskeleton and adhesion sites at the PM to affect EGFR activity [90–92], as well as at endosomal sites [93].

The PTPs play important role in suppressing aberrant RTK signalling. Reports show that in several solid tumors there is a reduced expression in some of the RPTPs: PTPRG, PTPRJ, PTPRD, and PTPRK [94]. PTPRG and PTPRJ also exhibit cancer growth suppressive potential [95, 96] and are considered established tumour suppressors amongst the classical PTPs. The cytosolic PTPN11 (SHP2) is also one of the most studied PTPs whose mutations have shown implications in human disease [97, 98].

All of the PTPs share a common catalytic mechanism [99], shown in Fig. 1.8. It is a two-step process based on a nucleophilic cysteine ($Cys-S^{-}$) with a low pKa within the PTP domain. In the first step, the cysteine executes a nucleophilic attack on the phosphorus atom in the phosphotyrosine residue of the bound substrate. As the ester bond is cleaved, a well positioned catalytic aspartate donates its proton to the oxygen in the leaving group of the substrate, thereby completing its reversion to its non-phosphorylated state. In the second

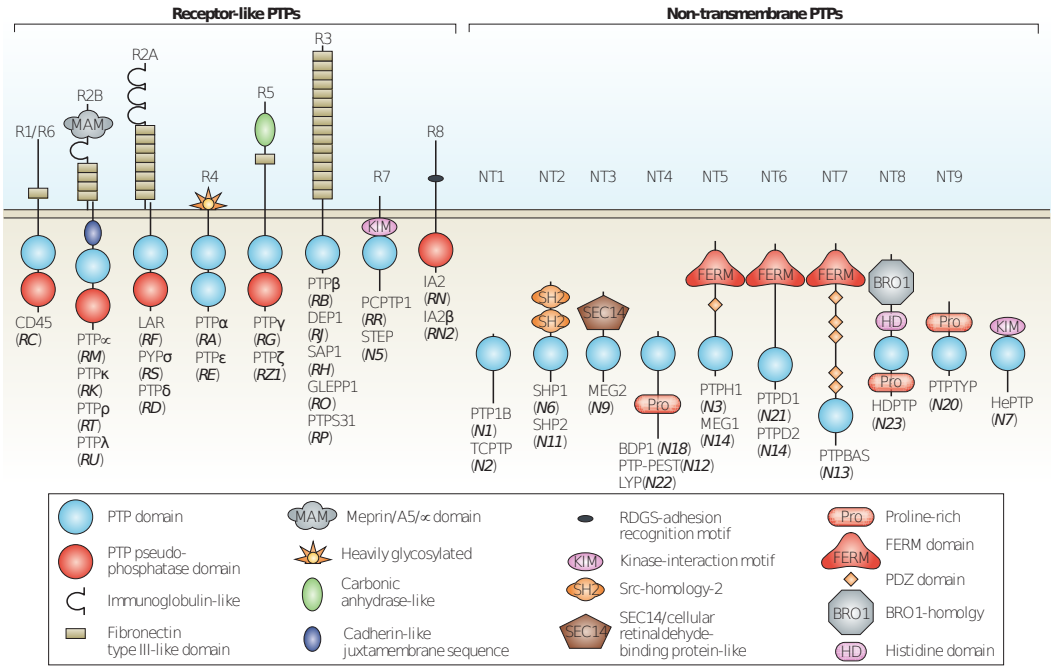

Figure 1.7 The family of classical PTPs. The classical protein tyrosine phosphatases (PTPs) are mainly categorised as receptor-like or non-transmembrane phosphatases. The distinct domains of the PTPs are presented in the inset, which determine the sub-classification based on sequence similarity. The nomenclature displays the protein names of the PTPs, commonly used in the literature, whereas the gene symbol is additionally included in parentheses. Reprinted from [81] with permission. Copyright © 2006, Springer Nature.

reaction, the cysteine-phosphate intermediate is hydrolysed by a water molecule, yielding the restored enzyme and inorganic phosphate.

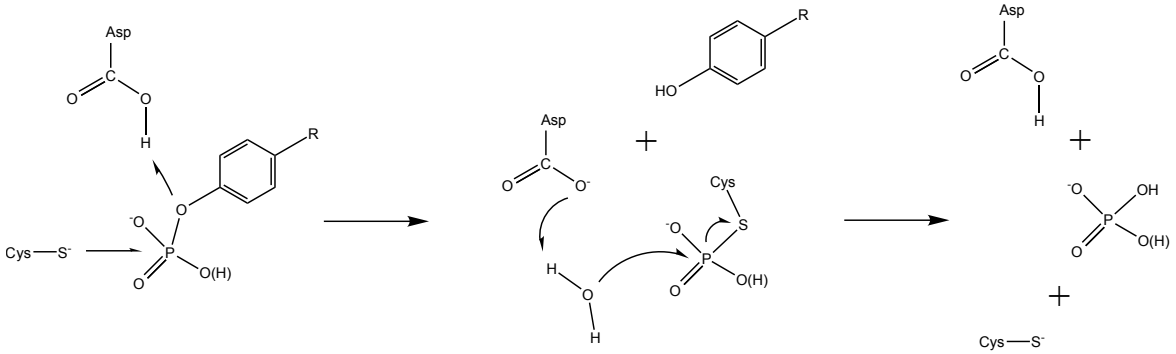

Figure 1.8 The catalytic mechanism of the PTP domain. The phosphorylated substrate is exposed to a nucleophilic attack by the active cysteine of the PTP domain, creating a phosphoenzyme intermediate. Hydrolysis then releases the phosphate group and reverses the active cysteine to its initial state.

1.3.2 PTP regulation by reversible oxidation

The low pKa of the active cysteine is crucial for the catalytic activity, therefore a very beneficial property [99]. It is achieved via many factors, mainly arising from the microenvironment of the cysteine residue [100]. However, this makes the PTPs more sensitive to oxidation by the reactive oxygen species - O_2-derived species that include superoxide anion (O_2^-), hydroxyl radical ($HO\cdot$) and the prominent hydrogen peroxide (H_2O_2) [101]. H_2O_2 possesses high reactivity towards cysteine residues in general, targeting the thiol group (Cys-SH) for oxidation to sulfenic acid (Cys-SOH). Cysteines with pKa values lower than the physiological pH are the ones susceptible to this attack, as their $-SH$ group becomes thiolated (to thiolate anion $-S^-$) [102]. Modification to sulfenic acid has major effects on the reactivity of the PTP, basically rendering it catalytically inactive. Secondary redox reactions occur to put the cysteine in a state from which it can revert back to the active one, mediated by the reducing agents [103]. These reactions also prevent irreversible overoxidation to sulfinic ($-SO_2H$) or sulfonic acid ($-SO_3H$), which typically occur only upon oxidative stress. These state transitions, summarised in Fig. 1.9, constitute the redox-based regulation of the PTPs.

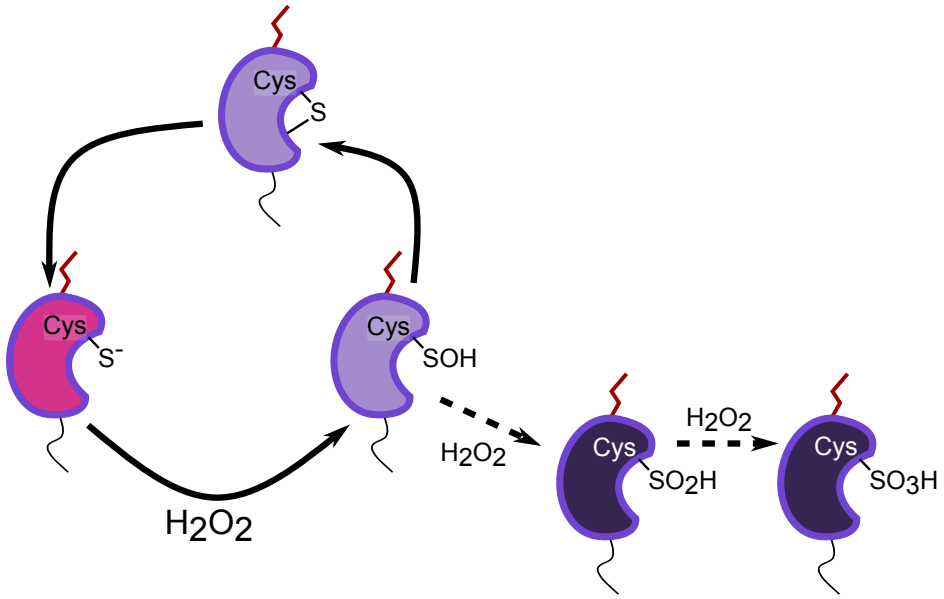

Figure 1.9 Redox regulation of the PTPs. Thiolate anion (-S$^-$) of the active cysteine is susceptible to oxidation by H_2O_2, forming a sulfenic acid (-SOH). Intra- or intermolecular disulfide is formed in a secondary reaction, that can transition back to the initial state, mediated by the reducing agents. Irreversible oxidation to sulfinic (-SO_2H) or sulfonic acid (-SO_3H) occur at a critically high H_2O_2 levels.

PTP inhibition by H_2O_2-induced oxidation is well studied in the literature. The widely used PTP inhibitor pervanadate, that is typically used as tyrosine phosphorylation enhancer,

carries out its function by irreversibly oxidising the PTPs [104]. PTPN1 (PTP1B) undergoes reversible oxidation in cells treated with insulin or EGF [105, 106], PTPN2 (TCPTP) similarly is oxidised with insulin [107], whereas PTPN11 (SHP2) is oxidised upon PDGF or EGF treatment [108, 109]. PTPRA on the other hand forms homodimers upon oxidation, as the oxidised D2 domains form a bridge [84, 110].

The RTKs exhibit their redox regulation via H_2O_2 production, mediated by the family of NADPH oxidase (NOX) complexes [111, 112]. The PM-localised NOX2 complex is the most studied isoform and is expressed in many cell types, showing high accumulation in protrusions and membrane ruffles [113]. Hydrogen peroxide is produced extracellularly by NOX2 and then transported inside by diffusion or via aquaporins (see Fig. 1.10). The mutual inhibition with the abundant peroxiredoxins then generates confined concentration of H_2O_2 near the PM [114]. Formation and activation of the complex is enhanced by PI3K-induced PI(3,4,5)P_3 formation and Rac1 activation [115]. EGFR, among other RTKs, can activate PI3K, thereby inducing H_2O_2 production near the PM [111, 116].

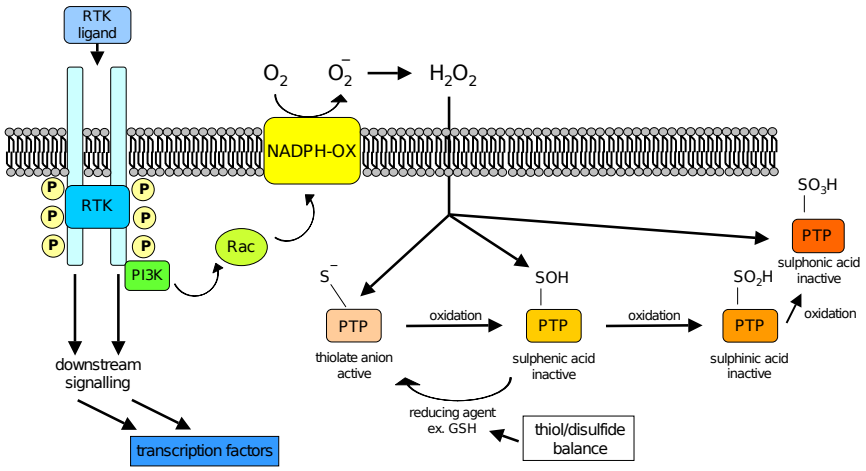

Figure 1.10 NOX-mediated ROS production and PTP inhibition. RTK-induced PI3K activation leads to formation of the NADPH-OX (NOX) complex at the plasma membrane, mediated by Rac and PIP_3. Extracellularly-produced H_2O_2 then enters the cytosol through the membrane to induce oxidation on the PTPs. Reprinted from [111]. CC BY 2.0.

1.3.3 PTP interactions with EGFR

Recursive interactions generate plasticity in EGFR response

Regulation of the PTP activity potentiates causal recursive EGFR-PTP coupling. The resulting interaction motif can generate non-trivial dynamical solutions, shaping the EGFR

activity in a more elaborate way than previously envisaged [76–79]. While the autocatalytic EGFR activation gives rise to a one-component positive feedback motif, the EGFR induced H_2O_2 production negatively regulates the interacting PTP, effectively creating a double-negative feedback motif [76]. This motif, also termed a toggle switch [80], can put the system in a bistable regime, where a discontinuous switch from low to high EGFR activity response can occur upon a certain input EGF threshold [76]. The switch effectively translates to a lateral phosphorylation propagation [77], where receptor activity is spread in a cascade fashion along the PM as a result of the autocatalytic activation mechanism [48].

Identification of major EGFR dephosphorylating activities

To identify which PTPs dephosphorylate EGFR, large scale studies have been performed in the literature. Based on enzymatic assays of purified PTPs, PTPN1/2/9 and PTPRA/B/C/E/G/J/O were identified as EGFR phosphatases [117]. In [118] a membrane two-hybrid assay was employed, and PTPN6/11/12, as well as PTPRA/B/E/G/H/K/S/T/U/Z were identified. Biochemical assays on cell extracts after siRNA knockdown found PTPRJ and PTPRK as PTPs that dephosphorylate EGFR [119], as well as PTPN1 [120], PTPN2 [121] and PTPN9 [122]. However, a more elaborate study that looks into the precise role of the PTPs in governing the phosphorylation dynamics of EGFR, which determines the strongest regulators in that sense, has not been conducted.

Previous work in the lab [123] addressed which of the PTPs associate directly with EGFR and strongly and negatively regulate its activity. Five major non-redundant PTPs that dephosphorylate EGFR were identified using cell array fluorescence lifetime imaging microscopy (CA-FLIM) screening [124] of 55 PTPs in combination with quantifiable opposed cDNA/siRNA genetic perturbations: the PM localised PTPRG, PTPRA and PTPRJ, the dual-specificity phosphatase DUSP3, as well as the ER associated PTPN2 (see Fig. 1.11, top left corner). In the subsequent analysis DUSP3 showed only weak and PTPRA showed modest temporal regulation [123], leaving three PTPs, localised on distinct membranes, as the major EGFR dephosphorylating activities.

Spatial temporal interactions

While the PM-localised RPTPs interact with EGFR in its principal location, the ER-bound PTPs interact with EGFR upon contact with EGFR-rich vesicles, following internalisation of EGFR (Fig. 1.12). Therefore, EGF-induced trafficking couples EGFR with these PTPs at distinct spatial as well as temporal points, imposing different functional PTP roles. Thus, EGFR's temporal phosphorylation dynamics is shaped by the spatially distributed EGFR-PTP interactions, showing how space and time are intertwined to determine sensing.

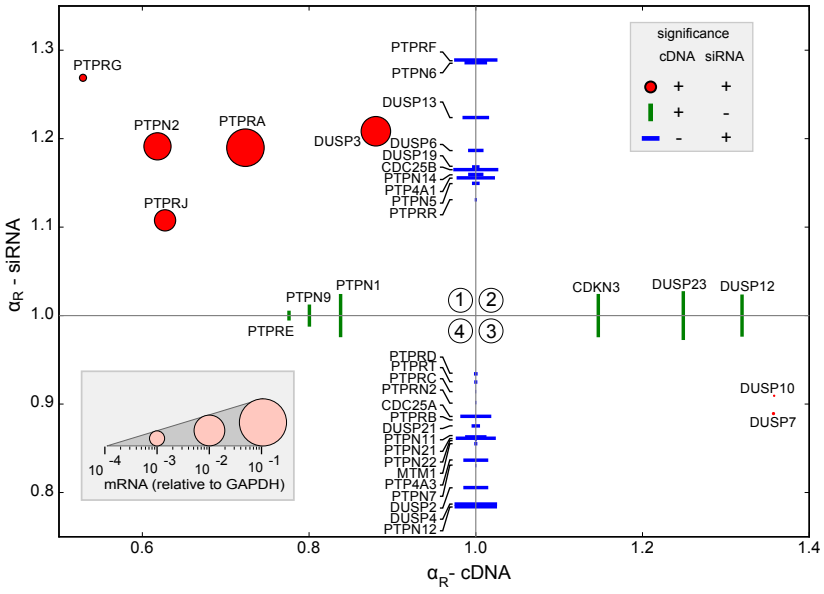

Figure 1.11 In situ EGFR phosphatome identification. Scatter plot of median EGFR phosphorylation fold-changes ($\alpha_R = \alpha_{PTP}/\alpha_{ctr}$) upon opposed siRNA-knock-down and ectopic PTPx-mCitrine perturbations, at 5 min after 200 ng/mL EGF stimulation. Significant changes upon both (red dots) or only one perturbation (green/blue lines, p<0.05) are shown. Marker size is scaled to relative PTPx-mRNA expression in MCF7 cells (legend: bottom inset). Reprinted from [123]. CC BY 4.0.

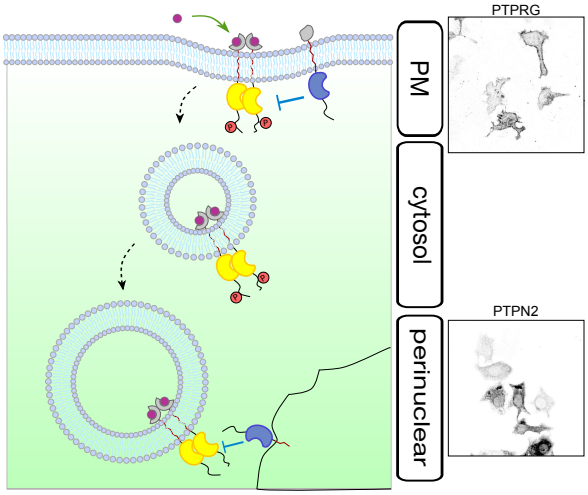

Figure 1.12 Spatially distributed EGFR-PTP interactions. Left: PTPs with different spatial localisations interact with EGFR on its characteristic vesicular trafficking routes. Right: Example images of PTPs with different localisations - RPTP (PTPRG) and ER-bound PTP (PTPN2).

However, it is not clear how these major PTPs interact with EGFR, how do they causally couple with each other, and how EGFR's sensing and responsiveness to growth factors is shaped as a result.

1.4 Dynamical solutions of underlying interaction motifs guide the cellular responses

Identification and understanding of associational/causal relationships and their unique mechanistic properties can be obtained by studying molecular interactions in cells. However, this is very often not sufficient to understand their biological function, thus one needs to study these interactions within the larger scope of their functioning, i.e. the systems in which they are embedded. While the systems are optimised towards performing certain functions [125], the 'optimisation' process itself imposes constrains on the possible solutions, hence their connections are far from random. Very often optimising certain signalling processes leads to requirements for similar functional forms, therefore successful evolutionary solutions are recurrent, in many different contexts [126]. This leads to ubiquitous presence of several unique network motifs in biological systems, whose forms can be more easily identified and used to study the organisational principles. To do so, we naturally turn to study how EGFR interacts with the three major PTPs and how the resulting dynamical behaviour governs EGFR sensing and responsiveness to EGF.

1.4.1 Geometrical representation of a dynamical system

While studying a given biological process it is important to define the representational form of the quantities whose change we are interested in analysing. This is typically a vector of quantities comprehensively representing the current state of the system. As EGFR response dynamics is determined by the activity regulation between EGFR and a given PTP, we represent out network state as a combination of $[EGFR_p, PTP_a]$, hence a two-dimensional vector of variables: $EGFR_p$ - the amount of phosphorylated (or active) EGFR molecules and PTP_a - the amount of active PTP molecules. The dynamical system defined by the interactions between these two molecules then describes the co-evolution of the two variables:

$$\begin{cases} \dfrac{\mathrm{d}EGFR_p}{\mathrm{d}t} = f(EGFR_p, PTP_a) \\ \dfrac{\mathrm{d}PTP_a}{\mathrm{d}t} = g(EGFR_p, PTP_a) \end{cases} \tag{1.1}$$

f and g describe the reaction kinetics (with the law of mass action) that are defined by the interaction motif itself (such as the one in Fig. 1.5). The state transition cycles between active and inactive state are modelled for each component, meaning there are two readouts, one for each activity state. However, we assume that on the time scale of the signalling process

there is a mass conservation, i.e. the total protein concentrations are constant. This renders the two activity states dependent, allowing us to reduce the dimensionality of the system by half. Therefore, we are only modelling the active states of the components (Eq. (1.1)). Even more, we can model them as fractions of the total protein concentrations, thus normalising their range in the [0,1] interval. Besides the variables, the system parameters appear in the equations for f and g. These are typically the reaction rate constants, protein concentrations and possibly input parameters (such as growth factor concentration).

In absence of any prior knowledge it could be assumed that $[EGFR_p, PTP_a]$ can acquire any possible combination, and all of these combinations define what is called the state space (or phase space, phase portrait), i.e. the multidimensional space enclosing all of the possible system states (Fig. 1.13, left). The tendencies (flow vectors) from each of the points in the state space, defined by the system in Eq. (1.1), constitute the so-called vector field. Given a starting point (initial condition/state) the dynamical system proceeds by following the vectors in the vector field, which will generate a trajectory in state space (Fig. 1.13, left, green line). However, all of the trajectories in the system starting from these different initial states typically converge to a small number of fixed points that define the stable configurations of the system. These are called stable steady states, or fixed point attractors, as they attract the neighbouring trajectories from every direction. Unlike them, the unstable steady states repel trajectories in at least one direction, hence are responsible for separating the state space into regions of different tendencies, called basins of attraction. In Fig. 1.13, left, there is one stable steady state, hence the complete state space is its basin of attraction.

In mathematical terms, a steady state $[EGFR_p^*, PTP_a^*]$ is defined as the state in which the system shows no change, i.e.

$$\begin{cases} \dfrac{\mathrm{d}EGFR_p^*}{\mathrm{d}t} = f(EGFR_p^*, PTP_a^*) = 0 \\ \dfrac{\mathrm{d}PTP_a^*}{\mathrm{d}t} = g(EGFR_p^*, PTP_a^*) = 0 \end{cases} \tag{1.2}$$

The relationship between $EGFR_p$ and PTP_a defined by setting of the derivative in the first equation to zero, $f(EGFR_p, PTP_a) = 0$, is called the $EGFR_p$-nullcline and it encloses all of the points in the state space where the change along the direction of the $EGFR_p$ axis is zero, i.e. the vector is aligned straight horizontally in the points on the nullcline. The PTP_a-nullcline is analogously defined. One way to think about a nullcline is by substituting its implicit form $f(EGFR_p, PTP_a) = 0$ with the explicit form, assuming we can find one: $EGFR_p = F(PTP_a)$. This imposes a parametric view of the variable on the x-axis, namely PTP_a. Thus the nullcline is defined by the steady state values of $EGFR_p$ when PTP_a is treated

as a parameter and varied from 0 to 1, i.e. when bifurcation analysis is performed using PTP_a as a bifurcation parameter. Analogous dependency $EGFR_p = G(PTP_a)$, is established for the other nullcline. The intersections between the two nullclines then determine the fixed points in the system.

Exemplary state space with its vector field, nullclines and steady states is presented in Fig. 1.13, left, for a simple EGFR-PTP motif, as shown in Fig. 1.5. A trajectory through state space translates into a trajectory in time (Fig. 1.13, right), representing the response of the system. In this case, it exhibits a transient phase initially and it converges to the steady state level. Although more complex attractors exist in nature, such as limit cycles (oscillations), strange attractors (chaos), the dynamics in our studied systems are mostly captured by point attractors (fixed points).

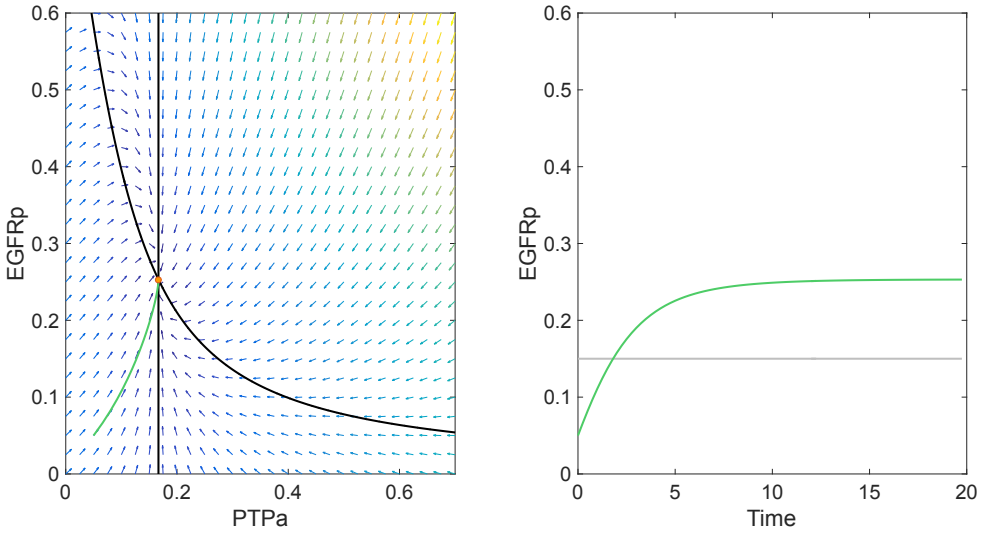

Figure 1.13 State space representation of a simple EGFRp-PTPa system. Left: State space with its vector field for the system shown in Fig. 1.5. Nullclines are depicted with black lines. Sample trajectory is shown in green. Right: The state space trajectory is translated into a temporal profile. The input fraction of ligand-bound EGFR is shown in grey.

Stable solutions are in many cases the most robust approach for achieving reliable and reproducible outcomes under various conditions. While the trajectories in state space generate the outcome, the fixed points in the system shape the state space geometry, defining the trajectory manifolds. Therefore in this thesis the system will be characterised by studying its convergence manifolds.

Rate balance plots to graphically examine stability

Generally, each of the equations f and g can be studied by splitting it into two parts: the forward reaction rate and backward reaction rate. This effectively groups the terms in the equation that activate or deactivate the component. Very often this step requires a quasi steady state assumption for all of the variables, except for the studied one. The rate balance plot then shows the dependence of both rates of change on the actual variable (Fig. 1.14).

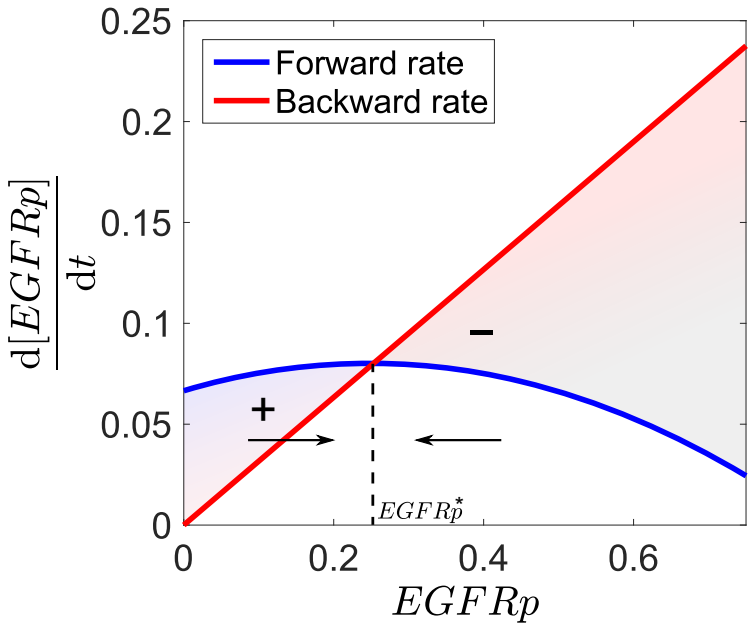

Figure 1.14 EGFRp rate balance plot. The forward and backward reaction rates are shown, which intersect in a single steady state (EGFRp*, dashed line). The sign of the difference between the rates left and right of the steady state is denoted, determining the system tendency.

The intersections give the balance points in the rates, i.e. the values for which there is no net change, hence the steady states of the system (EGFRp*). To asses steady state stability one has to observe the system tendency left and right of the steady state. In the example in Fig. 1.14 the forward rate is greater than the backward rate when EGFR's value is lower than the steady state value, thus higher activation will ensue, increasing the EGFRp value as a result. On the other side of the steady state the opposite is true, thus the EGFRp value will approach the steady state from both sides, indicating that it is a stable fixed point attractor. EGFRp* corresponds to the stable steady state value in Fig. 1.13.

Systematic study of dynamical systems using bifurcation analysis

Change of the parameters in the system has an effect on the shape of one or more of the nullclines, as they are included in the model functions, e.g. functions f and g in Eq. (1.2). Modification of the shape of the nullclines can then result in a change of the intersection points, either quantitatively - by altering the position(s) of intersection in the state space, or qualitatively - by increasing/decreasing the number of intersection points. The former modification alters the steady state values, while the latter changes the number of steady state solutions in the system.

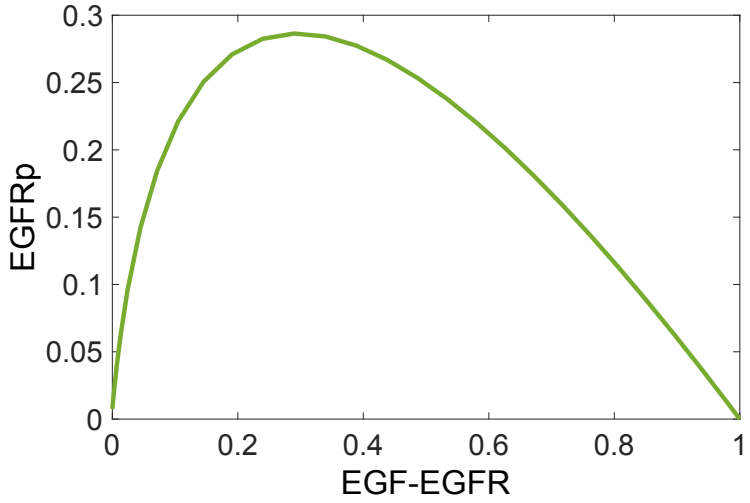

Figure 1.15 Bifurcation diagram showing dependence of EGFRp on EGF-EGFR. The green profile shows the quantitative change of the steady state value of EGFRp with modulation from 0 to 1 of the EGF-EGFR input.

Observing the quantitative and qualitative changes of the system when gradually modulating one or more of the parameters is called bifurcation analysis (origin from the Latin *bifurcatus* ('two-forked') - to divide or fork into two branches). The system's steady states are readout through one of its components, thus practically a projection, or dimensionality reduction of the fixed points in state space to the selected variable axis is observed on the y-axis of the bifurcation diagram, for every value of the parameter (Fig. 1.15). The modulated parameter on the x-axis is termed bifurcation parameter. Bifurcation point is thus defined as the parameter value on the x-axis at which a sudden qualitative change occurs in the system behaviour, i.e. a topological change in the state space due to modification of the nullclines, as described above. Different bifurcation types can be found, such as pitch-fork bifurcation and saddle-node bifurcation - where the system transitions from one to three fixed points or

vice versa, Hopf bifurcation and period doubling - where appearance and change in limit cycles occur, and many more.

Understanding of the bifurcation properties, or the topological changes, provides knowledge of the achievable dynamical solutions, hence of how can the system potentially behave. Therefore, studying the model parameters, or the factors that affect the system, through bifurcation analysis gives unique insight into the different operational regimes, allowing to infer in which of them the system is positioned, and to predict and hypothesise potential behaviours from there. An example for the EGFR-PTP system from Fig. 1.5 is shown in Fig. 1.15 where steady state values of EGFRp are examined in dependence of the input parameter EGF-EGFR. The steady state levels of EGFRp increase and reach maximum for ~30% receptor occupancy before decreasing to zero.

1.4.2 Identifying network motifs by probing their dynamical features

To understand the dynamical properties of the system, it is necessary to identify the underlying interaction network of proteins. This knowledge allows to further investigate the system properties by studying the network features under different conditions. Various network reconstruction methods have been employed in the literature to uncover the potential causal relations. Modular response analysis (MRA) is typically used when a relatively small network is studied and all of the components activities can be measured upon perturbation on each of the components individually [127].

On the other hand, network inference from temporal data has also been employed for large-scale networks. Typical experimental data consists of complete system observations at discrete time points after stimulation. Association matrix between all nodes is then constructed by thresholding the pairwise similarities from the observed data [128]. Causality can be inferred by taking into account of the pairwise time delays between the responses.

Reconstruction from single cell multivariate data takes advantage of the multidimensional distribution of the data and the cell-to-cell variance to estimate the dependencies between the variables. This is done using a directed probabilistic graphical model (Bayesian network) of relationships whose network structure is iteratively improved given a scoring function [129, 130].

In this thesis we are interested in how the response properties of EGFR arise from EGFR-PTP network motifs. However, only EGFRp can be observed experimentally and we cannot apply any of the previously described methods. Given our assumptions about the possible interactions, we can limit the number of networks that can emerge as potential candidates. The network that reflects the underlying dynamical signature can be then inspected and distinguished from the other candidate networks. Therefore, we probe the interaction network

itself via perturbing its model parameters and observing the activity of EGFR. Similar to a bifurcation analysis, studying the dynamical properties of the system in presence of a controlled parameter change provides a unique perspective on the functioning of the network: how is the response shaped by affecting the steady state solutions. While the biochemical constants are not straight-forward for experimental manipulation and the protein abundances need more complicated approach to control, the input EGF stimulus in the system is a highly controllable parameter that changes the response of the system. Therefore, this parameter will be probed experimentally and the dynamical properties will be studied theoretically.

1.5 Fluorescence microscopy for observing spatial temporal EGFR phosphorylation dynamics

Fluorescence microscopy is essential tool for observing and studying dynamical processes in living cells. Live single-cell imaging combines traditional imaging techniques with time-lapse microscopy to provide unique insight into the functioning of signalling networks. It is an important advancement in systems biology that can uncover dynamical details that might be obscured if average behaviour in a population of cells is observed. As living cells are translucent, typical approaches use expressed fluorescently-tagged proteins that are visible under a light microscope. Combined with live cell imaging techniques they provide quantifiable dynamics in space and time.

To maximise information extraction and establish recursive interaction between the computational modelling and the experimental design, it is necessary to grasp the principles of single cell imaging and optimise the work flow.

1.5.1 Photo-physical properties of fluorescence

In order for a protein to be visible under a microscope it must emit a light, or photons with specific wavelength. A fluorescent protein emits photons from its electrons, when they relax from an excited singlet state to the ground state. The electrons get to the excited state in the first place by absorbing photons from a light source with a higher frequency. This process is illustrated with a Jablonski diagram [131], shown in Fig. 1.16a. Electrons normally reside in the lowest energy state, indicated by S_0. Photon with corresponding energy may be absorbed by the protein, causing an electron to transition to one of excited states (S_1 or S_2 in Fig. 1.16a, blue line). The photon energy needs to correspond to the energy difference between the ground and the excited state in order to be absorbed. The electron excitation is a very fast process, on the order of 10^{-15} seconds. From the initial excited state the electron

loses its energy through the sub-levels to the lowest sub-level of the first excited state S_1 due to vibration. This non-radiative process, called internal conversion, is on the order of 10^{-12} seconds (black wavy lines, Fig. 1.16a). Fluorescent emission then takes place as the electron falls to one of the sub-levels of the ground state S_0. The energy of the emitted photon corresponds to the energy difference of the transition levels, and is thus lower than the energy of the initially absorbed photon. This process is on a time scale of nanoseconds (10^{-9}–10^{-8} seconds) after the initial photon absorption. The difference between the energy levels, i.e. wavelengths, of the absorbed and the emitted photons is called Stokes' shift, shown in Fig. 1.16b for the green fluorescent protein (GFP). There, the normalised spectrum depicts the probability that a photon with a specific wavelength will be absorbed (blue) or emitted (green). In this manner, the process of fluorescence converts light of one wavelength to another.

1.5.2 High-resolution confocal microscopy for observing fluorescently-tagged proteins in cells

The first step of the experimental design is deciding which fluorescent proteins and reporters are going to be introduced in the cells. The absorption and emission wavelengths of the fluorescent proteins restricts the system in the number of molecules that can be used simultaneously. The spectral overlap and skewed spectral distributions typically lead to unwanted photo-activation and photo-detection, or bleed-through from a neighbouring channel to the channel of interest. Therefore, careful selection of laser lines for activation and filters for selected detection are crucial for optimising imaging.

Multichannel time-lapse microscopy allows for image acquisition with suitable frequency over longer periods of time. The frequency of imaging is coupled to the rate of change of the signalling process, as it should provide enough temporal sampling of the process to capture its behavioural details. High spatial detail can be obtained by using a confocal laser scanning microscope, a point illumination system with a pinhole for focusing of the laser light to a relatively thin focal plane of interest, i.e. a slice of the cell at a given height (Fig. 1.16c). Another pinhole is used in an optically conjugate plane in front of the detector to eliminate fluorescent signal that comes from a source that is out of focus. Higher intensity and longer exposure are then used in addition to improve the signal-to-noise ratio and thus detection of lower levels of signalling quantities. However, there exists a trade-off between a good temporal signal and the health of the imaged cells and fluorescent proteins. High intensity and light exposure over longer periods of time lead to phototoxicity of the cells, while very

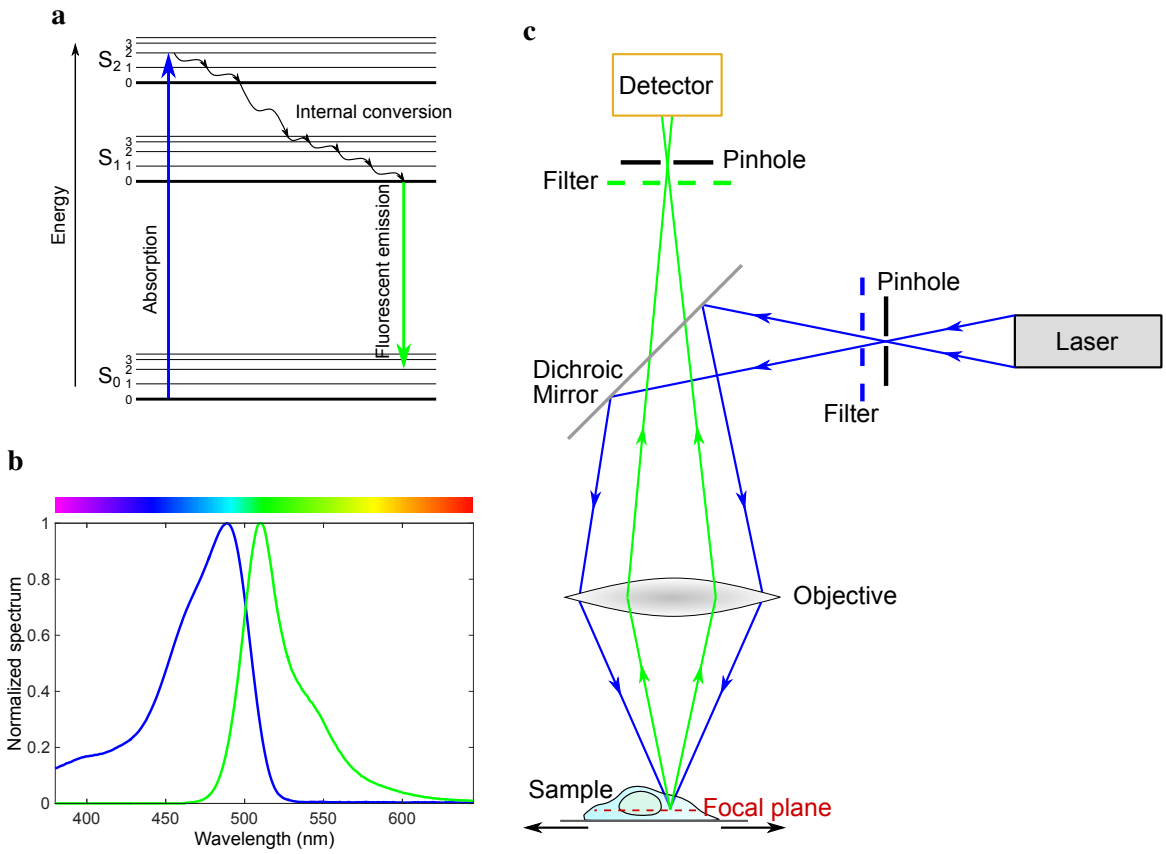

Figure 1.16 Principles of fluorescent microscopy. a) Jablonski diagram showing the excitation of an electron to a higher energy state (blue), internal conversion via vibrational relaxation to the lowest S_1 sub-level (black wavy lines) and fluorescent emission (green). b) Absorption (blue) and emission (green) spectrum of GFP. c) Diagram of a confocal microscope. Blue illumination light, filtered and then reflected using a dichroic mirror, is focused with a pinhole to a focal plane in the sample. The fluorescence emission signal is then transmitted through the dichroic mirror and filtered for wavelength and out-of-focus signal to the detector.

high frequency and intensity imaging lead to permanent photobleaching of the fluorophore, thus decrease of the signal.

Following the live cell imaging, tracking of the cells in time and image segmentation for extracting spatial data generate a single-cell spatial temporal data. Finally, the spatial temporal data can be used for information extraction by computational modelling and analysis of time series data. The results will guide the subsequent experimental designs and help pose and probe hypotheses for the signalling system in question.

1.6 Objectives

The main objective of this thesis is to reveal how EGFR can sense and respond to time-varying EGF signals. To understand the EGFR phosphorylation response we have to uncover the underlying principles of operation of the EGFR-PTP network. We set out to do this by identifying the network structure by experimentally probing the interaction motifs between EGFR and each of the PTPs of relevance - the PM-localised PTPRG/J/A and the ER-bound PTPN2. Using dynamical systems theory we then decipher the different levels of regulation and operation of the network. The unique properties of this spatially distributed EGFR-PTP system then give rise to the effective EGFR response, allowing the system to settle in a regime where it can process multiple subsequent GF stimuli. This provides understanding on multiple levels, from the dynamical properties of the network to its function as a whole, in this case the growth factor sensing capabilities of the cell. Finally, we probe the hypothesised cellular response experimentally to outline the functioning of the system.

Materials and Methods

2.1 Mammalian cell culture

MCF7 cells (ECACC, Cat. No. 86012803) were cultured in Dulbecco's modified Eagle's medium (DMEM) (PAN Biotech), supplemented with 10% heat-inactivated fetal bovine serum (FBS) (PAN Biotech), 10 mM glutamine (PAN Biotech) and 1% Non-Essential Amino Acids (PAN Biotech) at 37 °C with 5% CO2. The MCF7 cell line was authenticated by Short Tandem Repeat (STR) analysis (Leibniz-Institut DSMZ). Cells were regularly tested for mycoplasma contamination using MycoAlert Mycoplasma detection kit (Lonza).

2.2 Seeding

The cells were grown in culture until ~90% confluence, after which they were detached and seeded in new tissue culture flasks. The growth media was discarded, cells were washed once with PBS and Trypsin-EDTA was added for detachment. After 5–10 min incubation at 37 °C, fresh growth media, containing 10% FBS, was added to the cells and the cell density and viability was measured using a cell counter. Finally, the cells were seeded with the desired concentration in new tissue culture flasks or plates for experiments.

$\sim 2 \times 10^4$ MCF7 cells were seeded per well in an 8-well Lab-Tek chamber (Nunc) for the dose-response experiments and sustained EGF (S-EGF) live cell experiments. For the pulsed EGF (5P-EGF) stimulation experiments and for the multi-pulse experiments $\sim 1 \times 10^5$ MCF7 cells/well were seeded in a 6-well dish. Additionally, for the 5P-EGF experiment glass cover slides were placed in the wells on which the cells were then seeded, for subsequent use with a flow-through chamber.

For the siRNA multi-pulse experiments, following the siRNA and cDNA transfection, the cells were transferred to the CellASIC ONIX microfluidic switching plate (M04S-03, Millipore) in complete growth media for at least 3 h prior to serum starvation. The cells were

incubated with Accutase for ~15 min for gentler detachment, after which they were spun down and concentrated to 5 million cells/mL, as per the instructions manual. Finally, the cells were loaded and perfused using the CellASIC ONIX Microfluidic Platform (Millipore).

2.3 Transfection

Transfection was performed 24 h after seeding with a total of 0.22 µg (for 8-well Lab-Teks) or 1 µg (6-well dishes) of cDNA using FUGENE6 (Roche Diagnostics) transfection reagent. For the dose response experiments, expression plasmids were used of EGFR-mTFP (or EGFR-mCitrine where applicable), PTB-mCherry, TagBFP and either an empty pcDNA3.1 vector for the control case, Rab11^{S25N}-mTFP for the recycling inhibition or PTPx-mCitrine, for PTPx ∈ PTPRG, PTPRJ, PTPRA, PTPN2. For the trafficking and multi-pulse experiments, expression plasmids were used of EGFR-mCitrine, PTB-mCherry and cCbl-BFP and Rab11^{S25N}-mTFP where applicable. In experiments requiring siRNA transfection, the cells were transfected 6 h before cDNA transfection with DharmaFECT1 (Dharmacon) according to the manufacturer's instructions. Following cDNA transfection, the cells were incubated overnight.

2.4 EGF stimulation

In-house fluorescently mono-labelled EGF-Alexa647 was used in the experiment to observe its association with EGFR. The His-CBD-Intein-(Cys)-hEGF-(Cys) plasmid [132] was kindly provided by Prof. Luc Brunsveld, University of Technology, Eindhoven. Human EGF was purified from E. coli BL21 (DE3) and N-terminally labelled with Alexa647-maleimide as described previously [132] and stored in PBS at $-20\,^{\circ}$C.

Following transfection on the previous day, the cells were serum starved with supplemented DMEM with 0.5% FCS for at least 6 h before EGF stimulation.

For the dose response experiment, incremental doses of EGF-Alexa647 were administered in the working 8-well, to attain doubling concentrations ranging from 2.5 ng/µL to 640 ng/µL (0.64–87.67 nM), chosen to sample multiple data points in the early sensitive ligand-bound EGFR fraction range. Starting from an initial volume of 100 µL for 0 ng/mL of EGF-Alexa647, volumes of 30 µL were administered per each dose at 1.5 min time interval to reach a final volume of 370 µL with 640 ng/mL of EGF-Alexa647 in the well. The time interval was chosen to allow steady state convergence of the ligand-binding and phosphorylation processes, while minimising the total duration of the experiment.

A temperature-controlled in-house-developed [133] flow-through chamber was used to administer a 5 min pulsed 200 ng/mL EGF-Alexa647 stimulus (5P-EGF) with the aid of

a neMESYS low-pressure syringe pump (Cetoni GmbH). Media were exchanged with a constant flow rate of 3 µL/s to avoid cell detachment, while a constant flow with a low rate of 1 µL/s was maintained for the rest of the experiment.

The author thanks Dr. Jan Hübinger for helping in setting up the EGF-pulse instrumentation.

For the multi-pulse experiments with siRNA, the cells were seeded and starved in a CellASIC ONIX microfluidic switching plate (M04S-03, Millipore). An EGF pulse-washout program consisting of a 5 min pulse of EGF-Alexa647 (20 ng/mL) followed by continual perfusion with serum-free media for 25 min was delivered using the CellASIC ONIX Microfluidic Platform (Millipore). This step was performed per pulse, four times in total.

2.5 H_2O_2 production inhibition

For a subset of the dose response experiments H_2O_2 production was inhibited using Diphenyleneiodonium (DPI), that blocks formation of the NOX complex at the PM. The cells were incubated with 10 µM of DPI for 30 min prior to stimulation and imaging.

2.6 Confocal microscopy

Confocal images were recorded using a Leica TCS SP8 confocal microscope (Leica Microsystems). The microscope was equipped with an environment-controlled chamber (Life Imaging Services) maintained at 37 °C, an HC PL APO 63x/1.4NA CS2 oil objective and an HC PL APO 63x/1.2NA motCORR CS2 water objective (Leica Microsystems). mCitrine, mCherry and Alexa647 were excited with a 470–670 nm range white light laser (white light laser Kit WLL2, NKT Photonics) at 514 nm, 561 nm and 633 nm, respectively. mTFP was excited by the 458 nm Argon laser line, while BFP was excited with a 405 nm diode laser. Detection of fluorescence emission was restricted with an Acousto-Optical Beam Splitter (AOBS): BFP (425–448 nm), mTFP (470–500 nm), mCitrine (525–551 nm), mCherry (580–620 nm) and Alexa647 (655–720 nm). Notch filters 458/514 and 488/561/633 were used to suppress laser reflection where applicable. When the oil objective was used, the pinhole was set to 3.14 airy units and 12-bit images of 512×512 pixels were acquired in frame sequential mode with 2×frame averaging. The water objective was used for live cell EGFR trafficking experiments and the pinhole was adjusted (ranging from 3.44 to 2.27 airy units) for each separate channel to maintain optical sectioning fixed to 2.5 µm.

2.7 Imaging dose response experiments

Confocal laser scanning microscopy of live MCF7 cells was done on a Leica SP8 confocal microscope as described previously (section 2.6). EGF-Alexa647 doses were administered at 1.5 min time interval directly after image acquisition of the cell incubated with the previous dose. For NOX inhibition, cells were incubated with 10 µM DPI for 30 min prior to stimulation. The fluorescence of expressed TagBFP was used to identify the cytoplasmic region of the cell using Otsu's thresholding method [134] (scikit-image, scikit-image.org). The plasma membrane region of a cell in each time point was calculated by subtracting the cytoplasmic region from the cellular image mask. PTB–mCherry translocation to (pY1086, pY1148) PM-bound EGFR-mTFP(mCitrine) for a given EGF-Alexa647 dose $d \in D$ was quantified as:

$$PTB\text{-}EGFR(d) = \frac{[PTB_{PM}]/[PTB]_T}{[EGFR_{PM}]/[EGFR]_T}(d)$$

where PTB_{PM} is the PTB-mCherry translocated to the plasma membrane, whereas PTB_T is the total PTB-mCherry in the cell. The fraction of phosphorylated receptor was then calculated by normalising this value between the initial (unstimulated) and maximal value of the series

$$[pEGFR](d) = \frac{PTB\text{-}EGFR(d) - PTB\text{-}EGFR(0)}{\max_{i \in D} PTB\text{-}EGFR(i) - PTB\text{-}EGFR(0)}$$

where pEGFR refers to the fraction of phosphorylated EGFR, and D is the set of increasing doses. Similarly, the amount of liganded receptor for dose d was calculated from the ratio of integrated EGF-Alexa647 and EGFR-mTFP(mCitrine) fluorescence at the plasma membrane:

$$[EGF\text{-}EGFR](d) = \frac{[EGF_{PM}]}{[EGFR_{PM}]}(d)$$

The fraction of liganded receptor (lEGFR) was calculated as:

$$[lEGFR](d) = \frac{EGF\text{-}EGFR(d) - EGF\text{-}EGFR(0)}{\max_{i \in D} EGF\text{-}EGFR(i) - EGF\text{-}EGFR(0)}$$

The experiments were performed in collaboration with Dr. Rabea Stockert and Yannick Brüggemann. The author thanks them for their contribution.

2.8 Imaging EGFR vesicular dynamics

Confocal laser scanning microscopy of live MCF7 cells was done on a Leica SP8 confocal microscope as described previously (section 2.6). Flow-through chamber and a syringe pump were used to administer a 5 min pulsed 200 ng/mL EGF-Alexa647 (5P-EGF) (see section 2.4). Images were acquired for ~120 min at a 1 min time interval. Three pre-stimulation images were obtained. STMs were calculated as described in section 2.10 to track the spatial distribution (from the PM to the NM) of the measured quantities in time. STM of the fraction of liganded EGFR-mCitrine was estimated by the [EGF-Alexa647]/[EGFR-mCitrine] ratio normalised to the 5 min time point value, whereas the unliganded EGFR-mCitrine fraction by 1-[EGF-Alexa647/EGFR-mCitrine]. The fraction of phosphorylated EGFR at the PM was estimated using the translocation of PTB-mCherry to the PM-localised EGFR-mCitrine. The following quantity was normalised: $(PTB_{PM}/(PTB_T - PTB_{endo}))/(EGFR_{PM}/EGFR_T)$, where PTB_{endo} was estimated from the cytoplasmic population by intensity-thresholding (1.5*STD percentile) and removed from the total PTB pool as it is already bound to the phosphorylated EGFR-mCitine in the endosomes. Subsequently, the STMs of phosphorylation were estimated by $(PTB_{PM}/PTB_T)/(EGFR_{PM}/EGFR_T)$ normalised to the previously estimated phosphorylated PM fraction of EGFR. The resulting STMs in the figures are averaged STMs from the multiple cells and experiment repetitions.

2.9 Multiple EGF pulse experiment

For the Rab11^{S35N} cDNA multi-pulse experiment, identical image acquisition and PM-EGFR phosphorylation estimation was performed as for the single-pulse experiments. For the siRNA experiments, the cells were transferred to CellASIC ONIX microfluidic switching plate (see section 2.2) and stimulated with 20 ng/mL EGF-Alexa647 multiple times (see section 2.4). Confocal imaging was performed concurrently at 1 min time interval. PM phosphorylated fraction of EGFR-mCitrine was estimated in the same manner as for the single-pulse vesicular dynamics experiment.

The experiments were performed in collaboration with Dr. Wayne Stallaert. The author thanks him for his contribution.

2.10 Spatial-temporal maps (STMs)

The images were background-corrected. Cells were masked from the EGFR images using FIJI (https://fiji.sc/), the nuclei were segmented from the cCBL-BFP images. For each pixel

within the cell, the distances to the closest PM and nuclear membrane (NM) pixel were calculated to derive a normalised distance $r = \frac{r_{PM}}{r_{PM}+r_{NM}}$. All pixels were split in 10 segments according to their normalised distances. For each of the observables (EGFR-mCitrine, PTB-mCherry, and EGF-Alexa647 fluorescence intensities) the mean value was calculated for every segment, yielding a radial spatial profile for the given time point for the imaged cell. To calculate the radial distributions of the derived quantities (PTB-mCherry/EGFR-mCitrine, EGF-Alexa647/ EGFR-mCitrine, etc.), the respective spatial profiles were divided between the different observable quantities. Combining the spatial profiles of the consecutive time points compiles into a spatial temporal map (STM) of the cellular dynamics. Average STM was calculated from the different cells within the experiment.

2.11 Simulation of periodic pulses

Suprathreshold EGF pulse train was simulated to estimate the responsiveness of $EGFR_p$ in each of the different operation regimes (see section 3.4.3). For that, ligand-binding dynamics and dimerisation were introduced in Eq. (3.1) to capture the EGF-induced conversion from unliganded monomers to liganded dimers. The system equations were extended by adding:

$$\frac{\mathrm{d}[EGFR_p]}{\mathrm{d}t} \mathrel{+}= -k_f 2[EGFR_p]^2[EGF] + k_r[EGF\text{-}EGFR_p]$$
$$\frac{\mathrm{d}[EGF\text{-}EGFR_p]}{\mathrm{d}t} \mathrel{+}= k_f([EGFR_p]^2 + [EGFR]^2)[EGF] - k_r[EGF\text{-}EGFR_p]$$

Different $EGFR_\mathrm{T}$ parameter values (see table 2.2) were then chosen within each of the different regions in Fig. 3.25d that correspond to the $\gamma PTP_T/EGFR_T$ values.

2.12 Parameter estimation

To describe the dynamics of the effective EGFR-PTP network at the PM (Figs. 3.25c and 3.25d), the double-negative feedback model (Eq. (3.1)) containing

$$\frac{\mathrm{d}[PTPRG_a]}{\mathrm{d}t} = k_1[PTPRG_i] - k_2[PTPRG_a] - k_3[PTPRG_a](2[EGF\text{-}EGFR_p] + [EGFR_p])$$

was extended with:

$$\frac{\mathrm{d}[PTPN2_a]}{\mathrm{d}t} = \varepsilon(k_4[EGFRp][PTPN2_i] - k_2[PTPN2_a])$$

The dephosphorylation of EGFRp by PTPN2 was described by an additional term in Eq. (3.1): $\gamma_1[EGFRp][PTPN2_a]$. The EGFR-PTPN2 negative feedback is on a time scale (ε) approximately two orders of magnitude slower than the phosphorylation-dephosphorylation reaction, as estimated from the ~4 min recycling time (Fig. 3.11). The bifurcation analysis of this network was performed using the bifurcation analysis software XPPAUT (www.math.pitt.edu/ bard/xpp/xpp.html) and interpolated in MATLAB to generate 3D diagrams shown in Figs. 3.25c and 3.25d.

Aggregated parameters for fitting were calculated for the three candidate models in Fig. 3.15 where redundancy was present, and are shown as a, b and c in Table. 2.1. These represent for the double-negative feedback motif:

$$a = \frac{k_1 \gamma PTP_T}{k_1 + k_2}, \quad b = \frac{k_3 EGFR_T}{k_1 + k_2}$$

for the negative feedback motif:

$$a = \frac{k_2 \gamma PTP_T}{k_1 + k_2}, \quad b = \frac{k_4 EGFR_T}{k_1 + k_2}, \quad c = \gamma PTP_T$$

and for the negative regulation motif:

$$a = \frac{k_2 \gamma PTP_T}{k_1 + k_2}$$

The optimal parameter set that matched the dose response data was estimated using an adaptive Metropolis-Hastings algorithm, a variant of the Monte Carlo Markov Chain (MCMC) method for sequential sampling from the posterior joint probability distribution of the parameters [135]. Four parallel executions from different initial conditions were run for faster convergence results and avoidance of local minima. New high-dimensional parameter set candidates were sampled using a multivariate Gaussian distribution with adaptable variance to yield the target acceptance ratio, i.e. with a proposal scaling [136]. Correction step for the rejection of the sampled negative parameter values was also employed.

2.13 Parameter values and statistics

The following parameter values were obtained or used from/in the analysis, with the accompanying statistical analysis - goodness of fit and model selection results (Akaike information criteria):

Table 2.1 Dose response model parameters and statistics

		Common parameters				Model specific parameters			Goodness of fit			Model selection		
		α_1	α_2	α_3	k_5	a	b	c	SSE	RMSE	R^2	AIC	Akaike weights	Δ_i
control control non-targeting siRNA	Aggregated feedback model Aggregated feedback model	0 0	0.005 0.001	1.244 4.819	1.613 7.68	0.2 0.068	11.058 7.29	0.06 0.291	1.712 1.526	0.10684 0.09447	0.935 0.936			
PTPRG	Double-negative feedback	0.016	0.1	0.069	0.993	6.188	191.193		7.012	0.18405	0.806	487.13	0.999979	0
	Negative feedback	0	0.053	2.208	3.826	0.44	1078.868	0.29	7.377	0.18878	0.796	514.02	0.000001	26.888337
	Negative regulation	0	1.268	22.735	54.41	3.488			7.36	0.18856	0.796	508.86	0.000019	21.729155
PTPRG/DPI	Double-negative feedback	0.166	0.017	1.836	1.424	431.007	2278.328		10.121	0.22782	0.702	399.08	0.601412	0
	Negative feedback	0	0	244.759	371.022	0.265	285.392	46.366	10.201	0.22872	0.699	404.17	0.047388	5.08181
	Negative regulation	0	0.002	27.333	44.028	5.311			10.201	0.22872	0.699	400.16	0.351199	1.075853
PTPN2	Double-negative feedback	0.013	0.018	0.082	0.195	5.383	365.76		7.693	0.17867	0.787	479.93	0.067386	5.146119
	Negative feedback	0	0.055	1.426	3.103	0.392	98.026	0.258	7.671	0.17841	0.788	480.55	0.049467	5.764353
	Negative regulation	0	1.876	14.82	40.915	3.252			7.642	0.17807	0.789	474.79	0.883147	0
PTPN2/DPI	Double-negative feedback	0.036	0.103	0.078	0.836	5.277	105.314		10.742	0.18645	0.764	550.57	0.042709	6.168282
	Negative feedback	0.002	0.033	3.043	7.207	0.611	21.114	0.804	10.725	0.1863	0.765	551.71	0.024166	7.307148
	Negative regulation	0.003	3.22	12.944	56.261	4.694			10.659	0.18573	0.766	544.4	0.933125	0
PTPN2 siRNA	Double-negative feedback	0.046	0.107	0.998	2.959	18.491	337.586		1.454	0.10784	0.911	303.75	0.108	3.985
	Negative feedback	0	0.14	5.561	6.324	0.034	3672.836	0.251	1.445	0.1075	0.912	303.89	0.1	4.129
	Negative regulation	0.001	0.242	9.908	9.385	0.437			1.444	0.10748	0.912	299.77	0.792	0
PTPRJ	Double-negative feedback	0.063	0.001	0.247	3.268	96.906	1172.98		1.444	0.1012	0.928	285.031449	0.335645	1.150235
	Negative feedback	0	0.107	0.626	92.449	0.25	22733.744	0.312	1.45	0.10142	0.927	288.230432	0.0678	4.349218
	Negative regulation	0	0.022	0.111	14.882	0.058			1.448	0.10135	0.927	283.881214	0.596555	0
PTPRJ/DPI	Double-negative feedback	0.055	0.105	0.124	2.791	17.551	276.429		0.897	0.10274	0.923	180.672722	0.156907	3.2619
	Negative feedback	0.002	0.39	1.232	20.879	0.053	68.64	0.474	0.901	0.10294	0.923	183.332868	0.041495	5.922046
	Negative regulation	0.001	0.743	1.803	67.186	0.809			0.891	0.10237	0.924	177.410822	0.801597	0
PTPRJ siRNA	Double-negative feedback	0.03	0.076	0.337	2.014	8.197	185.103		0.762	0.09527	0.94	221.31	0.79	0
	Negative feedback	0	0.007	7.218	16.648	0.688	13058.206	0.724	0.78	0.09634	0.938	228.2	0.025	6.883
	Negative regulation	0.001	0.069	38.845	93.304	3.898			0.78	0.09635	0.938	224.23	0.184	2.917

Table 2.2 Model parameters used in 3-d bifurcation analysis and simulations of multi-pulse data

		α_1	α_2	α_3	k_5	k_1	k_2	k_3	k_4	γ	γ_1	ε	$EGFR_T$	$PTPRG_T$, $PTPN2_T$	k_f	k_r
EGFR-PTP interaction network	Fig. 3.25c	0.001	0.3	0.7	1.613	0.5	0.5	11	0	1.9	0	0.001-0.01				
EGFR-PTP interaction network	Fig. 3.25d	0.001	0.3	0.7	1.613	0.5	0.5	11	1.1	1.9	0.1	0.001-0.01				
EGFR responses	Fig. 3.27 (a/b/c)	0.001	0.3	0.7	1.613	0.5	0.5	11	1.1	1.9	0.1	0.001-0.01	(1.5/1.19/1.05)	1	0.001	0.0056

2.14 Statistical analysis

Area under the curve (AUC) of the dose-response profile of each cell was used as an integrated measure of the response function. The distributions of AUC values between two datasets were compared using two-sample Student's t-test.

Results

To characterise the sensing capabilities of EGFR, and how they are regulated, we study its phosphorylation response to EGF. Self-interactions of EGFR are responsible for recognising the EGF signal and triggering the response, thus they constitute the activation component of its embedding regulatory network. The spatial-temporal vesicular dynamics of EGFR is also an important facet of the signal processing and shaping of the response at the plasma membrane. Balancing out the phosphorylation is carried out by the PTPs, whose causal coupling to EGFR can generate different network motifs with complex phosphorylation dynamics.

Using experimental microscopy approaches and dynamical systems modelling we study the underlying regulatory network of EGFR and how it regulates and shapes its phosphorylation response to EGF. This ultimately provides understanding of the function of the network in growth factor sensing.

3.1 Phosphorylation response of EGFR to EGF

The phosphorylation response of EGFR is shaped by the dynamics of the regulatory network in which EGFR is embedded (see Fig. 1.5). On one hand, the self-interactions of EGFR comprise the activation mechanism, as they trigger the phosphorylation upon recognising presence of EGF. The canonical mechanism of trans-phosphorylation within stable ligand-induced EGFR dimers [137–139], and phosphorylation of unliganded EGFR within transient complexes [76, 8], by ligand-bound dimers, other phosphorylated monomers (autocatalytic activation) or other non-phosphorylated monomers (autonomous activation), govern the transition of EGFR to the active state. These causal interactions are depicted with green dashed lines in Fig. 1.5. Apart from the phosphorylated/unphosphorylated EGFR state we also distinguish between EGF-bound and unbound state, the ratio of which depends on the extracellular EGF concentration. Therefore EGFR can be in total of four states. We assume that the EGF-bound state is in a dimeric form, and hence its intrinsic trans-phosphorylation

is a first-order reaction. Phosphorylation of unliganded EGFR, caused by other EGFR molecules, is a second-order reaction. There we distinguish between autocatalytic activation as phosphorylated unliganded EGFR activates more unliganded receptors (left-most green arrow), ligand-bound-receptor-induced phosphorylation (middle green arrow) and autonomous activation (right green arrow). On the other hand, dephosphorylation by the PTPs comprise the inhibition mechanisms, and they are shown with blue dashed arrows in Fig. 1.5.

3.1.1 EGFR exhibits steep non-linear phosphorylation response upon ligand binding

To study EGFR's phosphorylation response to increasing doses of EGF, fluorescently tagged EGFR-mTFP or EGFR-mCitrine was ectopically expressed in breast cancer-derived MCF7 cells that have very low endogenous EGFR expression (~10^3 molecules per cell [140]). This model cell line was chosen to minimise the artefacts arising from the unobserved endogenously produced EGFR. The ectopic expression of EGFR-mTFP was engineered to fall within the endogenous EGFR expression range of the related non-tumorigenic MCF10A cells. Consequently, similar EGFR phosphorylation- and Akt activity responses to EGF were observed between both cell lines [123].

Confocal microscopy image series were obtained from single MCF7 cells exposed to increasing (doubling) doses of fluorescently tagged EGF-Alexa647 (Fig. 3.1). In this manner, dose-response analysis was employed to estimate the EGFR phosphorylation response to the ligand stimulation in single cells. We directly related the measured fraction of liganded receptors to EGFR phosphorylation to deconvolve the EGF binding kinetics from EGFR's response, which is not possible by analytical biochemical approaches on cell extracts.

Steady states of both ligand-binding and phosphorylation dynamics were reached within 1.5 minutes, with phosphorylation closely following the ligand-binding equilibration kinetics (see Fig. 3.2), implying that phosphorylation is not kinetic bottleneck in the system. Therefore, following the experimental design of obtaining fluorescent microscopy images every 1.5 minutes after new EGF-Alexa647 dose addition, the subsequent analysis was performed with the assumption that the system operates in a steady state regime.

As a readout for EGFR phosphorylation we used the fluorescently tagged phosphotyrosine-binding domain of Shc (PTB-mCherry), that is recruited to phosphorylated tyrosines 1086/1148 of EGFR [141]. Its rapid translocation to the phosphorylated EGFR-mTFP at the plasma membrane (see Fig. 3.1) determined the fraction of phosphorylated receptor (PTB translocation normalised to the total EGFR, Methods). The fraction of liganded EGFR-mTFP at the PM was determined by EGF-Alexa647/EGFR-mTFP, normalised to the saturating

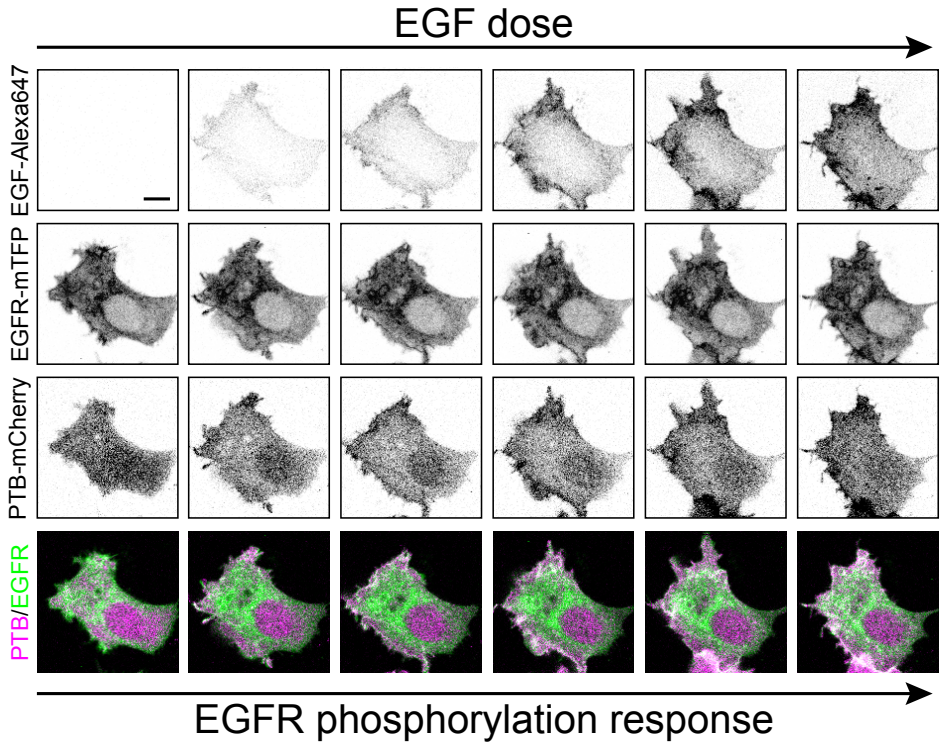

Figure 3.1 Setup of dose response experiments. Representative fluorescence image series of EGF-Alexa647, EGFR-mTFP, PTB–mCherry and PTB-mCherry(magenta)/EGFR-mTFP(green) overlay from the single-cell dose-response experiment. Cells were stimulated every ~1.5 min with increasing EGF-Alexa647 doses (2.5–600 ng/mL). Scale bar: 10 µm.

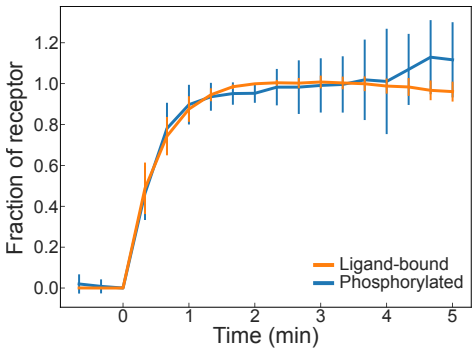

Figure 3.2 Ligand-binding and phosphorylation kinetics. Quantification of PTB-mCherry translocation kinetics to plasma membrane localised EGFR-mTFP (Average ± STD). MCF7 cells were stimulated with a saturating EGF-Alexa647 dose (320 ng/mL) and successive images were acquired every 20 s (n=10 cells). Translocated plasma membrane fraction of PTB-mCherry ($\frac{[PTB-mCherry_{PM}]/[PTB-mCherry]_T}{[EGFR-mTFP_{PM}]/[EGFR-mTFP]_T}$) converged to a steady state level in ~1.5 min, which was within the time frame of successive EGF-Alexa647 dose administration (Fig. 3.1).

EGF-Alexa647/EGFR-mTFP ratio. As changes of EGF in the environment are converted to changes in receptor occupancy with EGF in the cell, and the ligand-bound EGFR directly regulates the phosphorylation dynamics (see Fig. 1.5), we use it as an input into our system.

The ligand binding dynamics represents the relationship between the applied EGF-Alexa647 dose and the estimated fraction of ligand-bound EGFR-mTFP. To estimate this relationship, the following ligand-binding kinetics model was used (Fig. 3.3a):

$$[EGFR] + [EGF] \underset{k_r}{\overset{k_f}{\rightleftharpoons}} [EGF\text{-}EGFR]$$

with $K_D = k_r/k_f$ being the dissociation constant.

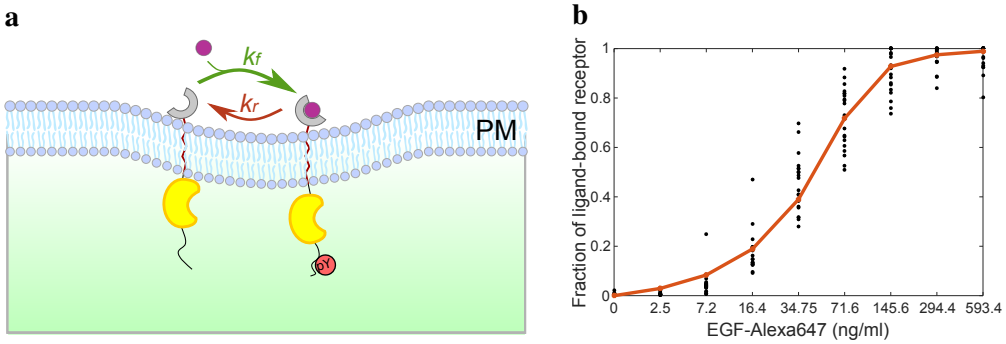

Figure 3.3 EGF-EGFR binding dynamics. a) Scheme of the binding dynamics at the plasma membrane. The unliganded receptors bind EGF (violet) with a forward rate constant k_f, while the the ligand-receptor complex dissociates with reverse rate constant k_r. b) Estimating fraction of EGFR-mTFP bound to EGF-Alexa647 in live cells: EGF-Alexa647/EGFR-mTFP quantified in single cells (data points) upon increasing EGF-Alexa647 doses was fitted (line) with the receptor binding kinetics model.

Assuming that at low EGF doses, the ligand can be depleted from the solution due to binding to EGFR [142], the fraction of ligand bound receptor in steady state gives the following closed-form solution:

$$\frac{[EGF\text{-}EGFR]}{[EGFR]_T} = \frac{\frac{n}{N_A}[EGFR]_T + [EGF]_T + K_D - \sqrt{(\frac{n}{N_A}[EGFR]_T + [EGF]_T + K_D)^2 - 4\frac{n}{N_A}[EGFR]_T[EGF]_T}}{2\frac{n}{N_A}[EGFR]_T}$$

where $[EGFR]_T = [EGFR] + [EGF\text{-}EGFR]$ is the total EGFR concentration on the plasma membrane and $[EGF]_T = [EGF] + \frac{n}{N_A}[EGF\text{-}EGFR]$ is the total input EGF dose, n is the number of cells, and N_A is Avogadro's number needed for converting the number of ligand-bound receptors into moles. This function was used to fit the experimental data (Fig. 3.3b) thereby mapping the input dose to a fraction of ligand-bound receptor. K_D was

obtained to be 762pM (427, 1097) with 95% confidence bounds, which is in line with values curated from the literature [143].

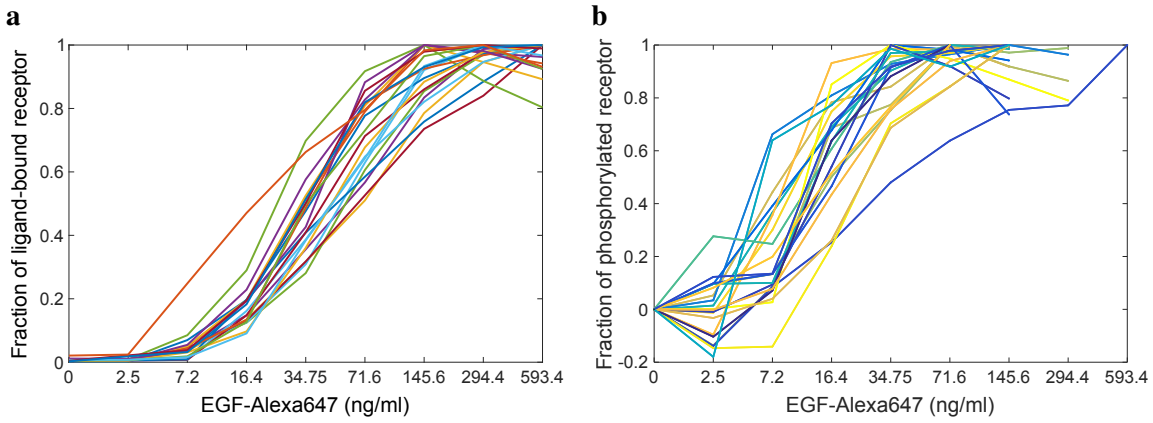

Figure 3.4 Dependence on ligand-binding and phosphorylation steady-state levels on EGF concentration. Single cell profiles of a) the fraction of ligand-bound EGFR-mTFP, quantified by [EGF-Alexa647$_{\mathrm{PM}}$]/[EGFR-mTFP$_{\mathrm{PM}}$], and b) the fraction of phosphorylated EGFR-mTFP, quantified by PTB-mCherry translocation to the plasma membrane ($\frac{[PTB-mCherry_{PM}]/[PTB-mCherry]_T}{[EGFR-mTFP_{PM}]/[EGFR-mTFP]_T}$), for increasing EGF-Alexa647 doses (n=21 cells, N=10).

Ligand-binding saturation levels were reached at 200–300 ng/mL of EGF-Alexa647, i.e. most of the receptors were bound to ligand (Fig. 3.4a). On the other hand, the phosphorylation response of EGFR reached saturation levels at around 50–70 ng/mL of EGF-Alexa647, with the activation threshold being at around 20 ng/mL of the ligand concentration (Fig. 3.4b). Combining of these results translates into a steep EGFR-mTFP phosphorylation response to the increasing ligand-bound fractions, as observed in most single cells (3.5a, with mean±std shown in 3.5b). While the ligand-bound EGFR contributes with a corresponding linear increase in the phosphorylation response (assuming high phosphorylation rate in-trans within the dimer), the observed steep non-linear dependency indicates that the amplified response is due to the increase of phosphorylation of the unliganded monomers. By subtracting the linear contribution of the liganded receptor (dash-dotted semi-transparent diagonal line) from the phosphorylation response profile we could estimate the contribution of the monomers, shown with the other dash-dotted profile in Fig. 3.5b. At the pick at around 25% ligand-bound receptors there are almost twice as many phosphorylated unliganded receptors than liganded ones. This indicates that the small ligand-bound EGFR fraction triggers the phosphorylation amplification via activity of the unliganded EGFR monomers. The amplification provides a stronger response to presence of EGF, and thus a more robust sensing. However, this immediate increase of sensitivity through the activation of the monomers may deplete the plasma membrane of receptors more rapidly and thus inhibit its prospective sensitivity as

a trade-off. Therefore, we set out to determine how the spatial-temporal organisation of EGFR modulates its plasma membrane abundance and thus affects the growth factor sensing system.

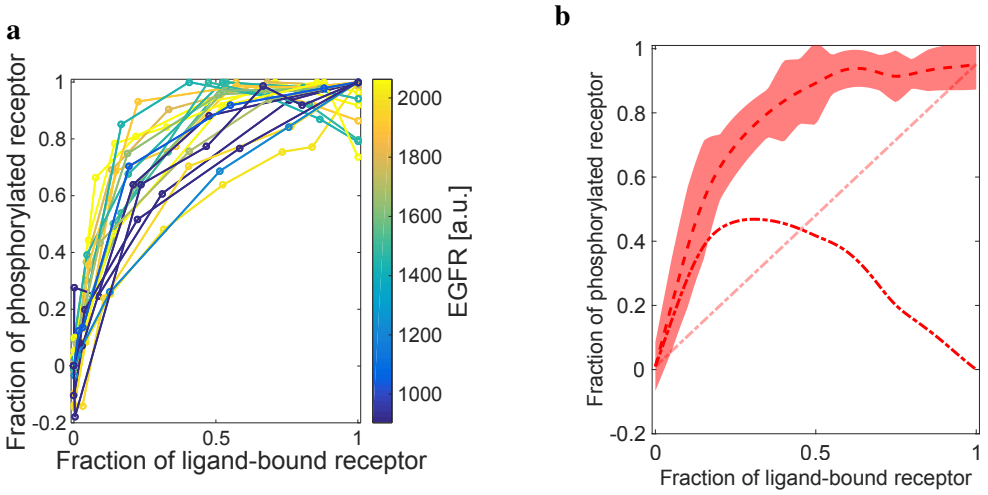

Figure 3.5 EGFR-mTFP phosphorylation response. a) Single cell EGFR-mTFP phosphorylation responses versus fraction of ligand bound receptors, derived from Fig. 3.4 (n=21 cells, N=10). The estimated fractions of phosphorylated vs liganded EGFR-mTFP are plotted and colour-coded by the average EGFR-mTFP fluorescence intensity per cell. Moving average ± STD are shown with dashed line and bounded regions in b). Dash-dotted lines depict the estimated contribution of unliganded (profile in front) and liganded (transparent linear profile) EGFR to the fraction of phosphorylated receptor.

3.2 Spatial-temporal vesicular trafficking dynamics of EGFR

Motivated by the distinct role of unliganded EGFR in shaping the response to EGF, we proceeded to study the vesicular trafficking organisation of EGFR and its influence on the phosphorylation of EGFR at the plasma membrane. Like many RTKs, EGFR undergoes internalisation into vesicles upon activation that fuse into larger endocytic compartments such as the early, late and recycling endosome, to be eventually distinctly redistributed. The receptor redistribution fate primarily depends on its molecular state and the system's capability of processing it. While the dimeric ligand-bound EGFR receptor has been shown to be ubiquitinated and undergoes a unidirectional trafficking towards the lysosome where it awaits degradation, the monomeric unliganded receptor exhibits constitutive recycling through the recycling endosome [8].

To distinguish between the trafficking routes of these two species, microscopy imaging experiments were performed on live MCF7 cells where the spatial distribution of an

ectopically-expressed, fluorescently-tagged EGFR-mCitrine was traced in time inside single cells exposed to EGF-Alexa647 stimulus. Phosphorylation dynamics were also traced, using the translocation of PTB-mCherry to EGFR-mCitrine, similar as in section 3.1.1. The spatial EGFR signal in Cartesian coordinates (x, y) was reduced to one-dimensional vector depicting the average EGFR signal at a relative position between the cellular and nuclear membrane in the cell in a given time point *t* (Fig. 3.6, columns 1-3). The radial symmetry in vesicular trafficking was exploited in this manner, as we are interested in the coarse spatial EGFR distribution between the plasma membrane and perinuclear areas. Tracing this spatial distribution in time then generates a 3-D spatial-temporal map (STM) consisting of space (r), time (t) and molecular quantity of interest (Fig. 3.6, fourth column), which can be any fluorescently measured quantity Q (EGFR-mCitrine, PTB-mCherry or EGF-Alexa647) as well as any other derived quantity that can characterise the receptor trafficking/phosphorylation dynamics.

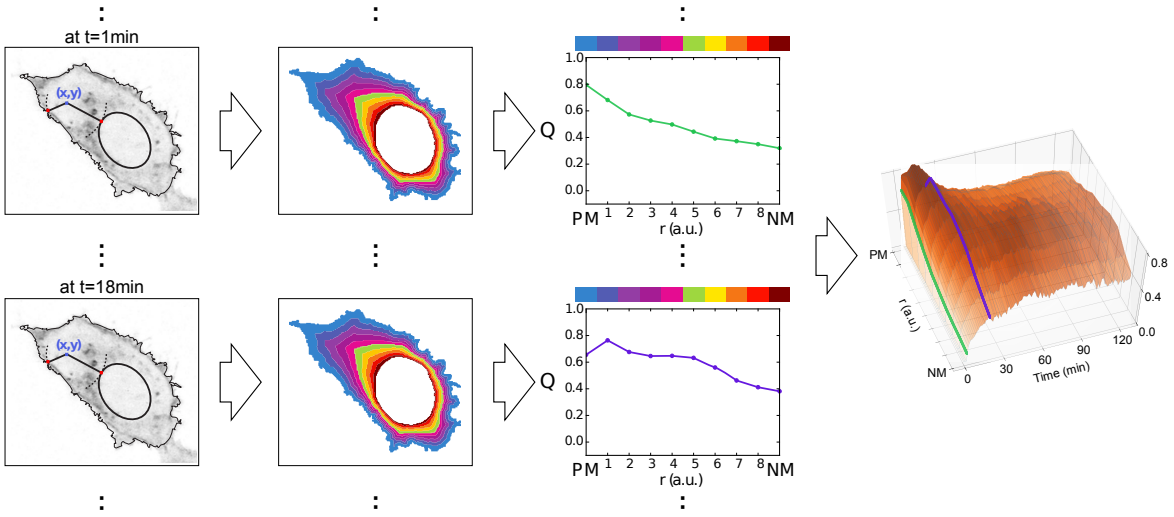

Figure 3.6 Spatial-temporal maps (STMs) of molecular quantity. Dimensionality reduction was performed from Cartesian (x, y) to normalised radial (r) distribution of molecular quantity (Q) between the plasma (PM) and the nuclear (NM) membrane in the cell at a given time point t (columns 1-3). Spatial distributions from multiple time points were joined to compile the STM of Q (column four).

3.2.1 Unliganded and liganded receptors have distinct trafficking fates

Stimulating the cells with EGF with different temporal durations generates distinct receptor occupancy and phosphorylation profiles, that will result in different distributions of EGFR in space. By comparing these profiles in space and time we can distinguish between the trafficking routes of our two species of interest - liganded ([EGF-Alexa647]/[EGFR-mCitrine]) vs unliganded (1 - [EGF-Alexa647]/[EGFR-mCitrine]) EGFR. To this end we performed two

types of experiments - stimulating the cells with sustained EGF-Alexa647 stimulus (S-EGF, 200 ng/mL, 2h) and with 5 min pulsed EGF-Alexa647 stimulus (5P-EGF, 200 ng/mL, 2h). In the former, the medium provides a continuous source of growth factor that maintains a constant fraction of ligand-bound receptor, whereas in the latter there is ligand-binding only during the presence of the pulse.

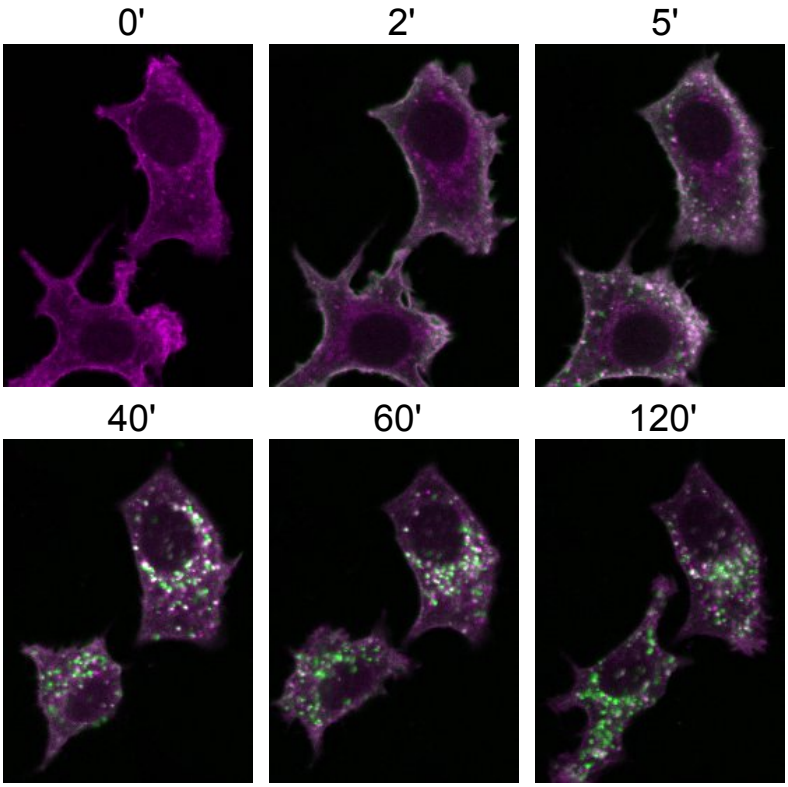

Figure 3.7 Spatial-temporal distribution of EGF/EGFR upon S-EGF stimulation. Representative fluorescence image series of EGF-Alexa647(green)/EGFR-mCitrine(magenta) overlay from single-cell trafficking experiment. Images were taken at 1 minute time interval for ~120 min, under sustained 200 ng/mL EGF-Alexa647 treatment.

We are interested in how the system is executing, and how the receptor state is influencing its spatial redistribution. In our experiments, upon S-EGF a significant fraction of the liganded EGFR was accumulated in the perinuclear area in the course of 2h, following the phosphorylation at the PM and internalisation (see Fig. 3.7). This accumulation can be observed from the average spatial-temporal map of the derived EGF-Alexa647/EGFR-mCitrine quantity (Figs. 3.8a to 3.8c). On the other hand, relatively smaller fraction of unliganded EGFR (1- EGF-Alexa647/EGFR-mCitrine) was recycling to the PM where it was exposed to constant presence of EGF in the surrounding medium, and was thus continuously depleted by re-internalisation from there (Fig. 3.8d). EGFR phosphorylation showed a

distinct spatial-temporal profile. EGFR phosphorylation profile on the PM was sustained over time, whereas it effectively decreased in the perinuclear area over the period of 2 h (relative to the respective ligand-bound profiles, Fig. 3.8e relative to Fig. 3.8c). This indicates that higher EGFR dephosphorylation activities take place in the cytoplasm. Hence, the spatial balance of EGFR was tipped towards the unidirectional trafficking route manifested by the accumulation in the perinuclear areas.

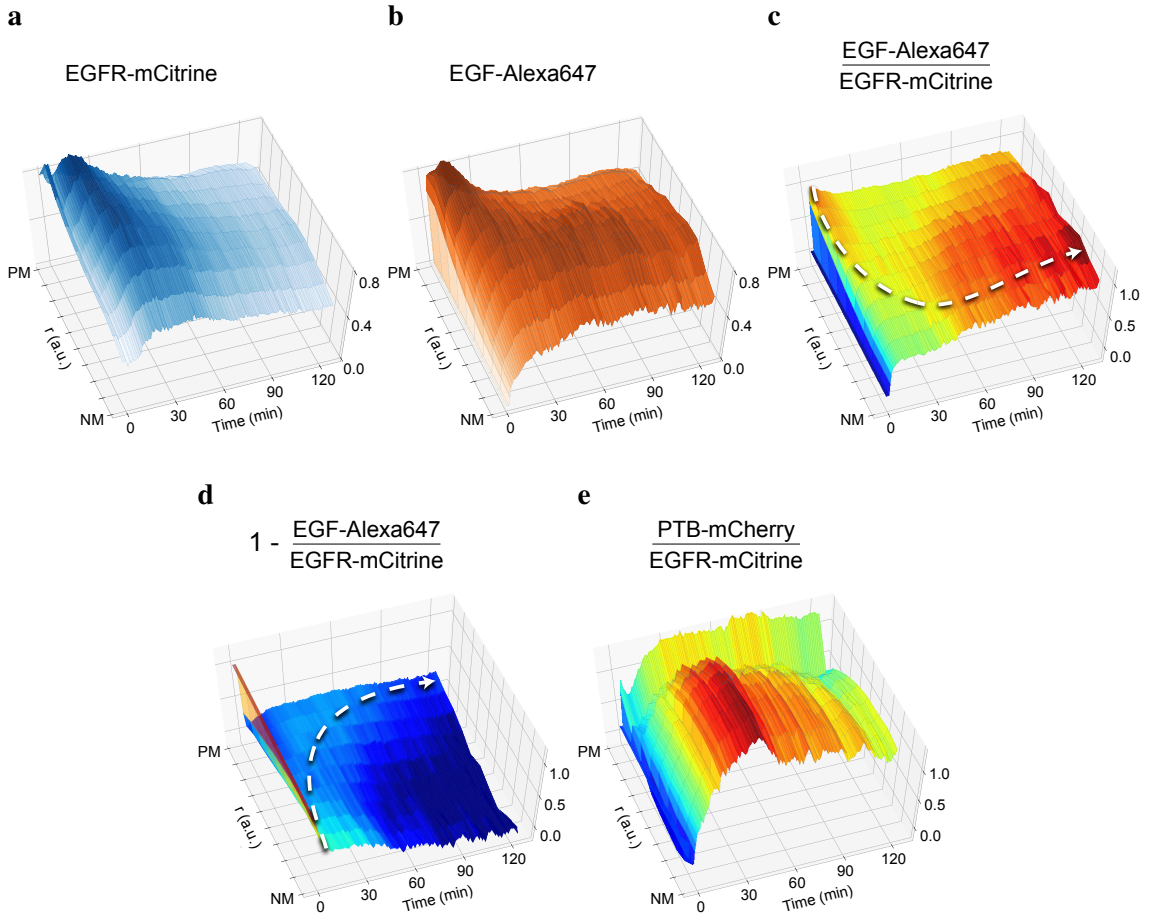

Figure 3.8 Quantification of spatial-temporal phosphorylation and trafficking dynamics of EGFR upon S-EGF. Average spatial-temporal maps (STMs) of corresponding molecular quantities obtained from live cells stimulated with 200 ng/mL S-EGF (n=16 cells, N=3). Depicted are the STMs of a) EGFR-mCitrine fluorescence, b) EGF-Alexa647 fluorescence, and estimated fractions of c) ligand-bound EGFR ([EGF-Alexa647]/[EGFR-mCitrine]), d) unliganded EGFR (1-[EGF-Alexa647]/[EGFR-mCitrine]) and e) phosphorylated EGFR, calculated by PTB-mCherry translocation ([PTB-mCherry]/[EGFR-mCitrine]). White dashed arrow denotes the change in spatial distribution over time.

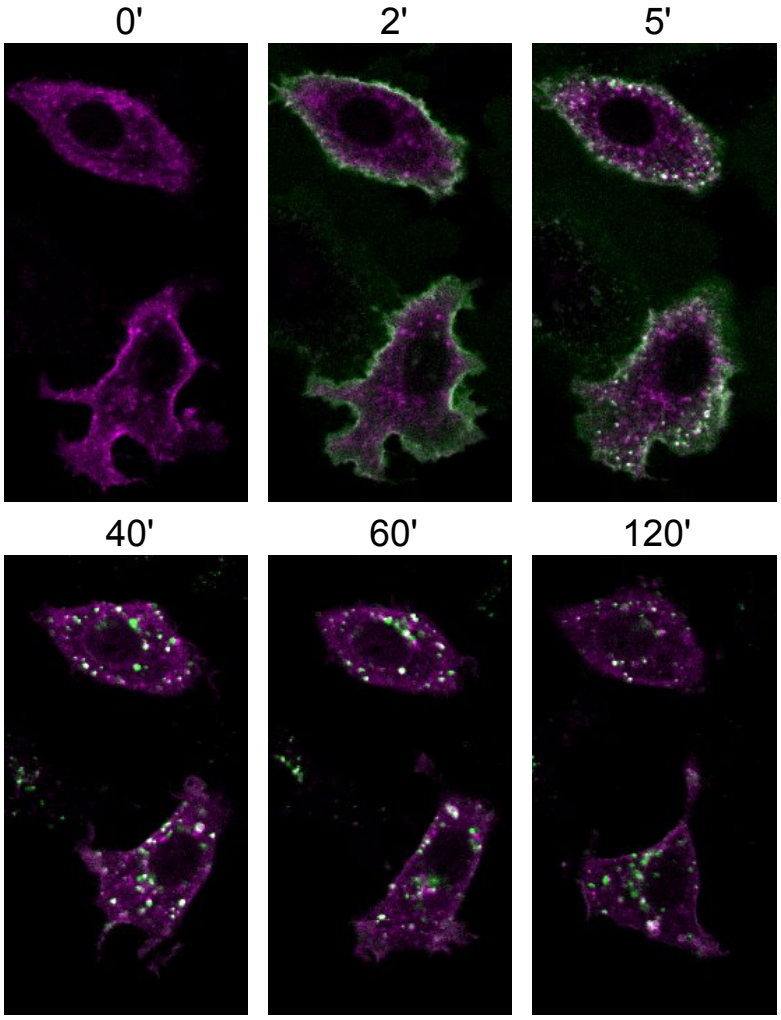

Figure 3.9 Spatial-temporal distribution of EGF/EGFR upon 5P-EGF stimulation. Representative fluorescence image series of EGF-Alexa647(green)/EGFR-mCitrine(magenta) overlay from single-cell trafficking experiment. Images were taken at 1 minute time interval for ~120 min, under 5 min pulsed 200 ng/mL EGF-Alexa647 treatment.

To investigate the spatial-temporal dynamics of EGFR trafficking and phosphorylation when cells see only a transient EGF stimulus, we stimulated the cells with 5 min pulse of EGF (5P-EGF) and followed the dynamics for 2h. This generated a different ligand-bound receptor levels at the PM following the pulse removal. The liganded receptors again undertook the unidirectional route from the PM towards the late endosome where they were degraded (Fig. 3.9), however in significantly reduced fraction than in the S-EGF case (Figs. 3.10a to 3.10c). The unliganded receptors in this case repopulated the PM shortly after the pulse with EGFR molecules susceptible to novel stimulus (Fig. 3.10d). Transient phosphorylation profiles were present at the PM and at the perinuclear area, albeit different than the ligand-

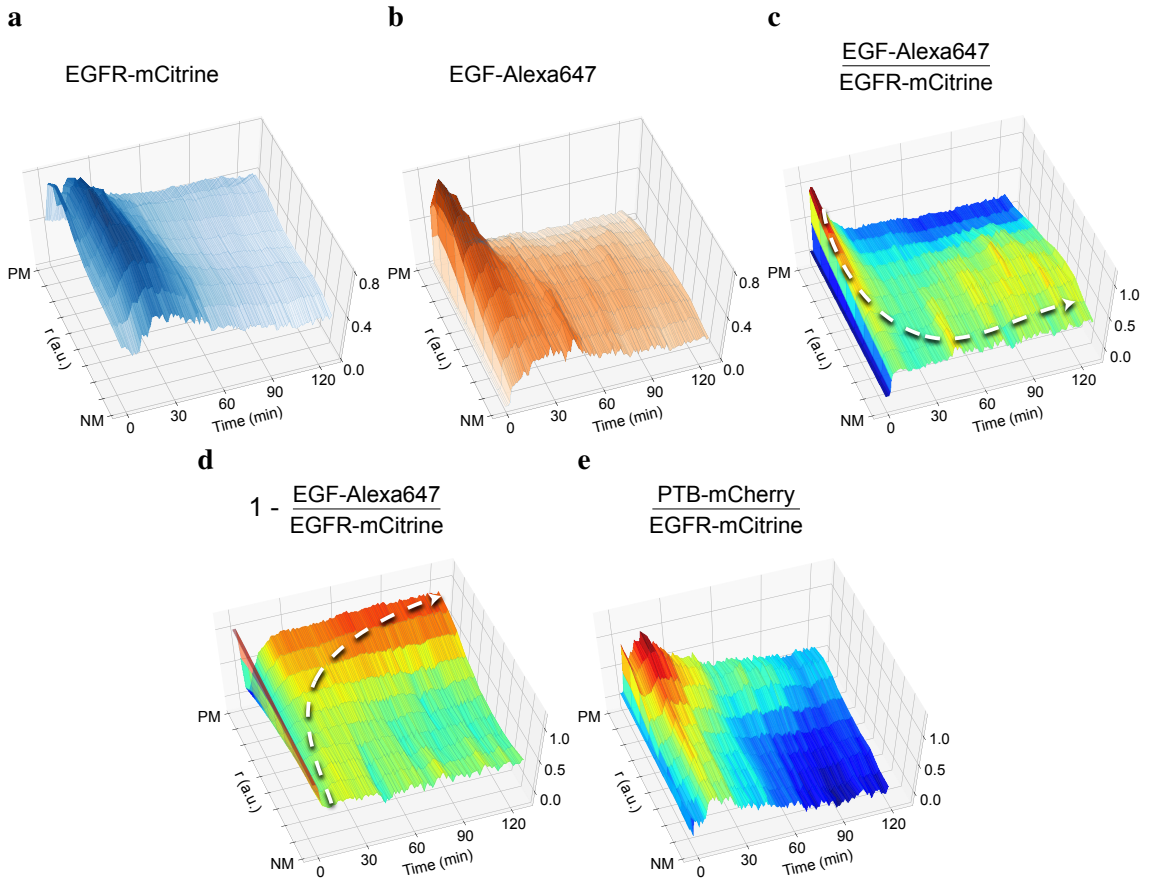

Figure 3.10 Quantification of spatial-temporal phosphorylation and trafficking dynamics of EGFR upon 5P-EGF. Average spatial-temporal maps (STMs) of corresponding molecular quantities obtained from live cells stimulated with 200 ng/mL 5P-EGF (n=14 cells, N=2), analogous to Fig. 3.8. Depicted are the STMs of a) EGFR-mCitrine fluorescence, b) EGF-Alexa647 fluorescence, and estimated fractions of c) ligand-bound EGFR, d) unliganded EGFR and e) phosphorylated EGFR.

bound ST profile (Fig. 3.10e). Decreasing phosphorylation towards the perinuclear area was observed in this case as well. The spatial cycle thus tipped the balance in favour of the recycling route in this case.

Continuous recycling of unliganded EGFR monomers repopulates the plasma membrane with unphosphorylated receptors. While when there is a sustained presence of EGF these receptors are reinternalised and depleted from the PM, after a transient EGF pulse they are recycled and can be reutilised at the PM, and thus they most likely serve as sensing entities for upcoming EGF stimuli.

Trafficking dynamics of unliganded EGFR maintains its plasma membrane levels

To determine the recycling dynamics of unliganded EGFR upon 5P-EGF stimulus, we constructed a dual-compartment model where EGFR internalisation from the PM to the endosomes occurs with rate constant k_{in} and EGFR recycles back to the PM with rate constant k_{rec} (Fig. 3.11a). During the initial 5 min stimulus, the PM fraction of unliganded EGFR ($EGFR_{PM}$) relative to the total unliganded concentration ($EGFR_T$) is reduced due to ligand binding.

After removal of EGF, replenishing of the unliganded EGFR at the PM takes place in the time span of ~5–35 min according to the following dynamics:

$$\frac{\mathrm{d}[EGFR_{PM}]}{\mathrm{d}t} = k_{rec}([EGFR]_T - [EGFR_{PM}]) - k_{in}[EGFR_{PM}]$$

yielding a closed-form solution

$$\frac{[EGFR_{PM}]}{[EGFR_T]}(t) = \frac{k_{rec}}{k_{rec}+k_{in}} - \left(\frac{k_{rec}}{k_{rec}+k_{in}} - \frac{[EGFR_{PM}]}{[EGFR]_T}(t_0)\right)\mathrm{e}^{-(k_{rec}+k_{in})(t-t_0)}$$

Here, $\frac{[EGFR_{PM}]}{[EGFR_T]}(t)$ represents the fraction of EGFR at the PM at a particular time t, and $\frac{[EGFR_{PM}]}{[EGFR_T]}(t_0)$ - the PM fraction at an initial time point $t_0 \approx 5min$. This model was used to infer the trafficking rates from the live cell data (Figs. 3.11b and 3.11c), where the first three (out of ten) spatial bins denoted the PM. Given that in steady state we have $\frac{[EGFR_{PM}]}{[EGFR]_T}^* = \frac{k_{rec}}{k_{rec}+k_{in}}$, it holds that

$$k_{in} = k_{rec}\frac{1 - \frac{[EGFR_{PM}]}{[EGFR]_T}^*}{\frac{[EGFR_{PM}]}{[EGFR]_T}^*}$$

Thus, the steady state PM fraction of unliganded EGFR, estimated from the k_{in} vs k_{rec} correlation scatter plot (Fig. 3.11d), was 0.43 with 95% confidence bounds (0.37, 0.49). The estimated average quantities (with 95% confidence bounds) were: $k_{in} = 0.31min^{-1}(0.12, 0.50)$, $k_{rec} = 0.23min^{-1}(0.08, 0.38)$, and the recycling half-life $t_{1/2} = \frac{ln2}{k_{rec}+k_{in}} = 4.32min(1.02, 7.62)$.

The high correlation between the cells in Fig. 3.11d indicates that most of them reach similar steady-state levels of unliganded EGFR fraction at the PM (Fig. 3.11b). This result suggests that the regulation on this level of spatial distribution of the unliganded receptor is ubiquitous and important cellular mechanism. Maintaining a certain fraction of receptors on the plasma membrane can impact the phosphorylation response and thus help the cell in sustaining sensitivity to EGF stimuli. To understand the implications of this organisation on the temporal EGFR phosphorylation response we examined the temporal phosphorylation dynamics at the PM in more detail.

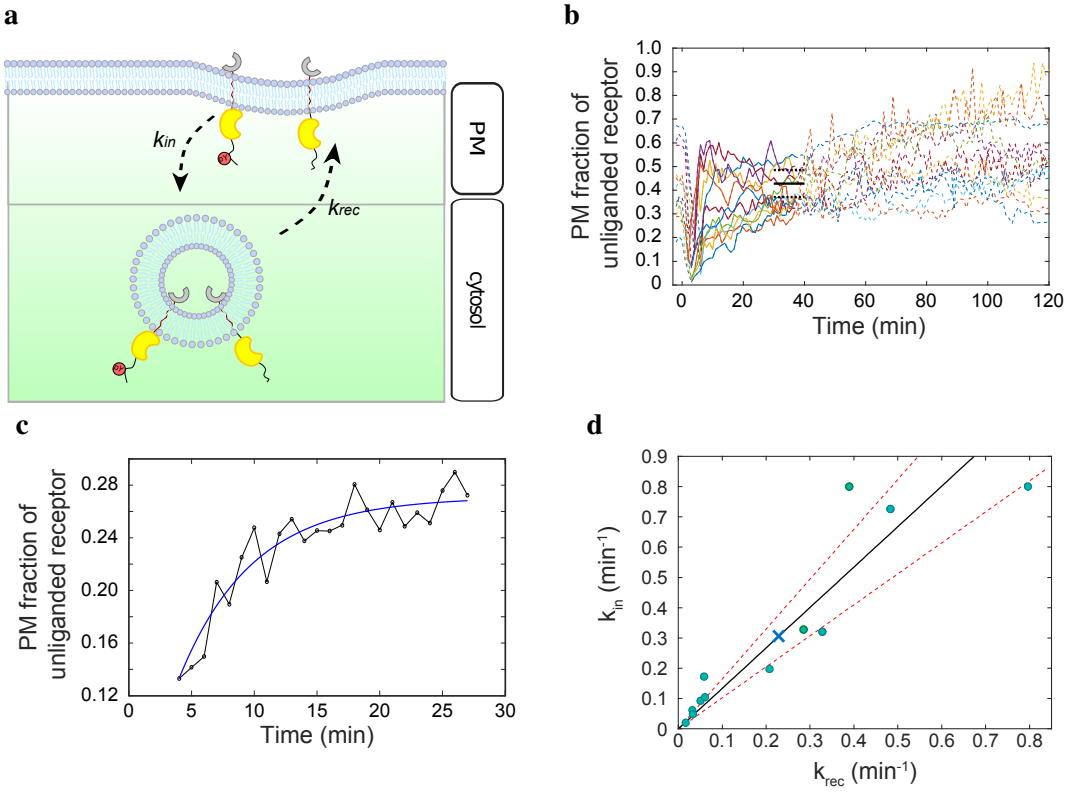

Figure 3.11 Quantification of recycling dynamics of unliganded EGFR-mCitrine upon 5P-EGF. a) Model scheme of EGFR recycling dynamics. Unliganded EGFR gets internalised with rate k_{in}, while endocytic EGFR gets recycled back to the plasma membrane with rate k_{rec}. b) Plasma membrane fraction of unliganded EGFR-mCitrine in single cells. Model-based estimation of the steady state level (95% confidence bounds) is shown with black line (inside dashed lines) (n=14 cells, N=2). c) Compartment-model-based fitting on 4–35 min time interval for the cells shown in b). d) Linear dependency in (k_{in}, k_{rec}) between single cells reflects that similar steady state plasma membrane fractions of unliganded EGFR are maintained in different cells by recycling. x: average (k_{in}, k_{rec}). Black line with red dashed lines depict linear fit with 95% confidence interval half-widths. Estimated rates: k_{in}=0.31 min^{-1} (0.12, 0.50), k_{rec}=0.23 min^{-1} (0.08, 0.38), with 95% confidence bounds.

3.2.2 Vesicular recycling of unliganded EGFR promotes prolonged activation at the plasma membrane

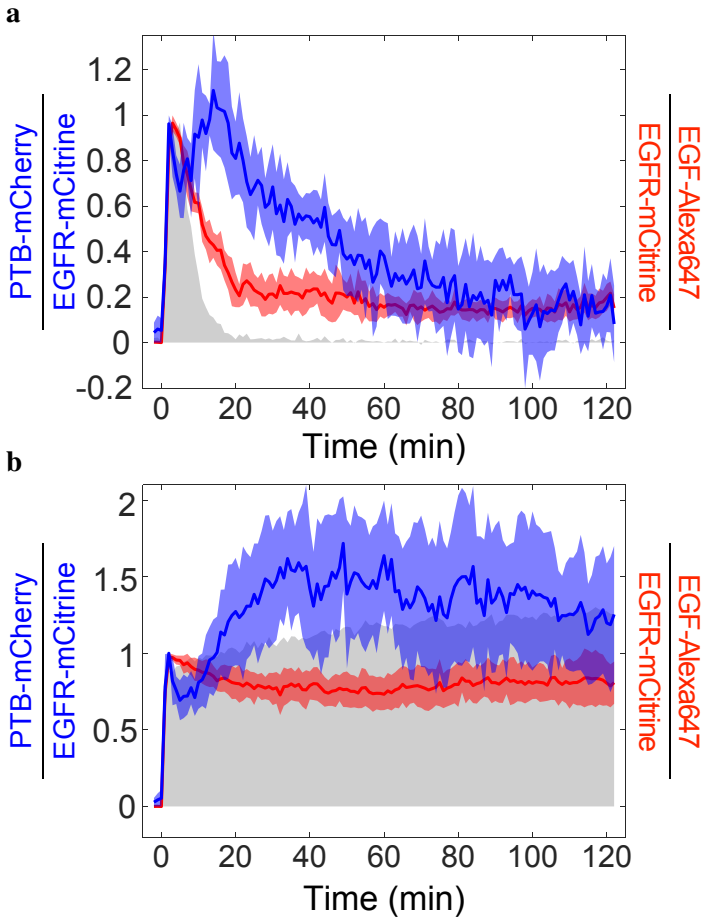

Figure 3.12 Temporal profiles of EGFR phosphorylation at the plasma membrane. The plasma membrane fractions of ligand-bound ([EGF-Alexa647]/[EGFR-mCitrine], red) and phosphorylated EGFR ([PTB-mCherry]/[EGFR-mCitrine], blue) derived from the respective STMs in Figs. 3.8e and 3.10e (median ± MAD). Extracellular EGF-Alexa647 fluorescence levels are shown in grey. The cells were stimulated with a) 5P-EGF (n=14 cells, N=2) and b) S-EGF (n=16 cells, N=3).

The PM EGFR phosphorylation profiles displayed characteristic temporal dynamics in both cases (Fig. 3.12). Upon 5P-EGF treatment the ligand-bound fraction (Fig. 3.12a, red profile) followed the EGF pulse dynamics (grey profile). However, the phosphorylation fraction (blue), following the minor dip after the initial EGFR internalisation (at around 5m), showed prolonged and elevated response that reached maximal level at 15–20 min and only after slowly decayed to the basal level (Fig. 3.12a). The time frame of this processes is in

line with the recycling kinetics (Fig. 3.11), suggesting that the recycled unliganded EGFR monomers induced the increase in EGFR phosphorylation, as they can be autocatalytically activated.

Upon S-EGF treatment the ligand-bound fraction (Fig. 3.12b, red) followed the continuous growth factor presence (grey) and showed sustained level at the plasma membrane. The phosphorylated fraction, similarly to the 5P-EGF case, showed the initial internalisation-induced dip at 5 min. Following the dip and the recovery period the cells sustained an elevated phosphorylation level at the PM (Fig. 3.12b, blue profile).

This highlights the importance of the spatial regulation in the system: elevating the PM abundance of EGFR via recycling brings more non-phosphorylated receptors that can be reutilised. They can trigger the autocatalytic mechanism, prolonging the plasma membrane EGFR signalling as a result (5P-EGF), or engage in ligand binding if there is a presence of growth factor (S-EGF). Such an organisation is thus crucial for increased sensing- and robust responding capabilities to upcoming growth factor stimuli.

Inhibition of recycling flattens the EGFR phosphorylation response

To verify that the vesicular recycling is one of the major determinants of EGFR phosphorylation dynamics, we probed the EGFR phosphorylation response experimentally (as in section 3.1.1) while inhibiting the recycling to the PM from the recycling endosome (RE). Major regulator of the exit from the RE is the small GTPase Rab11 [144]. It acts as a molecular switch that guides the exocytic transport of proteins to the cell surface via tubulation of the RE [145]. Its depletion has been shown to cause protein accumulation in the RE [145]. Ectopic expression of $Rab11^{S25N}$, a dominant negative form of Rab11 [146], was used to inhibit the function of the endogenously expressed Rab11, thereby shifting the EGFR spatial balance towards the perinuclear areas.

The results show flatter EGFR phosphorylation response, relative to the control case (Fig. 3.13, green vs red). While the ligand-bound fraction of receptors could still traffic unidirectionally through the 'degradation route', the inhibited recycling of the monomers disturbed the trafficking balance, resulting with reduced PM abundance of unliganded EGFR. This reduced amount of monomers then translated into weakened phosphorylation amplification. This underlined the importance of vesicular recycling in supporting the autocatalytic activation of EGFR by maintaining a fraction of unliganded monomers at the plasma membrane.

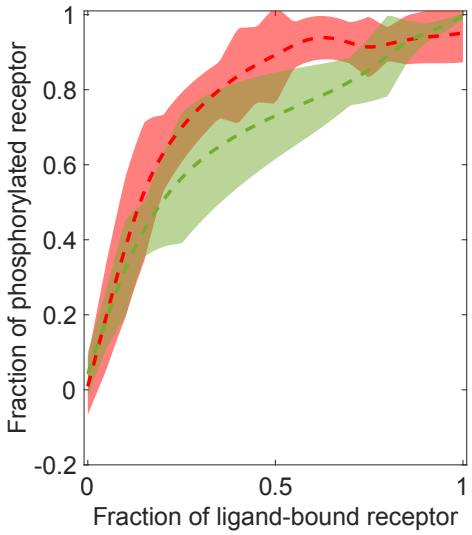

Figure 3.13 EGFR-mTFP phosphorylation response upon recycling inhibition. Dose-response of EGFR-mTFP phosphorylation (red, control) is significantly altered upon ectopic Rab11^{S25N} expression (green, p=0.02, n=12 cells, N=4). Moving average (dashed lines) ± STD (bounded regions) represents the single cell data.

3.2.3 Spatial organisation of EGFR established by distinct vesicular trafficking promotes the signal processing

These experiments show that unliganded and liganded EGFR exhibit distinct vesicular and phosphorylation dynamics that can be distinguished by 5P-EGF vs S-EGF stimulus (Fig. 3.14). Upon ligand binding at a subsaturating dose, unliganded monomeric EGFR is transformed into dimeric EGFR (green arrow, Fig. 3.14), which amplifies the response by activating the remaining monomeric EGFR (black arrow, Fig. 3.14). The monomeric EGFR can amplify its own activity by autocatalysis as well (black self-loop, Fig. 3.14). Active monomeric and dimeric EGFR then internalise into endocytic vesicles and traffic towards the early endosome (EE). Liganded EGFR unidirectionally traffics from there towards the late endosome where it gets inactivated by dephosphorylation and eventually degraded [8]. On the other hand, the unliganded EGFR recycles through the recycling endosome (RE) to repopulate the PM and can be reutilised in enhancing the phosphorylation response. Constant presence of growth factor redirects the traffic of EGFR from the continuous cycling route towards the unidirectional degradation route, depleting the plasma membrane of receptors. Inhibited recycling of the monomers, similarly to the degradation of liganded EGFR dimers, depleted the PM of the receptors and reduced the phosphorylation response. This indicates that a continuously maintained PM fraction of EGFR monomers provides the system with sensitivity and responsiveness to upcoming GF stimuli.

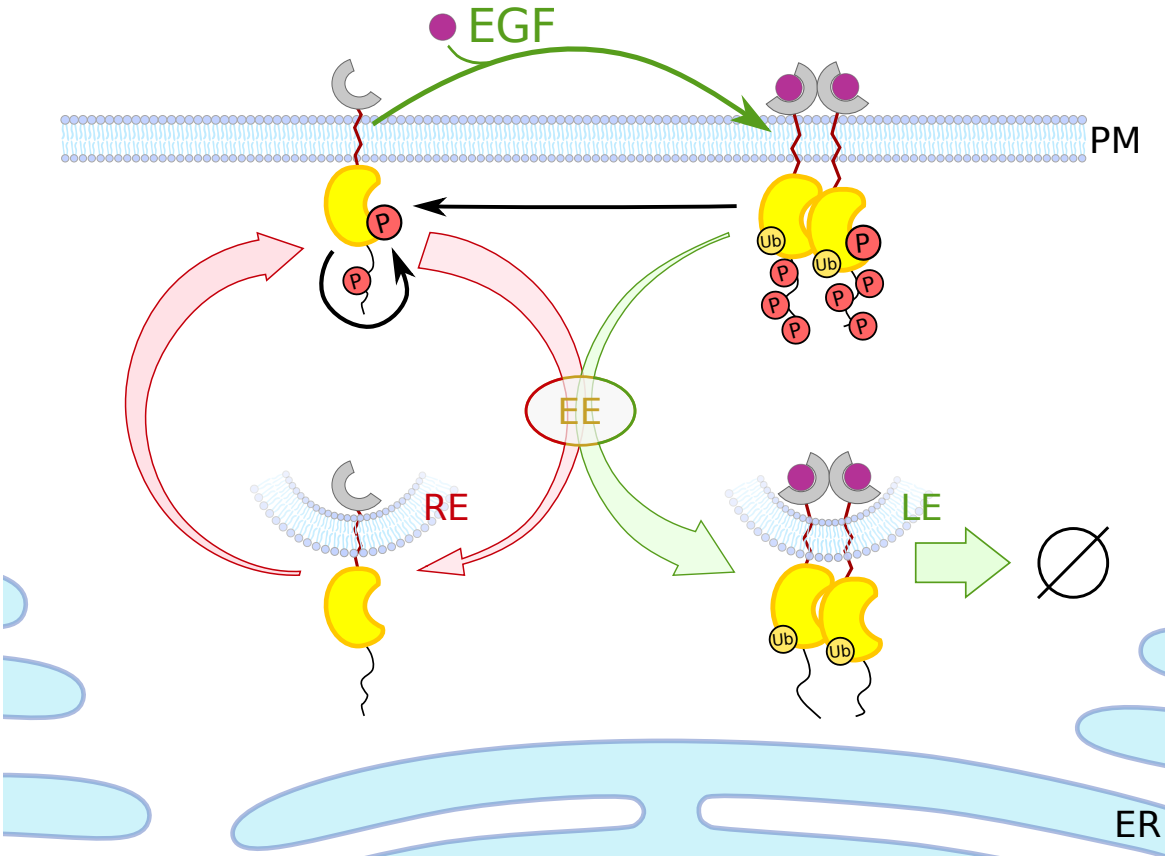

Figure 3.14 EGFR trafficking dynamics. Unliganded EGFR recycles via early (EE) and recycling endosomes (RE) to the plasma membrane (red arrows) whereas upon EGF binding (thin green arrow), ubiquitinated EGF-EGFR$_{Ub}$ unidirectionally traffickes via the early- to the late endosomes (LE, green arrow) to be degraded in lysosomes (∅). Causal links are denoted with solid black lines.

Major question that remains to be answered is how the interactions with the distinctly spatially distributed phosphates shape the characteristic EGFR phosphorylation dynamics.

3.3 EGFR response is determined by recursive interactions with the PTPs

EGFR's phosphorylation response to different EGF doses revealed the properties of the activation mechanisms depicted in Fig. 1.5. The steep non-linear profile (Fig. 3.5b) showcased the importance of the unliganded receptor species in the system in amplifying the response. As the dimeric liganded EGFR fraction was increased upon EGF addition, it activated

the monomeric one. Activity was further sustained by the autocatalysis of the unliganded monomers, as shown in Fig. 3.12a.

Counteracting the activation mechanisms of EGFR is carried out by the phosphatases, which regulate the phosphorylation of EGFR at their distinct localisations in the cell. As discussed previously, the PTPs under study are the direct and non-redundant strong regulators identified in [123]: the PM-localised PTPRG and PTPRJ, and the ER-bound PTPN2, as well as the weak regulator: the PM-localised PTPRA. The inhibitory mechanisms in the state transition diagram in Fig. 1.5 are depicted by the dephosphorylating activities of the phosphatases. However, the PTPs are not simple invariable entities, but as described in section 1.3.2 they can also be in multiple activity states and even further, they can be susceptible to regulation by EGFR itself. Only active PTPs can act as enzymes to dephosphorylate their substrates, and similarly, only phosphorylated EGFR molecules can induce PTP state change. Therefore, the specific causal coupling between the two species is a critical facet of the EGFR phosphorylation regulation as it will determine the activity states of both proteins. The essential role of the EGFR-PTP interdependence thus underlines the importance of determining the network motif of EGFR with each of its phosphatases. The topology of each network motif has specific dynamical properties that can contribute distinctly in shaping the phosphorylation response of EGFR.

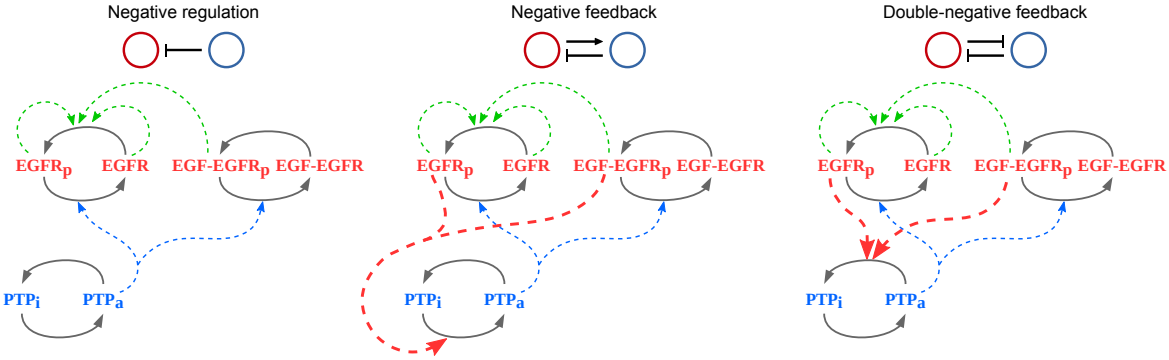

Figure 3.15 Possible EGFR-PTP interaction motifs. Solid arrows: molecular state transitions (p: phosphorylation, i: inactive, a: active), dashed arrows: causal links. Left: negative regulation, middle: negative feedback, right: double negative feedback. Top row insets: corresponding network motifs.

Given that we are studying two different species with inducible activity state transitions and given the additional regulation presumptions, there are three conceivable network topologies. They emerge by assuming that EGFR can regulate the PTP activity in any possible way, and are shown in Fig. 3.15. The motif on the left depicts the absence of causality from EGFR, hence there is only simple negative regulation from the PTP. In the motif in the centre, EGFR causes activation to its own inhibitor, the PTP, effectively generating negative

feedback to itself. Lastly, the mutual inhibition in the motif on the right produces a special type of positive feedback - a double-negative feedback. Each of these network motifs has its own distinct dynamical signature that can be utilised for performing specific function, but with which it can also be experimentally identified [80]. Therefore, dynamically probing the phosphorylation response of EGFR by introducing a phosphatase in the system can reveal the underlying EGFR-PTP network motif.

Assuming that in the control case the interaction of EGFR with the endogenously expressed PTPs (PTPe) encapsulates all of the aforementioned motifs, we created an aggregated interaction motif to fit the experimental dose-response data from Fig. 3.5b. The model effectively compiles to a double-negative-feedback-like motif (see Fig. 3.16a and Methods).

The reaction networks from Fig. 3.15 and Fig. 3.16a can be described by the generalised model:

$$\begin{cases} \dfrac{\mathrm{d}[EGFR_p]}{\mathrm{d}t} = [EGFR](\alpha_1[EGFR] + \alpha_2[EGFR_p] + \alpha_3[EGF\text{-}EGFR_p]) \\ \qquad\qquad - [EGFR_p](\gamma[PTP_a] + [PTPe]) \\ \dfrac{\mathrm{d}[EGF\text{-}EGFR_p]}{\mathrm{d}t} = k_5[EGF\text{-}EGFR] - [EGF\text{-}EGFR_p](\gamma[PTP_a] + [PTPe]) \\ \dfrac{\mathrm{d}[PTP_a]}{\mathrm{d}t} = k_1[PTP_i] - k_2[PTP_a] \\ \qquad\qquad - k_3[PTP_a](2[EGF\text{-}EGFR_p] + [EGFR_p]) \\ \qquad\qquad + k_4[PTP_i](2[EGF\text{-}EGFR_p] + [EGFR_p]) \end{cases} \tag{3.1}$$

Here, $[EGFR_p]$ and $[EGFR]$ are the concentrations of phosphorylated and non-phosphorylated unliganded EGFR monomers respectively, $[EGF\text{-}EGFR_p]$ and $[EGF\text{-}EGFR]$ - phosphorylated and non-phosphorylated liganded EGFR dimers respectively and $[PTP_a]$ and $[PTP_i]$ - active and inactive ectopically expressed PTP respectively. α_1, α_2 and α_3 are rate constants of the autonomous, autocatalytic and ligand-mediated activation respectively (dashed green arrows in Fig. 3.15 and Fig. 3.16a), k_5 is the intrinsic dimeric trans-phosphorylation rate constant, while γ is the dephosphorylation rate constant (dashed blue arrows). k_1 and k_2 are the intrinsic PTP activation and inactivation rate constants respectively, while k_3 and k_4 are the EGFR-induced deactivation and activation rate constants of the PTP respectively (dashed red arrows in Fig. 3.15). The contribution of the endogenously expressed PTPs is

$$[PTPe] = c + \frac{1}{a + b(2[EGF\text{-}EGFR_p] + [EGFR_p])}$$

Due to conservation of mass balances we were able to reduce the system in Eq. (3.1) to three variables using:

$$[EGFR] = [EGFR]_T - [EGF\text{-}EGFR]_T - [EGFR_p]$$

$$[EGF\text{-}EGFR] = \frac{1}{2}[EGF\text{-}EGFR]_T - [EGF\text{-}EGFR_p]$$

$$[PTP_i] = [PTP]_T - [PTP_a]$$

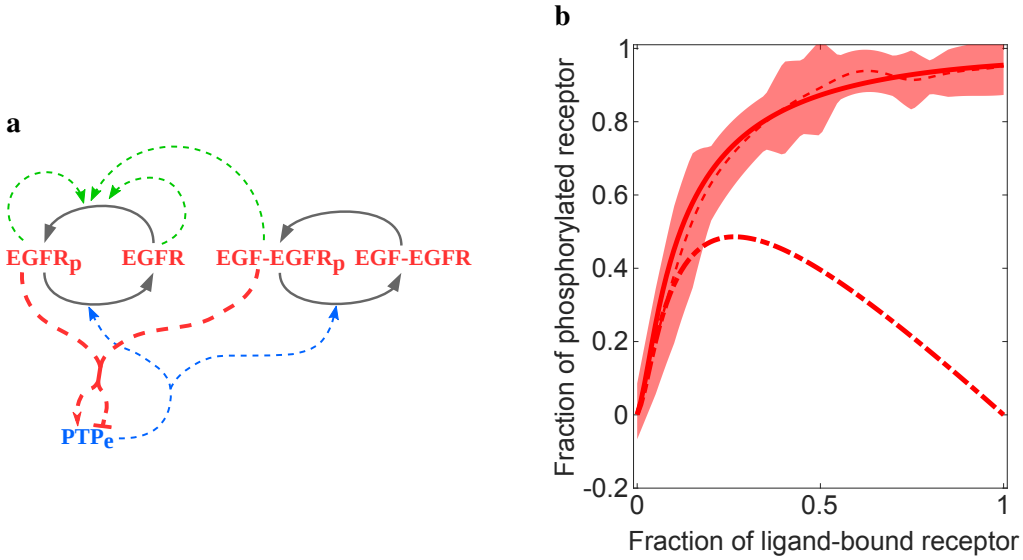

Figure 3.16 EGFR phosphorylation response upon interaction with the endogenously expressed PTPs. a) EGFR-PTPe double-negative-feedback-like interaction motif. b) Model fit of dose-response experimental data in the control case is shown with a solid red line. Dash-dotted line denotes the phosphorylation contribution from the unliganded EGFR. The data was fitted with the model shown in a). Moving average ± STD are shown with dashed red line and bounded region.

To describe the aggregated effect of endogenous PTP activity on EGFR phosphorylation, the quantities describing ectopic PTPx expression are set to 0, and a, b and c are arbitrary parameters that approximate the aggregated activity of multiple endogenously expressed PTPs. This overall activity was modelled as a combination of double-negative and negative feedback topology as well as negative regulation motifs. In case of ectopic PTPx-mCitrine expression on the other hand we have $\gamma > 0$. Additionally, the following parameter restrictions were imposed: double-negative feedback ($k_3 > 0$, $k_4 = 0$), negative feedback ($k_3 = 0$, $k_4 > 0$) or negative regulation ($k_3 = 0$, $k_4 = 0$).

Experimentally, administration of every subsequent dose was performed after ligand-binding steady state convergence with the previous dose. As the phosphorylation kinetics followed the ligand-binding equilibration closely (Fig. 3.2), we assume the system is under steady state conditions. Therefore, for a given parameter set, we solve the system in Eq. (3.1) by finding a set of variables $(EGFR_p^*, EGF\text{-}EGFR_p^*, PTP_a^*)$ that satisfies:

$$\begin{cases} \dfrac{\mathrm{d}[EGFR_p^*]}{\mathrm{d}t} = 0 \\ \dfrac{\mathrm{d}[EGF\text{-}EGFR_p^*]}{\mathrm{d}t} = 0 \\ \dfrac{\mathrm{d}[PTP_a^*]}{\mathrm{d}t} = 0 \end{cases}$$

To fit the model that best represents the experimental EGF dose - EGFR phosphorylation response in the control case, the model and data were transformed by expressing the dependency of the fraction of phosphorylated EGFR ($[pEGFR] = (2[EGF\text{-}EGFR_p] + [EGFR_p])/[EGFR]_T$) to the fraction of liganded EGFR-mTFP. The optimal parameter set was estimated using an adaptive Metropolis-Hastings algorithm, a variant of the Monte Carlo Markov Chain (MCMC) method for sequential sampling from the posterior joint probability distribution of the parameters [135] (see section 2.12 for more technical details).

The resulting profile, shown in Fig. 3.16b closely matches the experimental data. Having modelled the unliganded species specifically, we can easily estimate its contribution to the phosphorylated fraction in the response. Here it again shows significant contribution to the phosphorylation response from the unliganded EGFR (dash-dotted profile). This contribution diminishes as the unliganded receptors are increasingly converted to ligand-bound ones.

3.3.1 EGFR-PTPRG toggle switch shapes the EGFR response

To understand how EGFR sensitivity to GFs is regulated by the distinct activity of PTPRG/J/A at the PM and PTPN2 on the ER, we determined the EGFR-mTFP phosphorylation response to EGF-Alexa647 doses upon ectopic expression or knock-down of the respective PTPx. This was performed in single cells analogous to the experiments presented in Fig. 3.16b. The positive perturbation magnify the interaction between the ectopically expressed PTPx-mCitrine and EGFR-mTFP, isolating the effect of their interaction motif. This allowed us to simplify the models from Eq. (3.1) by setting $PTPe = 0$. The causality coupling between PTPx and EGFR was determined by analysing the goodness of fit of the aforementioned three possible interaction motifs (Fig. 3.15) to the dose-response data. The network motif

was subsequently established by comparing the relative qualities of the model fits using the Akaike information criterion [147] (see section 2.13 for the fitting results).

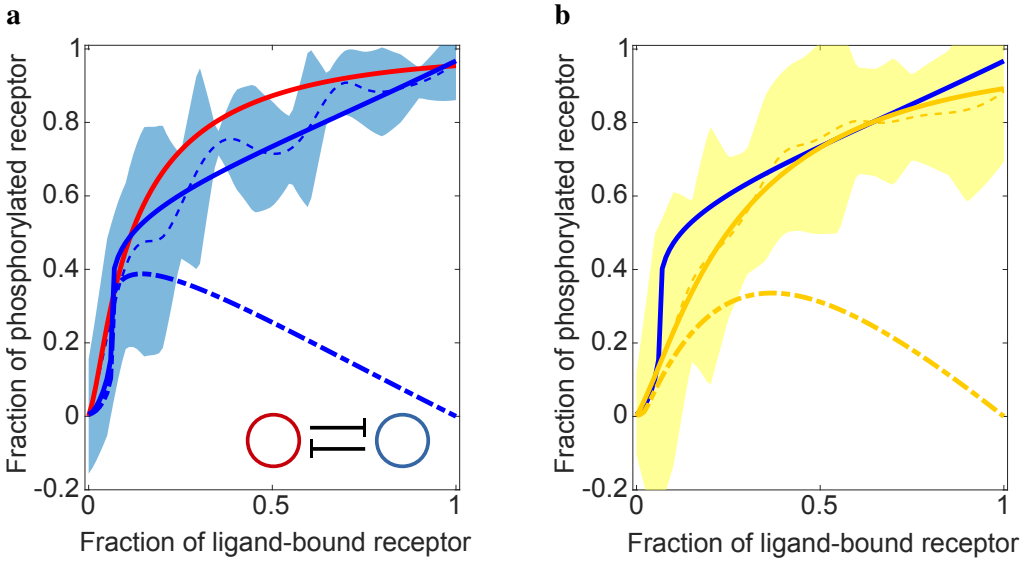

Figure 3.17 EGFR phosphorylation response with ectopic co-expression of PTPRG-mCitrine. Solid lines: model-based fits to the phosphorylated EGFR fraction. Dash-dotted lines: contribution of the unliganded monomers. Moving average ± STD are shown with dashed lines and respectively coloured bounded regions. a) Dose-response of EGFR-mTFP phosphorylation (red) is significantly altered with co-expression of PTPRG-mCitrine (blue lines, p=0.027, n=28 cells, N=14). Best fit was achieved with the model shown in inset. b) NOX-inhibition with DPI (10 µM, 30 min pre-incubation) significantly flattens dose-response of EGFR-mTFP phosphorylation with co-expression of PTPRG-mCitrine (yellow lines, p=0.06, n=26 cells, N=10).

A remarkable switch-like EGFR phosphorylation response (blue), compared to the control case (red fit), was observed upon ectopic PTPRG-mCitrine expression (Fig. 3.17a). A threshold of EGFR activation at around 6-7% receptor occupancy with EGF was imposed by PTPRG. Above the threshold the response was abruptly switched on, mainly contributed by the autocatalytically activated unliganded EGFR monomers (Fig. 3.17a, blue dash-dotted profile). Such a response was most consistent with a double-negative feedback (Fig. 3.17a, inset). Hence, with a subthreshold stimulus the negative regulation by PTPRG dominates the response, while the situation is reversed in the suprathreshold case, where the autocatalytic activation overcomes the inhibition and suppresses the activity of PTPRG.

Dose response experiments with knock-down of PTPRG were not performed, as it was shown that MCF7 cells treated with PTPRG siRNA exhibit preactivation of EGFR [123].

EGFR regulates PTPRG through oxidation-mediated mechanism

The biochemical mechanism with which EGFR can regulate the activity of PTPRG is via H_2O_2-mediated oxidation, as discussed in section 1.3.2. EGFR induces activation of H_2O_2 production by NADPH-oxidases (NOX), which potentially reversibly oxidises the catalytic cysteine of PTPRG. To test whether the dose response of EGFR is affected by H_2O_2, we inhibited NOX activity with diphenyleneiodonium (DPI) before the dose-response experiment. This suppressed H_2O_2 production, thus effectively lowering the PTP regulation from EGFR. The switch-like activation observed upon PTPRG-mCitrine expression (Fig. 3.17b, blue profile) was converted to a flatter gradual response as a result of the DPI pre-treatment (Fig. 3.17b, yellow profile). The increased PTPRG activity reduced the phosphorylation of EGFR. The double-negative feedback was thus weakened and almost effectively reduced to a negative regulation, which was reflected in the model fits (section 2.13). The enhanced PTPRG activity was most strikingly observed from the contribution of the unliganded monomeric receptor (Fig. 3.17b, dash-dotted profile), suggesting that PTPRG is strongly suppressing the autocatalytic activation of EGFR.

3.3.2 EGFR-PTPRJ negative regulation motif suppresses the phosphorylation of EGFR

Unlike PTPRG, ectopic PTPRJ-mCitrine expression flattened the dose-response profile strongly and uniformly throughout the whole ligand-bound fraction range, relative to the control case (Fig. 3.18a, blue). This uncovered the underlying interaction motif as a simple negative regulation (Fig. 3.18a, inset). Perturbing the network motif with the NOX inhibitor DPI resulted with no change in the response profile, excluding the PTP regulation from EGFR as a possible causal link (Fig. 3.18b, yellow).

On the other hand the knock-down of PTPRJ showed no significant effect on increasing the phosphorylation response of EGFR (Fig. 3.18c, blue). However, the single cell data reveal the manifestation of switch-like response (Fig. 3.18d), reminiscent of the data in Fig. 3.17a. Furthermore, the double-negative feedback model fit was the most consistent with the experimental dose-response data. This indicates that the knock-down of PTPRJ revealed the underlying EGFR-PTPRG double-negative feedback, therefore the role of PTPRJ is likely in modulating the response established by the EGFR-PTPRG recursive interaction.

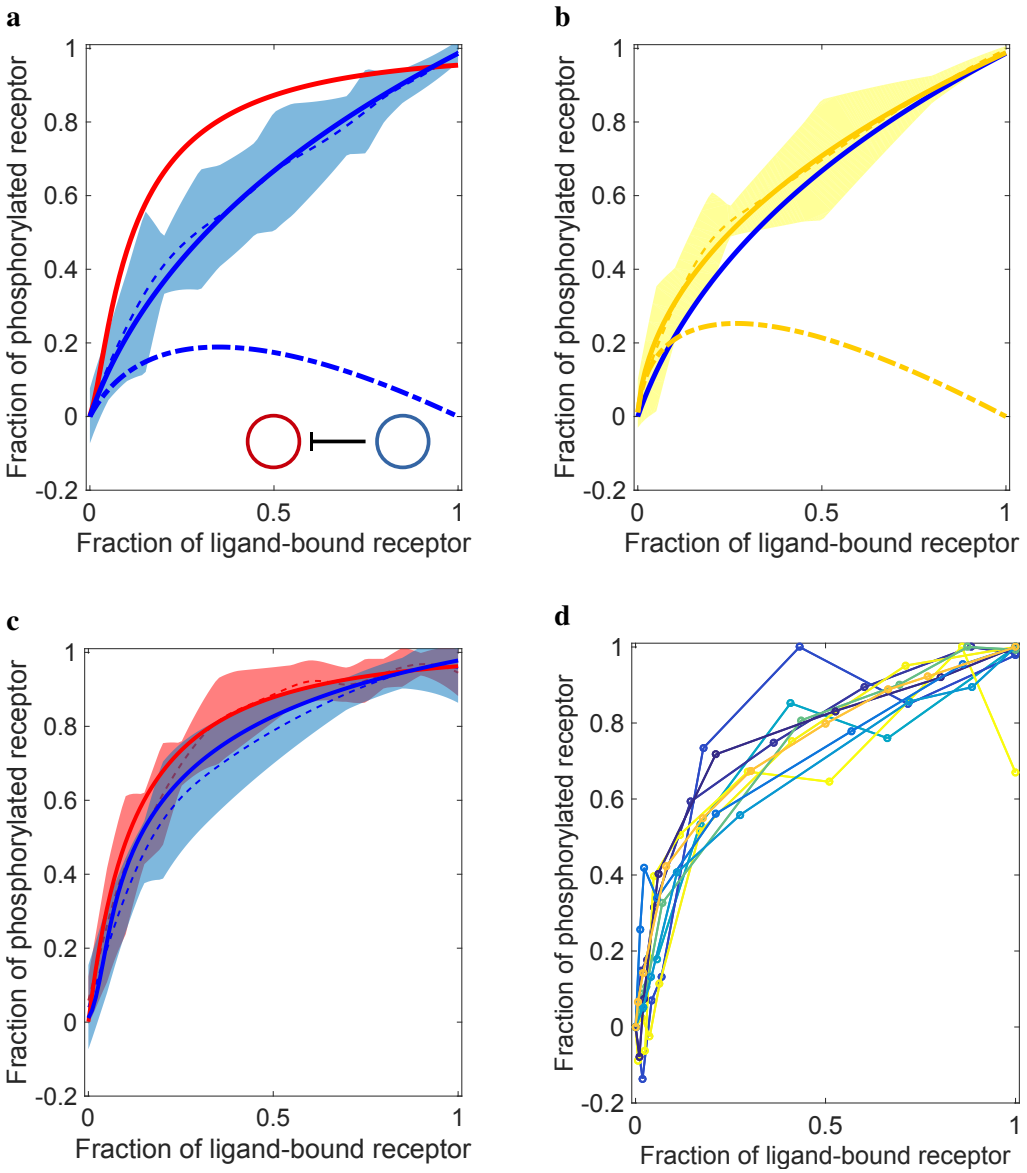

Figure 3.18 EGFR phosphorylation response upon perturbation of PTPRJ expression. Moving average ± STD are shown with dashed lines and respectively coloured bounded regions. Solid lines: model-based fits to the phosphorylated EGFR fraction. Dash-dotted lines: contribution of the unliganded monomers. a) Dose-response of EGFR-mTFP phosphorylation (red) is significantly altered with co-expression of PTPRJ-mCitrine ($p=4\times10^{-4}$; n=16 cells, N=7). Best fit was achieved with the model shown in inset. b) NOX-inhibition by DPI (10 µM, 30 min pre-incubation) has no effect upon PTPRJ-mCitrine co-expression (p=0.162, n=10 cells, N=5). c) Dose-response of EGFR-mCitrine phosphorylation upon siRNA-mediated PTPRJ knock-down (blue line, n=11 cells, N=3). The corresponding single cell profiles are shown in d).

3.3.3 PTPRA has minor effect on EGFR's phosphorylation response

One of the receptor-like phosphatases that was also identified, albeit as a minor regulator, was PTPRA [123]. Consistent with those results, the EGFR-mTFP phosphorylation response upon ectopic expression of PTPRA-mCitrine showed weak insignificant suppression (Fig. 3.19a, blue) relative to the control case (red). It is however known that the activity of PTPRA is affected by the redox mechanism, inducing it into self-inhibitory state via homodimer formation [84, 110]. If PTPRA is indeed a strong regulator of EGFR, but its activity is inherently inhibited, the release of the oxidation-mediated inhibition would result in enhanced PTPRA activity and thus suppressed EGFR response to EGF. Therefore, we again probed this hypothesis by inhibiting the H_2O_2 production with DPI. The phosphorylation response of EGFR showed no enhanced suppression (Fig. 3.19b, yellow) compared to the case without ROS inhibition (blue). The absence of regulation from PTPRA was further corroborated by the PTPRA siRNA-mediated knock-down dose response experiment, which showed no significant phosphorylation elevation, compared to the control case (Fig. 3.19c).

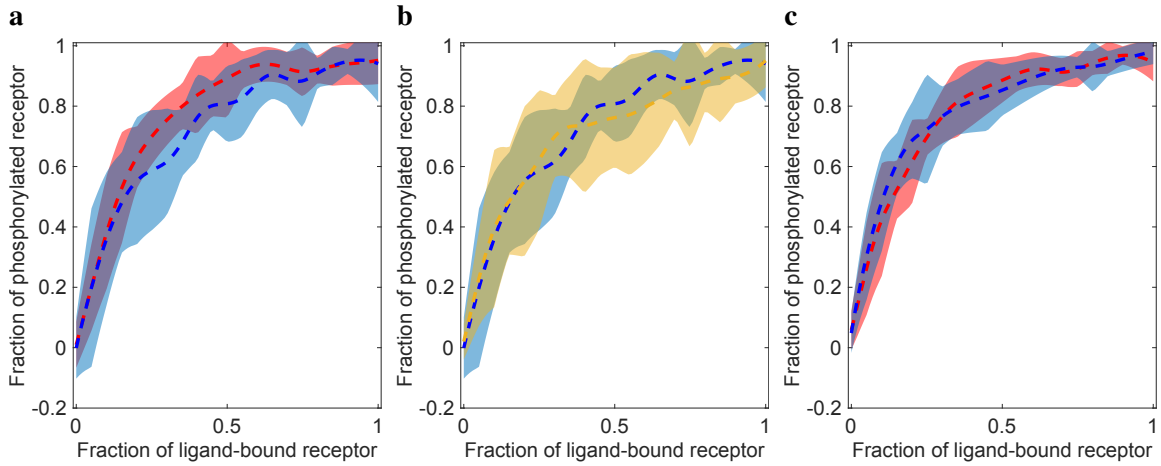

Figure 3.19 EGFR phosphorylation response upon perturbation of PTPRA expression. Moving average ± STD are shown with dashed lines and respectively coloured bounded regions. Dose-response of EGFR-mTFP phosphorylation (control, red) is not affected upon a) siRNA-mediated PTPRA knock-down (blue, p=0.823, n=14 cells, N=7) or b) PTPRA-mCitrine co-expression (blue, p=0.225, n=34 cells, N=16). c) NOX-inhibition by DPI (10 µM, 30 min pre-incubation) has no effect (yellow, p=0.937, n=38 cells, N=16) on the dose-response of EGFR-mTFP phosphorylation with ectopic co-expression of PTPRA-mCitrine (blue, same as in b)).

3.3.4 Spatially established EGFR-PTPN2 interaction motif regulates the phosphorylation response of EGFR

The function of PTPN2 as a strong and direct regulator of EGFR is an intricate case. Its localisation is predominantly in the perinuclear areas, determined by its ER-binding domain, and declines towards the PM. Nevertheless, the effect of the ectopic expression of PTPN2-mCitrine on the phosphorylation response of EGFR is strong (Fig. 3.20a, blue). Unlike PTPRG and more similar to PTPRJ, this effect is uniform, flattening the response throughout the whole ligand-bound EGFR range, implying a negative feedback or a negative regulation mechanism (Fig. 3.20a, inset). This was further reinforced by the invariant phosphorylation response upon ROS production inhibition with DPI (Fig. 3.20b, yellow). On the other hand, PTPN2 knock-down perturbation resulted in increase in EGFR phosphorylation, where EGFR transitioned to the high phosphorylation state at even lower fraction of ligand-bound receptor, compared to the control (Fig. 3.20c, blue vs red). This amplification at low EGF dose is due to the increase of phosphorylation of the unliganded EGFR monomers, hence the absence of PTPN2 from the system causes the active monomers to elevate their activity at the PM. This confirmed that PTPN2 is indeed a strong and non-redundant regulator of EGFR, coupled with it in a negative feedback or negative regulation fashion.

The strong negative regulation that PTPN2 exerts on EGFR's phosphorylation response then prompts whether and how the coupling between EGFR and PTPN2 is established via vesicular trafficking. Given the previously determined relation between vesicular trafficking and phosphorylation response of EGFR (section 3.2.3), we hypothesise that the two proteins interact on the contact points between endosomal and ER membranes. Therefore, we inhibited the exit from the recycling endosome using the dominant negative Rab11^{S25N} mutant (as in section 3.2.2) and observed the effect on the phosphorylation response at the plasma membrane in presence or absence of ectopic PTPN2 expression. Ectopic expression of PTPN2-mCitrine generated no significant flattening on the phosphorylation response of EGFR-mTFP when the dominant negative Rab11^{S25N} mutant was present in the system (blue with PTPN2 relative to red without PTPN2 in Fig. 3.20d). The absence of additional inhibition of EGFR phosphorylation at the plasma membrane with ectopic expression of PTPN2 indicates that it is the monomers, which are concentrated at the RE in this case, that were affected the most in the analogous experiment without ectopic expression of Rab11^{S25N} in Fig. 3.20a. Therefore, PTPN2 exerts its strong effect on EGFR through dephosphorylation of the recycling monomers. The interaction mechanism is trafficking mediated and occurring mostly in the perinuclear areas. Moreover, the interaction is promoted by the internalisation

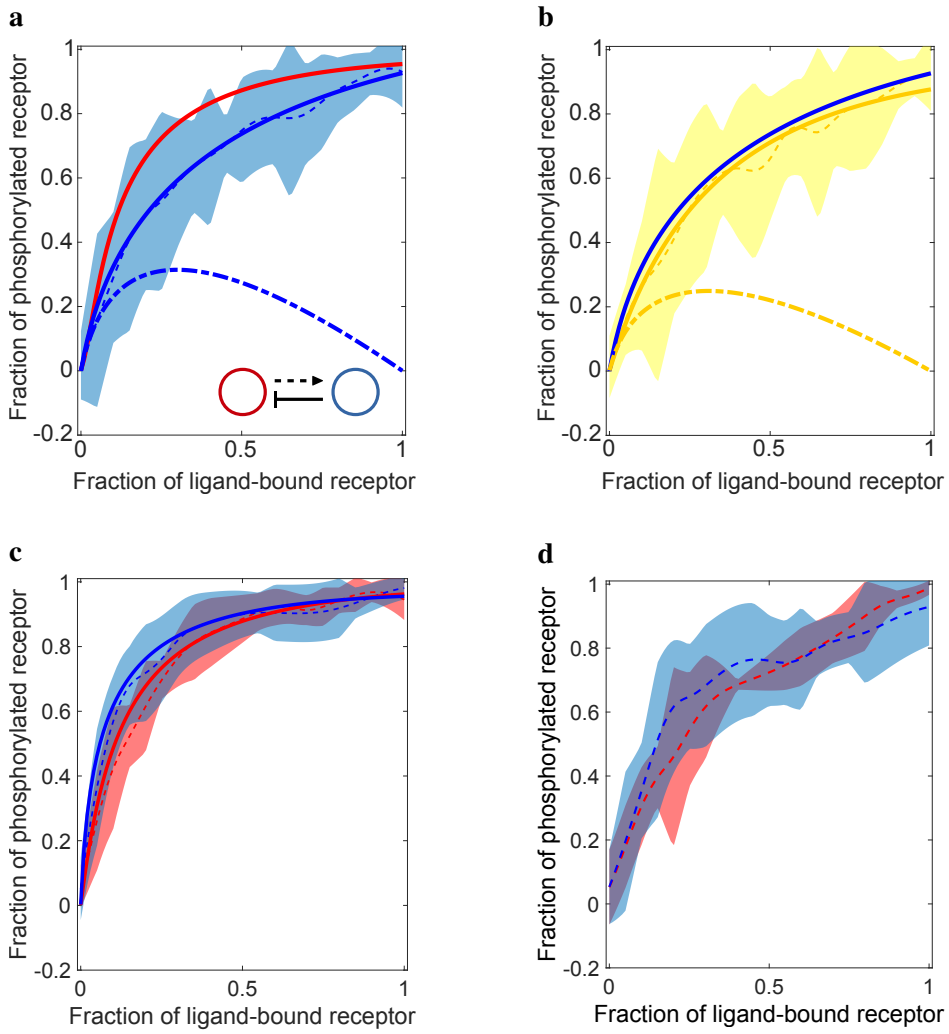

Figure 3.20 EGFR phosphorylation response upon perturbation of PTPN2 expression. Solid lines: model-based fits to the phosphorylated EGFR fraction. Dash-dotted lines: contribution of the unliganded monomers. Moving average ± STD are shown with dashed lines and respectively coloured bounded regions. a) Dose-response of EGFR-mTFP phosphorylation (red) is significantly altered with co-expression of PTPN2-mCitrine (blue, p=0.001, n=34 cells, N=13). Best fit was achieved with the model shown in inset. b) NOX-inhibition by DPI (10 µM, 30 min pre-incubation) has no effect upon PTPRJ-mCitrine co-expression (p=0.19, n=45 cells, N=12). Dose-response of EGFR-mCitrine phosphorylation c) upon siRNA-mediated PTPN2 knock-down (blue line, p=0.17; n=14 cells, N=6) and d) with co-expression of Rab11^{S25N}-BFP for recycling inhibition (red, n=15 cells, N=4). Additional co-expression of PTPN2-mCitrine has no effect on the response (p=0.35, n=19 cells, N=7).

of EGFR, hence it is conditioned on its activity. This in effect generates a spatially established negative feedback.

3.4 Dynamical systems properties of the EGFR-PTP network

The previously presented results demonstrated that EGFR responsiveness to EGF is mainly determined by a double-negative feedback with PTPRG that is established by phospho-EGFR-induced NOX-mediated production of H_2O_2, and modulated by PTPRJ activity at the plasma membrane and PTPN2 on the ER. Phosphorylation of the unliganded monomers plays crucial role in amplifying the response through autocatalysis, thereby providing increased sensitivity in the system. Regulating that phosphorylation then happens on two levels: PTPRG imposes threshold for the switch-like activation at the plasma membrane by countering the autocatalysis through dephosphorylation of the monomers, while the internalised phosphorylated monomers are dephosphorylated and recycled back to the plasma membrane by PTPN2 and can again engage in the autocatalytic activation mechanism. Hence, vesicular trafficking couples the activities of these PTPs on different cellular membranes into a unified EGFR-PTP network that determines the phosphorylation response (Fig. 3.21a).

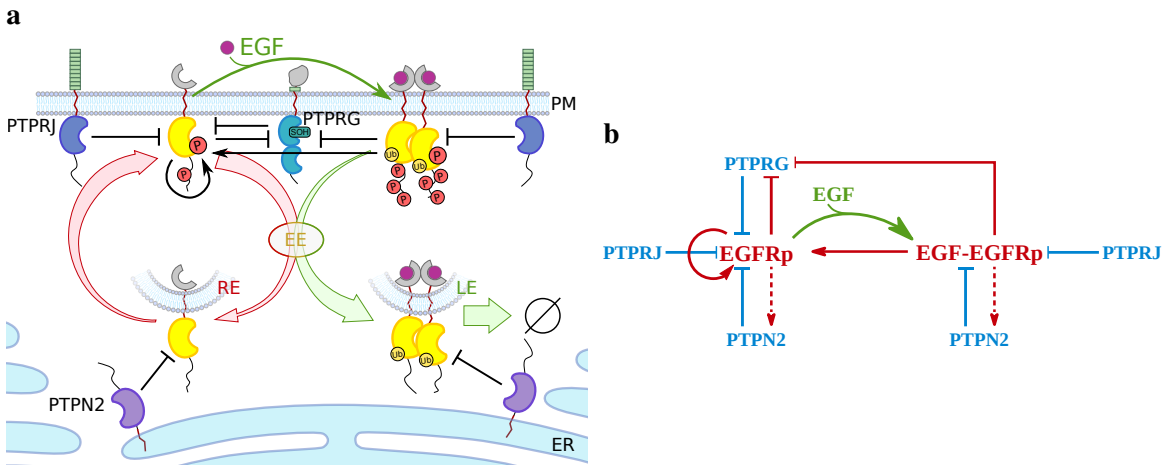

Figure 3.21 Unified EGFR-PTP network. a) Scheme of the EGFR-PTP interaction network established through EGFR trafficking dynamics. EGFR interacts with PTPRG/PTPRJ at the PM and PTPN2 in the cytoplasm. All notations as in Fig. 3.14. b) Causality diagram of the unified EGFR-PTP network. Red/blue lines: causal interactions, green arrow: ligand binding.

To better understand how the central EGFR-PTPRG double-negative interaction that determines sensitivity to EGF is modulated by negative regulation by PTPRJ and negative feedback by PTPN2, we transformed this spatial scheme into a unified causality diagram (Fig. 3.21b). This enables us to explore the dynamical properties of this network using

bifurcation analysis (see section 1.4.1). For this purpose, the model in Eq. (3.1) was simplified by parametrising EGF-EGFR, as we assume that the dimer is always in a phosphorylated state.

3.4.1 Bistable dynamics of the EGFR-PTPRG double-negative feedback motif generates switch-like activation of EGFR

The mutual EGFR-PTPRG inhibition combined with the autocatalytic activation of EGFR generates interdependence between the two proteins with two stable solutions in the system: one where EGFR is active while PTPRG is inactive and vice versa. Simultaneous existence of two stable steady states is termed bistability [148]. When in bistability, the system is poised in one of the two stable steady state solutions (see Fig. 3.22a), defined by the intersections of the nullclines (see section 1.4.1). Sudden transition from one stable steady state to the other due to destabilisation results in a switch-like activation or deactivation. As both of them are attainable in bistability, the convergent phosphorylation state of EGFR is determined based on the initial phosphorylation level, i.e. is history-dependent. Third, unstable saddle fixed point, repels the system trajectories in one direction, thus separates the state space into two regions defined by the trajectories that are attracted to a common stable steady state (Fig. 3.22b, blue vs orange trajectories and steady states). These regions thus determine the basins of attraction around each of the stable steady states, and are analogous to valleys in an extended 3-D space - a landscape that depicts the system potential, where the trajectories descend towards the stable steady states that have zero potential change [149] (Figs. 3.22b and 3.22c). The ridge between the two valleys is determined by the unstable fixed point.

There is a range of input dose for which the phosphorylation dynamics operates in a bistable regime with both low and high phosphorylation levels of EGFR potentially attainable. The phosphorylation dynamics can be analysed by studying the state space topology changes during a presence and removal of input signal, as shown in Fig. 3.23. Prior to addition of EGF the resting phosphorylation state is occupied (Fig. 3.23a). Thresholded switch-like activation then arises from a saddle-node bifurcation: a change in EGF dose at which the occupied stable low EGFR phosphorylation state merges with the unstable fixed point, abruptly annihilating each other (see Fig. 3.23b). This change in the topology of the state space comes about as the nullclines no longer intersect in three fixed points, but in one, as a result of the input parameter change. Consequently, the system state transitions towards the single remaining stable steady state - the high EGFR phosphorylation state (Fig. 3.23b, green trajectory). The resulting dose-response profile has the shape as the one shown in Fig. 3.17a. Therefore, while PTPRG's activity suppresses the autocatalysis of EGFR and dominates in the bistable regime

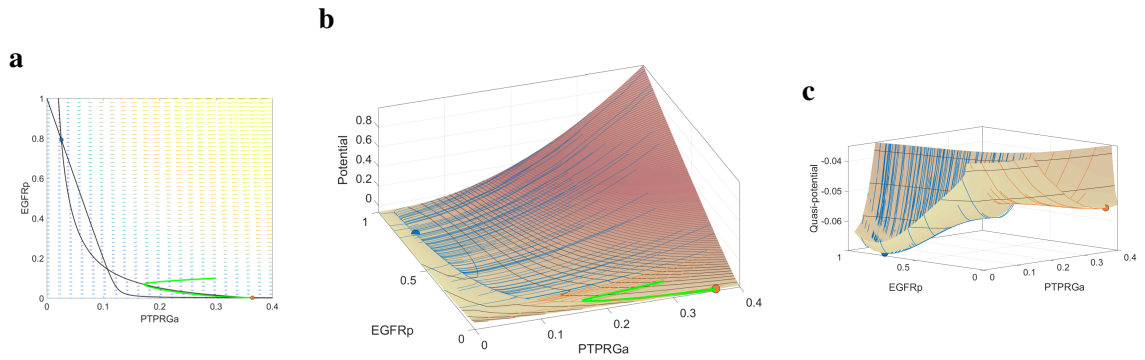

Figure 3.22 Bistable behaviour of EGFR-PTPRG double-negative feedback. a) State space of the EGFR-PTPRG system. Solid black lines represent nullclines which intersect at three different points. The vector field is shown in the background. Green line shows a trajectory that converges to one of the stable steady states. b) Corresponding estimated quasi-potential landscape representation. Blue trajectories converge to high-, while orange trajectories to low EGFR phosphorylation steady state, outlining their basins of attractions. c) Enhanced view showing the potential-valleys, defined by the basins of attraction, separated by an unstable-saddle-node-established ridge.

under a subthreshold stimulus condition, it can no longer contain the activity of EGFR with suprathreshold stimulus and becomes inactive as a result. However, the amplification via autocatalytic activation inflicts a trade-off, as the phosphorylation level is maintained after the pulse removal. The state trajectory stays in the high phosphorylation state upon reinstating of the initial bistability as it remains stable (Fig. 3.23c). A suprathreshold EGF pulse thus causes an irreversible activation of EGFR, where the autocatalysis alone is sufficient to maintain the monomeric unliganded receptors phosphorylated after the pulse removal. This effectively generates a memory in the system, as the monomeric species preserve the knowledge of a previous stimuli.

3.4.2 Sensitivity to novel growth factor stimuli depends on PTP/EGFR plasma membrane abundance

Shapes of the nullclines determine the number of intersection points between them, hence existence of bistability depends on the parameters in the system. These include the biochemical rate constants and the protein concentration levels. Unlike the former which depend on the biochemical properties of the molecules, the latter can vary depending on the context, and are thus tunable parameters for the cell. The gene regulatory expression profile of the cell, as well as the spatial regulation in the system, will determine the protein concentration levels at the plasma membrane, and consequently the operation regime of the cell. More accessible

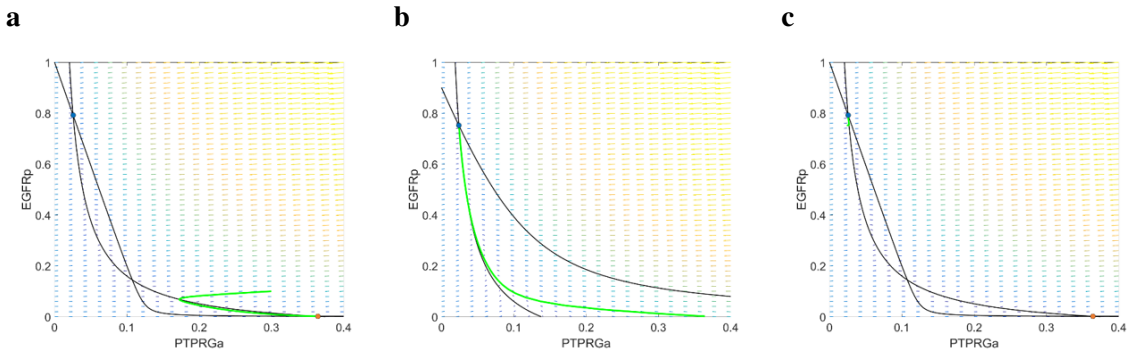

Figure 3.23 Memory from bistable dynamics in EGFR phosphorylation upon pulsed EGF stimulation. State space representation of the EGFR-PTPRG system as in Fig. 3.22a. a) Pre-stimulus (Bistability): The trajectory converges to the resting phosphorylation state. b) Suprathreshold stimulus (Monostability): Transition of the state trajectory to the remaining stable, high EGFR phosphorylation state from bistability. c) Pulse removal (Bistability): The state is maintained at the high EGFR phosphorylation level when bistability is reinstated.

experimental perturbations of these mechanisms also provide an advantage in characterising the dynamical properties of the network.

Therefore, the phosphorylation dynamics of monomeric unliganded EGFR (EGFRp) at the plasma membrane was analysed theoretically as function of the system's parameters: liganded EGFR (EGF-EGFR), which will show the response properties, and PTPRG/EGFR expression levels, which will determine the regime of operation. Dependence on PTPRG/EGFR with EGF-EGFR=0 can be observed in Fig. 3.24a, where the bistability region spans between the two annotated saddle-node bifurcation points. To understand further how the system will respond to a given EGF concentration depending on where it is positioned in respect to PTPRG/EGFR, the EGFRp response was studied using 3-D bifurcation analysis. The EGFRp steady state surface, also termed *cusp catastrophe* surface [148], is shown in Fig. 3.24b in dependence of both of the parameters. The surface folds over on itself in certain points of the parameter space, defining the bistable region where three fixed points coexist. Profiles parallel to the EGF-EGFR axis show the phosphorylation response of EGFRp for a given PTPRG/EGFR ratio. Therefore, studying the difference between the responses is performed in relation to the PTPRG/EGFR concentration ratio at the plasma membrane, and the four distinct response types, i.e. operation regimes, that were identified are denoted on the PTPRG/EGFR axis. Their respective EGFRp responses are captured in the bifurcation diagram against the input EGF-EGFR, shown in Fig. 3.24c, where representative profile (vertical slice) was taken from each of the operation regimes. Finally, to interpret the activation/deactivation points in each of the responses, a top view of the 3-D bifurcation diagram, describing the

PTPRG/EGFR - EGF-EGFR parameter space, is shown in Fig. 3.24d, where the overlay of the high and low phosphorylation states in the bistable region is denoted with purple.

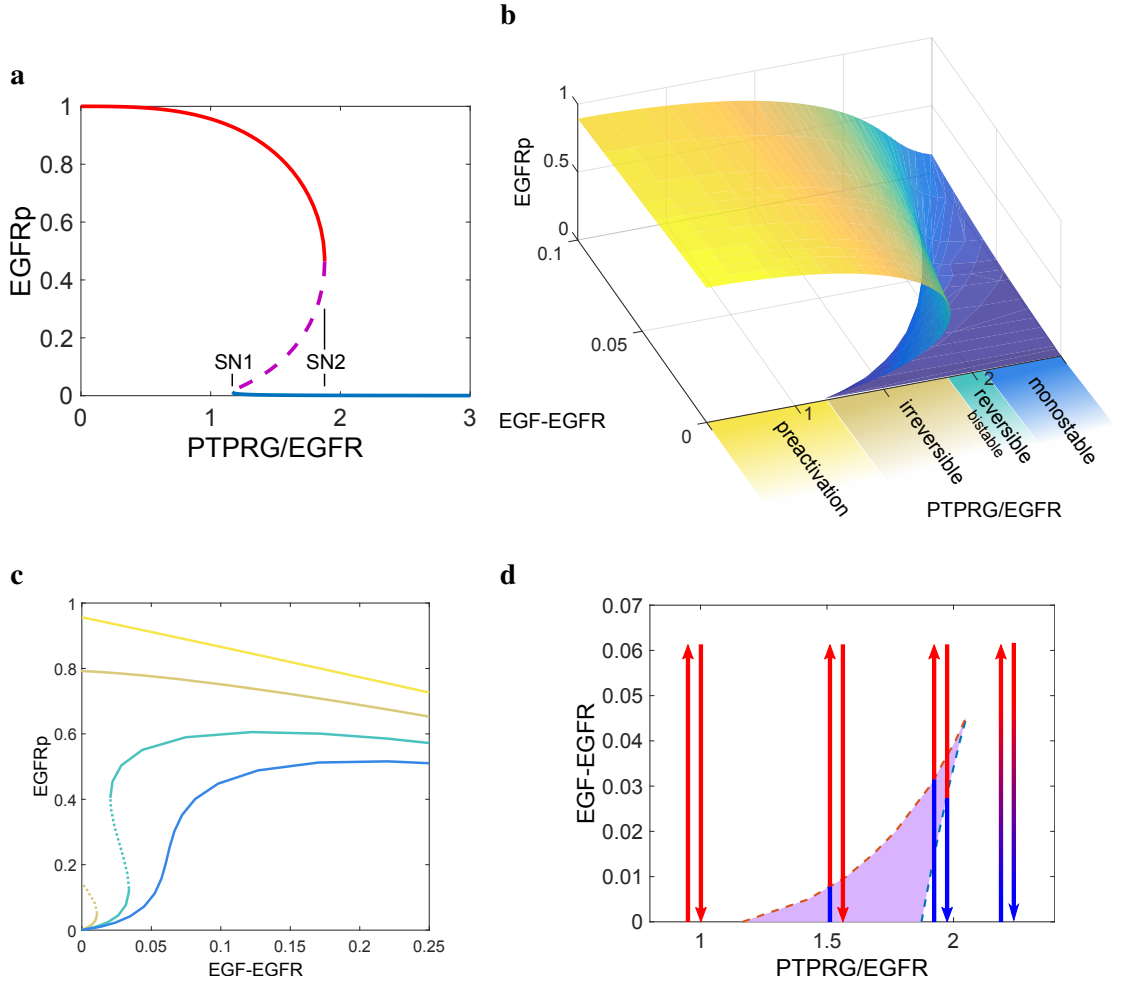

Figure 3.24 Bifurcation analysis of the EGFR-PTPRG system. a) Bifurcation diagram of unliganded EGFRp as a function of PTPRG/EGFR. Stable branches are depicted with solid lines (red - high-, blue - low phosphorylation), while unstable branch is shown with dashed line. The saddle-node bifurcations, SN1 and SN2, define the bistable region. b) 3-D bifurcation diagram of EGFRp as a function of liganded EGF-EGFR and PTPRG/EGFR. Different regimes of operation are denoted along the PTPRG/EGFR axis. c) Bifurcation diagram of EGFRp on EGF-EGFR. Representative responses are shown from the four operation regimes. Colours are matching the respective region colours along PTPRG/EGFR axis in b). d) PTPRG/EGFR - EGF-EGFR parameter space depicting the possible dynamical regimes. Bistable region is denoted with purple colour. Arrows illustrate forward and backward EGF-EGFR dose-response trajectories within each operation regime. Blue colour in arrow depicts low-, while red depicts high EGFRp state is occupied along the trajectory.

For high concentrations of EGFR or low PTPRG concentrations (as with a knock-down), hence low PTPRG/EGFR ratio, the autocatalysis is sufficiently strong to maintain stable phosphorylation levels of EGFR even in the absence of signal (EGF-EGFR), leading to preactivation and no response to EGF (Fig. 3.24b, yellow region; Fig. 3.24c, yellow profile).

For a wide range of PTPRG/EGFR concentration at the PM the system resides in bistability in the absence of signal (Fig. 3.24b, brown region). Increase in liganded EGFR then leads to saddle node bifurcation and abrupt switch in activity (Fig. 3.24c, brown profile; Fig. 3.24d, third arrow), as described previously. Removal of EGF, i.e. EGF-EGFR, from the system results in reinstating of bistability. However, since the convergent state depends on the previous state in bistability, the system will continue to reside in the high phosphorylated state in this case (Fig. 3.24c, upper branch of orange profile; Fig. 3.24d, fourth arrow).

Moving the system further on the right on the PTPRG/EGFR axis, by decrease of EGFR or increase of PTPRG abundance, can weaken the self-sustaining autocatalytic activation mechanism and place the system away from the irreversible regime of operation (Fig. 3.24b, green region). The system operates in a monostable regime there, however, upon increase in EGF-EGFR it can enter bistability while still occupying the low phosphorylation state of EGFR. Exit from bistability generates the switch in activation (Fig. 3.24c, green profile; Fig. 3.24d, fifth arrow), as in the previous case. The backward EGF-EGFR trajectory will again occupy the high phosphorylation state when it is in bistability but the system will reset when it is back in the initial low monostable state (Fig. 3.24d, sixth arrow). The discrepancy between the EGF-EGFR points of activation and inactivation (saddle-node bifurcations), resulting from operating in bistability in history-dependent manner, is called hysteresis (see Fig. 3.24c, green profile). However, unlike in the previous case where the hysteresis was extending back past the y-axis, locking the system in a phosphorylated EGFR state (Fig. 3.24c, brown profile), it operates in a reversible regime in this case.

Still further right on the PTPRG/EGFR axis, the system operates in a completely monostable manner (Fig. 3.24b, blue region). Starting from the low phosphorylation state in the absence of stimuli, EGFR is gradually, albeit still ultrasensitively activated (Fig. 3.24c, blue profile; Fig. 3.24d, seventh arrow). The backward EGF-EGFR trajectory overlaps with the forward trajectory, thus the system is in a reversible regime again.

The bistable response is modulated by PTPRJ and PTPN2

Determining the conditions under which bistability occurs is necessary to understand the response profile. Bistability can arise from a presence of ultrasensitive response coupled to a positive feedback in the system, either a double-positive or a double-negative feedback [150]. The EGFR-PTPRG system satisfies these conditions as the autocatalytic activation

mechanism of EGFR, as well as the double-negative feedback, provide non-linearities necessary for bistability. This can be observed in Fig. 3.25a, where bistability arises when the phosphorylation and dephosphorylation rates balance each other (intersect) in three different points, two of which are stable. The bifurcation from bistable to monostable dynamics occurs when the changes in forward and backward rate due to increase of EGF result in intersection in a single point. From this graphical analysis it is straightforward to perceive how the absence of either of the two preconditions will result in loss of non-linearity of the respective forward/backward rate, thus in loss of bistability. This can also be seen from the first equation in the main model in Eq. (3.1), where setting $\alpha_2 = \alpha_1$ to remove autocatalysis lowers the order of the forward rate from second to first.

The extent of the bistable region shapes the phosphorylation response of EGFR and determines the operation regime of the network. While the interaction of EGFR with PTPRG constitutes the central motif that generates bistability, the interactions with the other PTPs modulate the extent of the bistable region, hence the EGFR response. The contribution from the negative regulation by PTPRJ or negative feedback from PTPN2 in the backward rate of EGFR phosphorylation is of the same shape. It adds a linear term to the rate and therefore steepens its profile (Fig. 3.25b), effectively decreasing the region where the two profiles intersect in three points. The previous wide PTPRG/EGFR region of irreversible bistability provided a response where the forward EGF-EGFR trajectory (green) lead to switch-like activation and the backward trajectory (red) remained in the high phosphorylation state (Fig. 3.25c, using the original model from Eq. (3.1)). The narrowing of the bistability by PTPRJ and PTPN2 shifted the system poised at the same PTPRG/EGFR ratio to a reversible region (bistable or monostable) of the bifurcation diagram (Fig. 3.25d). The negative feedback with PTPN2 that is established by the vesicular recycling thus plays a similar role to PTPRJ. However, the vesicular recycling of activated EGFR monomers that are dephosphorylated by PTPN2 in the cytoplasm is also essential to maintain sufficient number of EGFR molecules at the plasma membrane for autocatalysis to manifest.

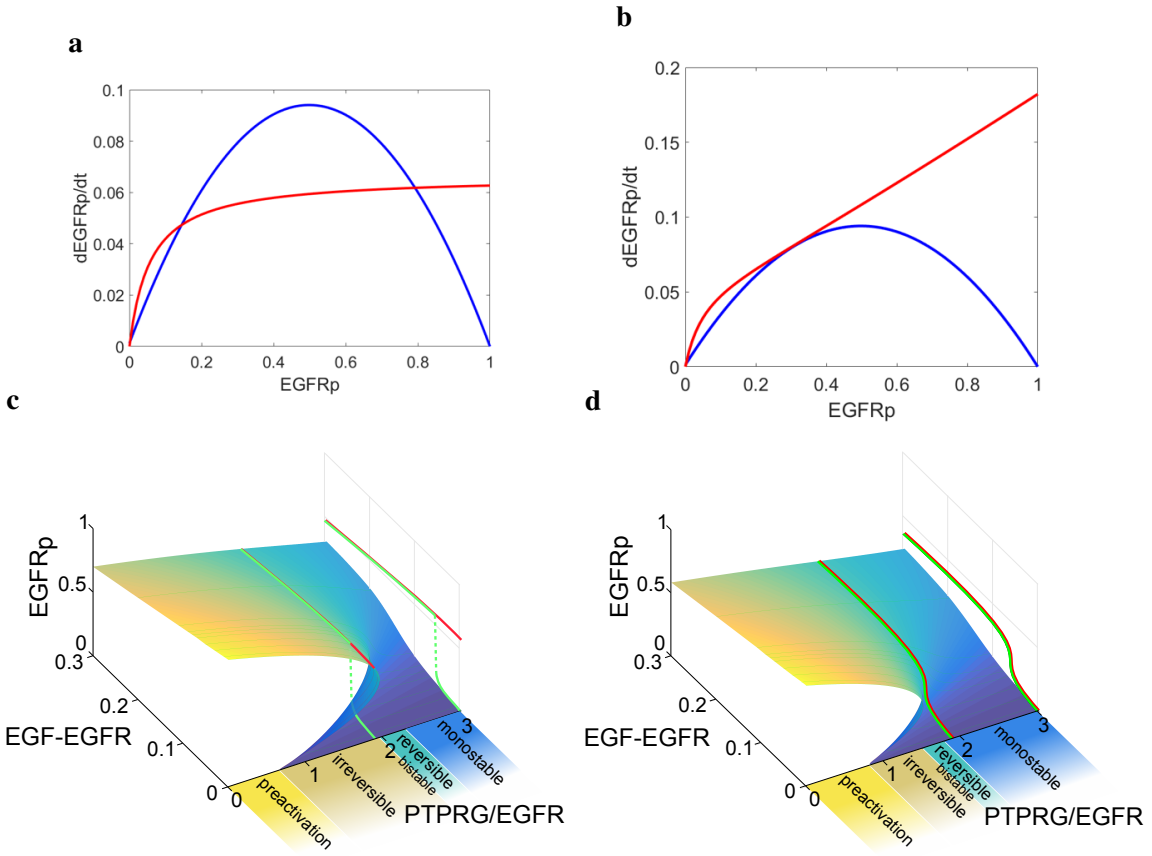

Figure 3.25 Modulation of the range of the bistable EGFRp response by PTPRJ/PTPN2. a) Rate-balance plots of EGFRp captures the bistable dynamics in the EGFR-PTPRG system. Blue shows the forward-, while red shows the backward non-linear phosphorylation rate of EGFRp. b) Rate-balance plot with additional negative regulation in the system. c) 3-D bifurcation diagram as in Fig. 3.24b. Forward (green) and backward (red) dose-response trajectories are shown for PTPRG/EGFR=1.9, with corresponding orthographic projections on the right profile plane. d) 3D-bifurcation diagram for the combined toggle-switch/negative regulation/negative-feedback network topology established by vesicular recycling of unliganded EGFR.

3.4.3 Periodic pulses to probe the network sensitivity

Whether and how this EGFR-PTP system will respond to time-varying cues will depend on where the system is organised in parameter space (PTPRG/EGFR). To explore how the system will respond in the different parameter regimes, we simulated EGFR responsiveness to a train of periodic EGF pulses (see Methods). If the dynamics of the EGFR-PTP system is dominated by the bistable properties of the PTPRG-EGFR toggle switch, the simulation shows that EGFR will remain irreversibly “trapped” in the active state after the first EGF

pulse removal and decrease of EGF-EGFR (Fig. 3.26a). The system is thereby not able to sense and respond to subsequent EGF cues. However, if the system is organised close to the bifurcation point, just outside the irreversible bistable region, the response dynamics exhibit reversible but delayed phosphorylation relaxation (Fig. 3.26b). Hence, the system can respond to all of the subsequent pulses, while transiently maintaining memory of the previous pulse.

Further away in the monostable regime, EGFR phosphorylation closely follows the EGF input (Fig. 3.26c).

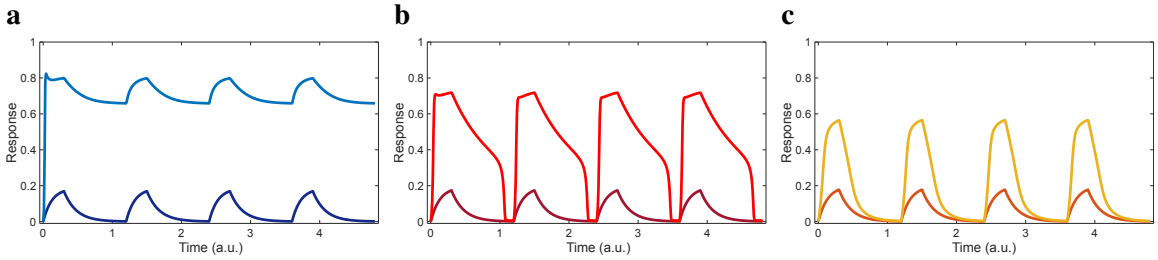

Figure 3.26 Different temporal responses to train of EGF pulses. Simulated temporal profiles of the fractions of liganded (dark) and phosphorylated receptors (light) in response to a train of EGF pulses, when the system is organised in a) the bistable regime, b) close to the bistability region, and c) in the monostable regime.

The EGFR-PTP system is poised at criticality, close to bistability

To identify where the EGFR-PTP system is poised and whether it can sense time-varying EGF signals, four subsequent non-saturating (20 ng/mL) 5 min EGF-Alexa647 pulses followed by 25 min washout were administered every 30 min to live MCF7 cells expressing EGFR-mCitrine. The fraction of liganded receptor (EGF-EGFR=EGF-Alexa647/EGFR-mCitrine) as well as the fraction of phosphorylated EGFR (EGFRp=PTB-mCherry/EGFR-mCitrine) were ratiometrically determined at the plasma membrane as a function of time, similar to the analysis in section 3.2.2 (see Methods).

Cells with knock-down of PTPRG showed strong response to the initial EGF pulse, followed by limited response to the subsequent pulses, restricted within the boundaries of the higher EGFR phosphorylation state. The EGFR activation did not relax back to the basal inactivated state in these cells (Fig. 3.27a, light blue). This result is consistent with the irreversible bistable EGFR phosphorylation dynamics with low levels of PTPRG (Fig. 3.26a). It confirms that PTPRG is a central regulator of EGFR activation dynamics through a double negative feedback motif. We also observed a subpopulation of cells (4 out of 9 cells) that

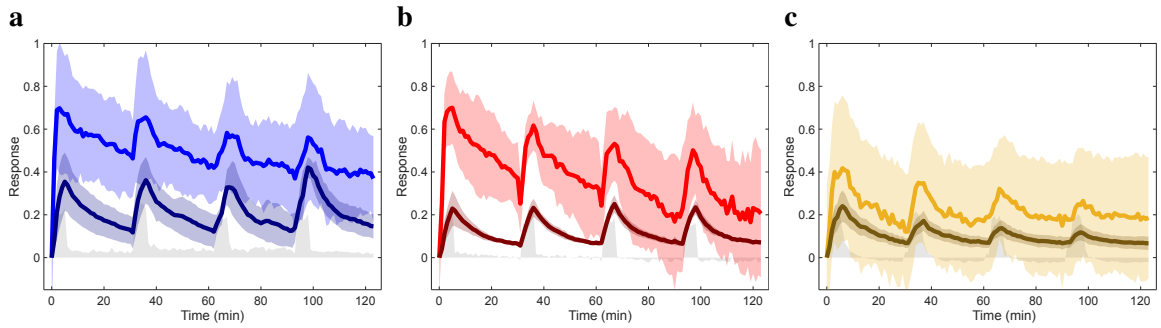

Figure 3.27 Temporal responses to train of EGF pulses upon experimental PTPRG/EGFR perturbations. Temporal traces of the fraction of ligand bound ([EGF-Alexa647]/[EGFR-mCitrine], dark colour) and phosphorylated EGFR estimated by PTB-mCherry translocation to the plasma membrane ([PTB-mCherry]/[EGFR-mCitrine], light colour) in live MCF7 cell. Data was acquired at 1 min intervals following 20 ng/mL 5P-EGF every 30 min. Average ± STD are shown with solid line and coloured bounds from single cell data upon a) siRNA-mediated knock-down of PTPRG treatment (n=5 cells, N=2), b) non-targeting siRNA treatment (n=4 cells, N=1), and c) ectopic Rab11^{S25N}-mTFP expression (n=16 cells, N=2).

relaxed back to the basal state after each EGF pulse (data not shown), presumably due to variability in PTPRG knock-down with respect to EGFR expression levels.

In the control cells, EGFRp response showed prolonged relaxation (Fig. 3.27b, light red) after each EGF pulse, reminiscent of the simulated response of a system poised close to the bifurcation, at the criticality point (Fig. 3.26b). This differed from the relaxation of the liganded EGF-EGFR that displayed a more monotonic decay function (Fig. 3.27b, dark red), which is due to depletion of liganded receptors from the plasma membrane by endocytosis. The more rapid activation of EGFRp with respect to EGF-EGFR at the onset of each pulse is a manifestation of the autocatalytic EGFR phosphorylation amplification. The prolonged relaxation shows that the EGFR-PTP system is organised close to the bistable region, narrowly escaping irreversible activation, enabling both sensing, as well as robust activation upon time-varying EGF stimuli.

EGFR abundance at the plasma membrane regulated by vesicular trafficking determines the sensing

This reflects on how the PTPRG/EGFR concentration ratio distinctly poises the system on the bifurcation diagram, and thus dictates the dynamics of the system (Fig. 3.24b). To perturb the positioning of PTPRG/EGFR at criticality we manipulated the spatial organisation of the system. As shown previously, ectopic expression of the dominant negative Rab11^{S25N}

mutant impairs the vesicular recycling of EGFR monomers. This generates a lower steady state plasma membrane abundance of EGFR, hence shifts the system to the right on the PTPRG/EGFR axis of the bifurcation diagram, to the monostable regime of operation. In this case, a dampened phosphorylation response, relative to the control case, to a train of EGF pulses was observed, where EGFRp followed closely the EGF-EGFR relaxation (Fig. 3.27c). This corroborated the previous findings that recycling of EGFR monomers is essential to generate a sufficient concentration at the plasma membrane for autocatalytic amplification of phosphorylation after each EGF pulse. This is apparent from the strong decrease in both autocatalytic EGFR activation, as well as the dampening of both EGFRp and EGF-EGFR in amplitude in the course of the experiment (Fig. 3.27c). In this case, the system loses its robustness in response to time varying stimuli and becomes more rapidly insensitive to upcoming EGF pulses.

How long the system can respond to time-varying EGF stimuli generally depends on the total amount of expressed EGFR that is recycling in the cell, and how quickly, thus how much of this pool is depleted by the unidirectional trafficking of liganded EGFR, which in turn is determined by the magnitude of EGF stimuli.

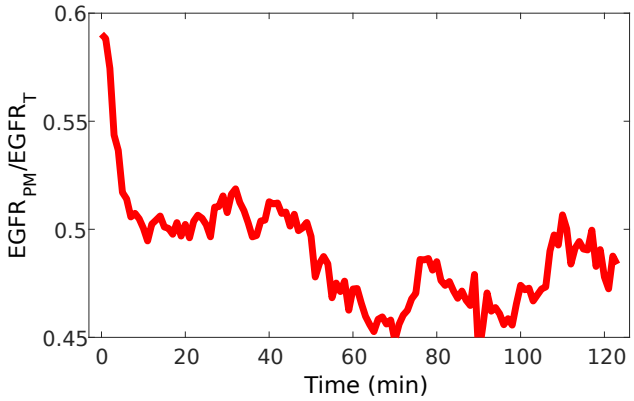

Figure 3.28 Temporal profile of the fraction of EGFR at the PM upon stimulation with train of EGF pulses. Average $[\text{EGFR-mCitrine}_]\text{PM}/[\text{EGFR-mCitrine}]_\text{T}$ is shown for the single cell data upon non-targeting siRNA treatment (n=4 cells, N=1), corresponding to Fig. 3.27b.

We also observe decrease in response amplitude and extent of phosphorylation in the control case (Fig. 3.27b). To examine whether this indeed comes as a result of the decrease in the dynamically maintained PM EGFR abundance, we plotted the fraction of EGFR at the plasma membrane, relative to the total abundance. Sharp decrease in relative concentration due to ligand-binding can be observed after the first pulse (0–30 min), followed by an additional decrease after the second pulse (30–60 min), after which the concentration did not

decrease further (see Fig. 3.28). This correlates with the decrease in amplitude and temporal extent in the phosphorylation response, more accentuated after the second pulse (Fig. 3.27b). Hence, the lowering steady state plasma membrane abundance of EGFR that shifts the system to the right on the PTPRG/EGFR axis of the bifurcation diagram (Fig. 3.24b), is pushing the system towards the fully monostable regime of operation.

Growth factor sensing is optimal at criticality

To understand the extended phosphorylation relaxation after each EGF pulse in the control case, we turn again to the state space representation of the system. The PTPRG/EGFR parameters poise it just outside of the irreversible bistable regime. There, next to the saddle node bifurcation point, the nullclines no longer intersect at three different points, but are rather very close to each other near the point where the high EGFR phosphorylation state and the unstable steady state merged and annihilated each other, while they still intersect on the other end at the low EGFR phosphorylation state (see Fig. 3.29a). The quasi-potential has very small derivative at this position because of the closeness of the nullclines, hence the landscape's slope is fairly flat there (see Fig. 3.29b). The system dynamics at this criticality point are slowed down as a result.

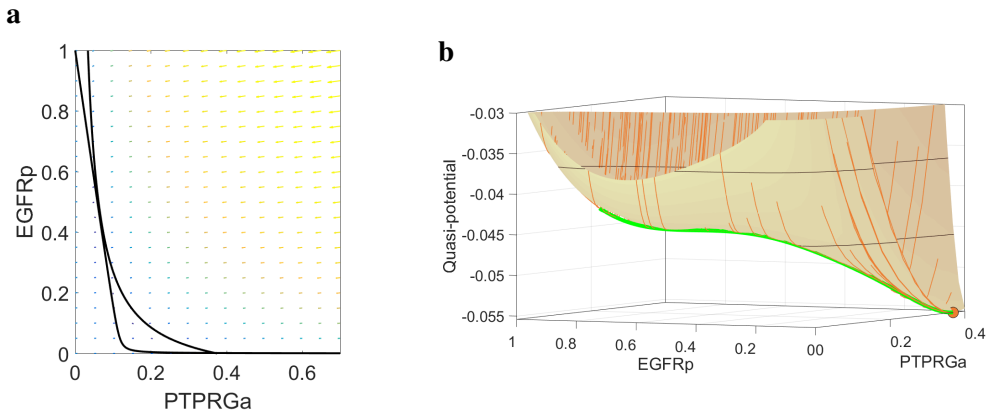

Figure 3.29 Behaviour of the EGFR-PTP system close to criticality. a) State space representation of the EGFR-PTP system as in Fig. 3.22a. The nullclines are very close to each other at (EGFRp≈0.5, PTPRGa≈0.1). b) Corresponding quasi-potential landscape showing the flat slope at the narrow part of the stable manifold near (EGFRp≈0.5, PTPRGa≈0.1). The green line outlines a trajectory from a high EGFRp initial state to the low EGFRp steady state.

Arrival of suprathreshold EGF pulse changes the topology of the state space by changing the nullclines and therefore the points of intersection. This dynamics was simulated using

a stochastic numerical simulation (see Methods) and three snapshots of a representative simulation are shown in Fig. 3.30. We can observe the history of the trajectory (green) overlaid over the current state space (Figs. 3.30a to 3.30c, left panels). Moreover, we can observe how the generated state space trajectory is translated into a temporal profile of extended EGFR phosphorylation, shaping the response dynamics (Figs. 3.30a to 3.30c, right panels).

From the initial state the system rapidly converged to the low phosphorylation stable steady state (EGFRp≈0, PTPRGa≈0.4) in the absence of stimulus (Fig. 3.30a). Signal presence altered the nullclines' intersection points which destabilised the occupied steady state (Fig. 3.30b). Thus, from the low EGFR phosphorylation monostable mode (single intersection point), through the bistable region (two intersection points), the state space topology settled at the high EGFR phosphorylation monostable mode (single intersection point, distant from the initial one) where the switch-like activation took place (EGFRp≈0.6, PTPRGa≈0.1; Fig. 3.30b). Finally, signal removal reinstated the initial state space topology, where the 'ghost attractor' captivated the relaxing system trajectory for a transient period of time before it continued to converge back to the initial stable steady state (EGFRp≈0, PTPRGa≈0.4, Fig. 3.30c). In this manner the signal processing with the metastable steady state is translated into a temporal EGFR phosphorylation profile with transient memory of the perceived stimulus. The EGF-induced topological changes in the state space provided such robust signal processing, while also allowing EGFR phosphorylation resetting to the ground state. The EGFR-PTP network thus acts as a sensory system of single cells, adopting these information processing capabilities in the vicinity of the saddle-node bifurcation point.

Another important feature of the dynamics of the network in which EGFR is embedded is to ensure maximal dynamic range of the receptor's phosphorylation response to minimal growth factor dose that activates the system (EGF-EGFR=0.15, see Fig. 3.24c). We therefore determined the amplitude of EGFR phosphorylation when changing the PTPRG/EGFR concentrations on the PM (Fig. 3.31). The maximal EGFR phosphorylation response amplitude gradually increased when decreasing the PTPRG/EGFR concentration as the system moved from the monostable towards the bistable regime, exhibiting a clear peak at the PTPRG/EGFR ratio that corresponds to the saddle-node bifurcation. After the bifurcation point, the discontinuous drop in amplitude corresponds to switching and maintenance of continuously high EGFR phosphorylation state in the bistable regime and further on the left in the preactivation regime. Organisation at criticality thus also ensures optimal dynamic range of EGFR phosphorylation response.

As mentioned before, reversibility is a crucial feature of the EGFR-PTP system when operating at criticality. Following the prolonged EGFR phosphorylation, the system converges

back to the resting state, and is therefore susceptible again to upcoming growth factor stimuli. However, should a subsequent pulse arrive within the duration of the transient memory, the response amplitude of the system will be low, comparable to the amplitude of a system that operates in an irreversible bistable regime (Fig. 3.31). To determine how is the response changed and how is the transient memory affected by a concurrent arrival of a second pulse, we performed stochastic simulations as in Fig. 3.30. The results show that with the second pulse the trajectory revisits the high EGFR phosphorylation steady state from the currently occupied narrow region of the stable manifold in state space, thus the response amplitude is indeed reduced (Fig. 3.32a). However, persistent memory is not developed, as the transient memory is extended by an additional prolonged duration.

This hypothesis was also tested experimentally by applying short pulses of 20 ng/mL EGF-Alexa647, as in the experiments from section 3.4.3. To determine the transient memory duration, a single EGF pulse, followed by a wash, was applied to single cells (Fig. 3.32b). The resulting dynamics showed a prolonged phosphorylation of 20–30 min after the pulse wash, in line with the previous results from Fig. 3.27b. When a second pulse was applied within the duration of the phosphorylation response (at ~15 min), the transient memory was extended accordingly, in agreement with our simulations (Fig. 3.32c).

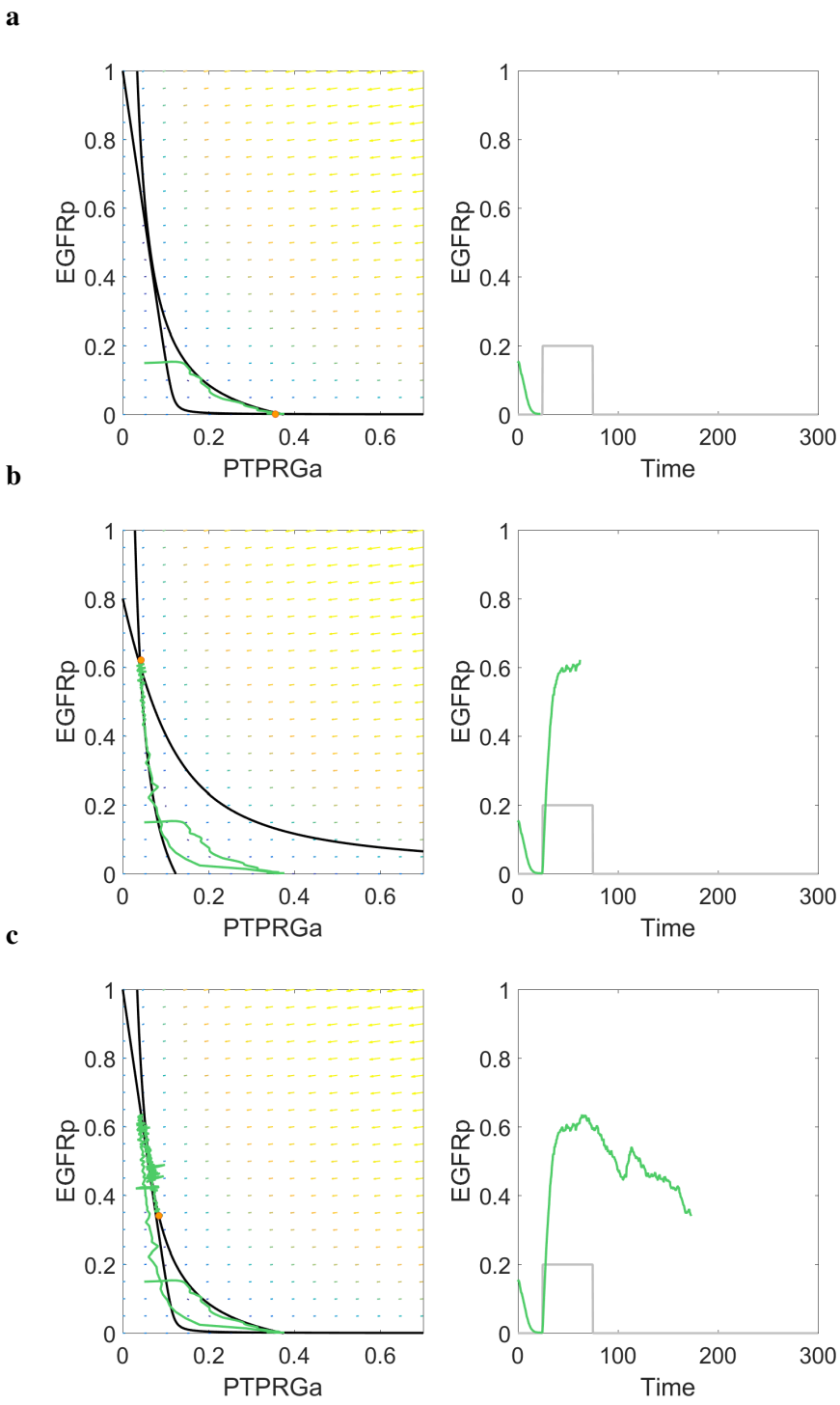

Figure 3.30 EGFR phosphorylation dynamics upon EGF pulse near criticality. Stochastic simulations of the EGFR-PTP system. Left panels show the state spaces as in Fig. 3.22a, in the corresponding regimes. Right panels show the corresponding EGFRp trajectory in time (green). The presence of the EGF pulse is shown with grey. a) Pre-stimulus: The trajectory converges to the resting phosphorylation state. b) Suprathreshold stimulus: Transition of the state trajectory to the high EGFR phosphorylation state. c) Pulse removal: The state is transiently maintained at a high EGFR phosphorylation level when the system returns to criticality, before it converges back to the ground state.

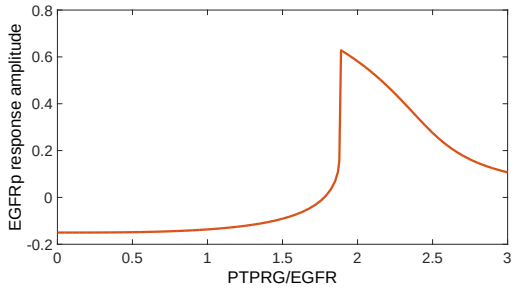

Figure 3.31 Phosphorylation response amplitude of unliganded EGFR. The maximal EGFR phosphorylation response amplitude is shown for different PTPRG/EGFR values, estimated by the difference in the responses from EGF-EGFR=0 to EGF-EGFR=0.15.

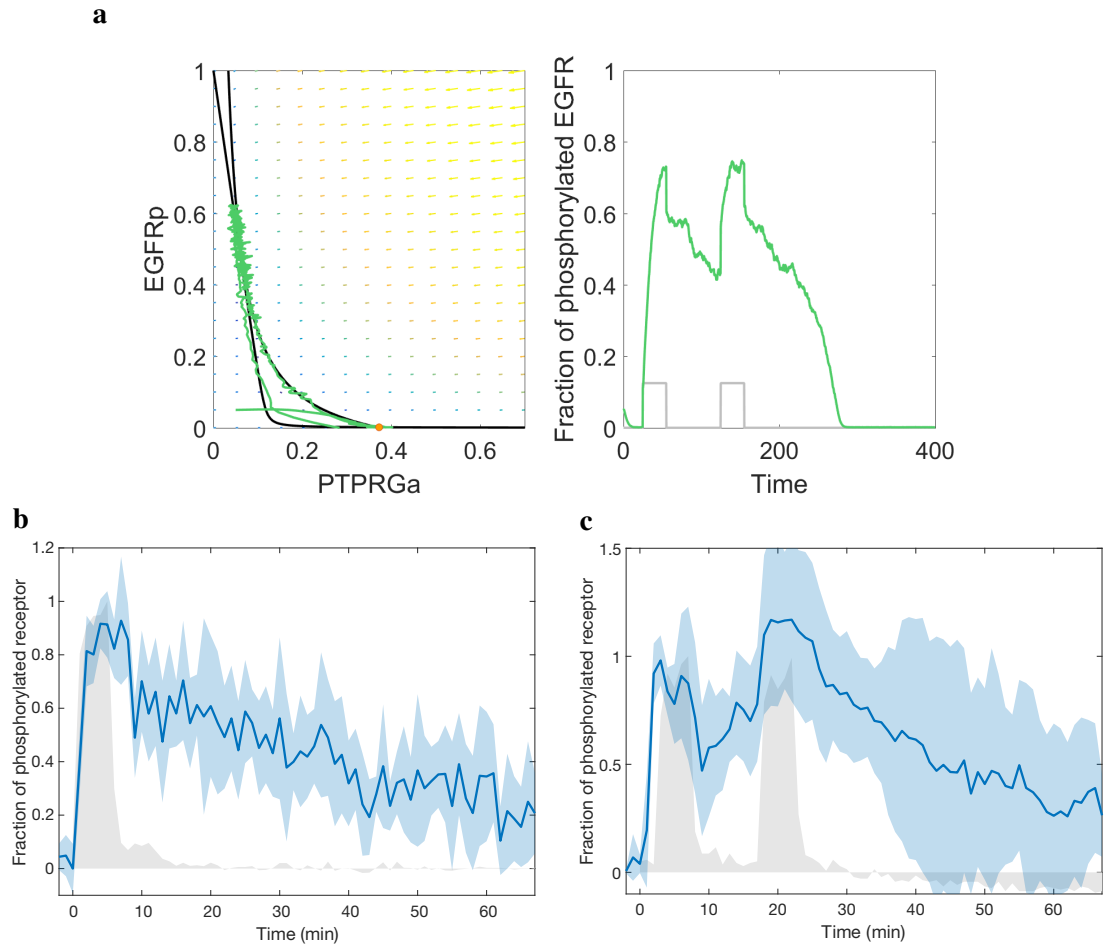

Figure 3.32 Temporal EGFR phosphorylation dynamics upon second EGF pulse in quick succession. a) Stochastic simulations of the EGFR-PTP system, as in Fig. 3.30. Temporal traces are shown of the fraction of phosphorylated EGFR-mCitrine upon b) single (n=7 cells, N=1) and c) double EGF-Alexa647 pulse stimulation (n=5 cells, N=1). Data was acquired and processed as in Fig. 3.27b.

Discussion

How cells sense and respond to extracellular EGF concentration is determined by the response dynamics of EGFR. This means that the spatial-temporal growth factor signal is translated through the EGFR phosphorylation, resulting in activity propagation downstream by recruitment of SH2- or PTB-containing effector proteins. EGFR's phosphorylation regulation is still not well understood, as the state transitions by the canonical and non-canonical activation mechanisms, as well as the coupling interactions with the phosphatases have not been well characterised on a systemic level. In this thesis, the main objective was to reveal how sensing and responding to time-varying EGF signals is determined by the EGFR-PTP network in which the receptor is embedded.

4.1 Vesicular trafficking of EGFR regulates its phosphorylation dynamics at the plasma membrane

To understand sensing, it was first necessary to determine which species are able to sense the time-varying cues and how is their cell surface abundance regulated to support the sensing. Upon occurrence of growth factor signal, fraction of the receptor population gets bound to ligand, ubiquitinated and depleted from the plasma membrane, that is determined by the ligand concentration. The remaining unliganded receptor fraction remained sensitive to upcoming stimuli. It is thus the unliganded EGFR that is sensing the time-varying cues, therefore the regulation of its plasma membrane abundance is crucial for maintaining or diminishing the sensing capabilities. The balance between plasma membrane and endosomal fractions of EGFR is determined by the spatial organisation of the receptor, and it is established via vesicular trafficking. It has been shown in a recent study that the unliganded EGFR undertakes a different trafficking route than the liganded EGFR upon activation at the plasma membrane and internalisation [8]. Whereas the liganded and ubiquitinated EGFR, tagged for degradation, from the early endosome traffics unidirectionally towards the late

endosome and lysosome, the unliganded EGFR exits the early endosome and recycles back to the plasma membrane through the recycling endosome. We distinguished between these two trafficking routes by exposing the cells with EGF stimulus of different duration - pulsed vs sustained stimulation. By tracking the spatial distribution of the receptors over time, we could observe plasma membrane depletion and accumulation in the perinuclear areas of the ligand-bound EGFR upon exposure to sustained EGF stimulation (Fig. 3.8c). On the other hand, transient stimulation emphasised the trafficking route of the unliganded receptor, which was rapidly recycling to repopulate the plasma membrane (Figs. 3.10d and 3.11). The effect of such spatial organisation came to light when studying the phopshorylation dynamics on the plasma membrane. The recycling of the unliganded EGFR upon 5P-EGF, which increases the plasma membrane abundance, resulted in prolonged phosphorylation there, due to triggering of the autocatalytic mechanism of activation (Fig. 3.12). On the other hand, with S-EGF the monomers engaged in ligand-binding and maintained constant and elevated levels of phosphorylation.

4.2 Autocatalytically activated EGFR forms distinct coupling interactions with PTPs on different membranes

To understand the phosphorylation dynamics, the regulation network in which EGFR is embedded was studied. On one hand, the activation mechanisms triggered phosphorylation of EGFR across the plasma membrane. These include the canonical model for EGFR activation of the ligand-bound dimers via trans-phosphorylation [44, 139], as well as the autocatalytic, autonomous and ligand-bound-induced activation of the unliganded EGFR [76, 77]. Unliganded EGFR molecules can initiate and propagate the signal among the receptor population, even in the absence of stimulus [46]. The phosphorylation propagation has been directly observed initially in [48], where local EGF stimulation led to global EGFR phosphorylation across the plasma membrane. This non-linear self-amplification is a manifestation of the autocatalytic activation of EGFR. Using single-cell dose-response analysis we characterised the EGFR phosphorylation response to increasing doses of EGF. This allowed to establish that the autocatalytic activation of the unliganded receptors indeed significantly enhanced the EGFR phosphorylation in the low doses stimulation scenarios. While the ligand-bound fraction of receptors contributed linearly to the increase of phosphorylation, the unliganded receptors introduced non-linearity and thus generated an ultrasensitive response to EGF, rather than a graded one (Fig. 3.5). The unliganded receptors can get trans-phosphorylated in a transient complex by another unliganded receptor - comprising the autonomous or autocatalytic activation, or by a ligand-bound receptor, that promotes the autocatalysis at low

dose. The basis for such phosphorylation propagation through autocatalytic EGFR activation is most likely the phosphorylation of the regulatory Y845 in the kinase activation loop, which stabilises the active conformation of the receptor [47, 8]. This could be established by direct autophosphorylation in transient receptor complexes or by indirect phosphorylation via Src [151] that is in turn activated by EGFR [152]. A recent study revealed in detail the molecular basis behind the autocatalytic activation mechanism [153].

EGFR response dynamics, however, is not solely determined by its activation mechanism, but results also from the coupling interactions with the PTPs. It has been shown previously, for example, that a double negative EGFR-PTP feedback determines the ultrasensitive lateral phosphorylation propagation mechanism [76, 77]. Using dynamical systems modelling we uncovered the role of the plasma membrane-localised PTPRG as such regulator, coupling with EGFR in a toggle switch manner to shape its responsiveness to EGF (Fig. 3.17a). This coupling is mediated by the phospho-EGFR-induced H_2O_2 production near the plasma membrane, that oxidised the catalytic cysteine of PTPRG, thereby making it inactive. Inducing NOX complex inhibition therefore resulted in decreased EGFR phosphorylation response, following from the increased PTPRG activity (Fig. 3.17b). The mutual inhibition of EGFR and PTPRG gave rise to a bistable response, where two stable solutions exist simultaneously in the system - one where EGFR 'dominates' over PTPRG and vice versa. Therefore, with low EGF dose PTPRG dominates the EGFR-PTPRG balance and inhibits the autocatalytic activity of EGFR, while given high enough stimulus, EGFR overcomes the inhibition by PTPRG and propagates the signal laterally. The critical EGF dose upon which the system exhibits discontinuous switch-like activation sets an activation threshold for EGFR. This toggle switch interaction motif between EGFR and PTPRG practically implements an activation safeguarding filter for EGFR, as stimuli with low signal-to-noise ratio are deemed insufficient for triggering a phosphorylation response and are thus filtered out. Due to bistability, however, irreversible activation that is maintained even after removal of the signal, occurs as an adversary side effect. Permanent memory is formed in the network, as EGFR maintains its phosphorylation level as a result of a previously perceived signal.

A question arose therefore as to how is this vulnerability overcome in order for the signal to be terminated. We identified that the negative regulation through PTPRJ at the plasma membrane helps in pushing the system towards reversible activation that is necessary to sense upcoming growth factor cues (Fig. 3.18a). It modulates the bistable response established by the double-negative feedback between PTPRG and EGFR. This was corroborated by a knock-down of PTPRJ, which exposed the underlying switch-like activation (Fig. 3.18c). The internalisation following the activation removes the active receptors from the plasma membrane where the routes of liganded and unliganded EGFR diverge. This promotes

the interaction with the ER-bound PTPN2, which exerts its strong effect on EGFR by dephosphorylating the recycling monomers, effectively generating a spatially established negative feedback. Thus, a flatter EGFR phosphorylation response was observed upon ectopic expression of PTPN2 (Fig. 3.20).

4.2.1 Spatial segregation of PTPs allows signal processing

The autocatalytic activation of the unliganded EGFR is coupled to a mutual inhibition with PTPRG at the plasma membrane, whose bistable switch-like response permits a threshold activation of EGFR. This interaction is spatially unified with the EGFR-PTPN2 interactions through the recycling of the EGFR monomers. The stronger dephosphorylating PTP activities in the perinuclear areas reset the monomeric EGFR activity states before they return to the plasma membrane. The spatial segregation of high PTPN2 activity from the plasma membrane ensures that EGFR phosphorylation is not immediately suppressed upon exposure to ligand. This is also in line with the relatively low mRNA expression of the RPTPs with respect to PTPN2 (PTPR/ER-PTP mRNA 0.045, [123]). The system therefore can initiate signalling due to a clear segregation of tyrosine kinase and phosphatase activity and shuts down by their co-localisation over time due to vesicular traffic. Such stronger endosomal dephosphorylation over time was observed by comparing the plasma membrane vs endosomal distribution between Fig. 3.8e and Fig. 3.8c upon S-EGF, and between Fig. 3.10e and Fig. 3.10c upon 5P-EGF. Similar effect was observed in [8], where the increasing concentration of PTP1B towards the perinuclear area led to a decreasing EGFR spatial activity gradient.

4.2.2 Spatially unified EGFR-PTP coupling interactions establish growth factor sensing network

The spatial organisation of the system is summarised in Fig. 4.1. Unification of the interactions of EGFR with the PTPs on different membranes establishes a system for growth factor sensing: the autocatalytic EGFR monomers coupled with the RPTPs in a double-negative-feedback fashion amplify the response after a signal threshold, while upon internalisation their phosphorylation state is reset as a result of the interactions with the ER-bound PTPN2, before they recycle back to the plasma membrane to respond to upcoming stimuli. Presence of growth factor in the environment re-routes ligand-bound EGFR molecules from the unliganded recycling to the liganded-ubiquitinated unidirectional degradation route and thus decreases the total concentration of EGFR at the plasma membrane. Dynamically

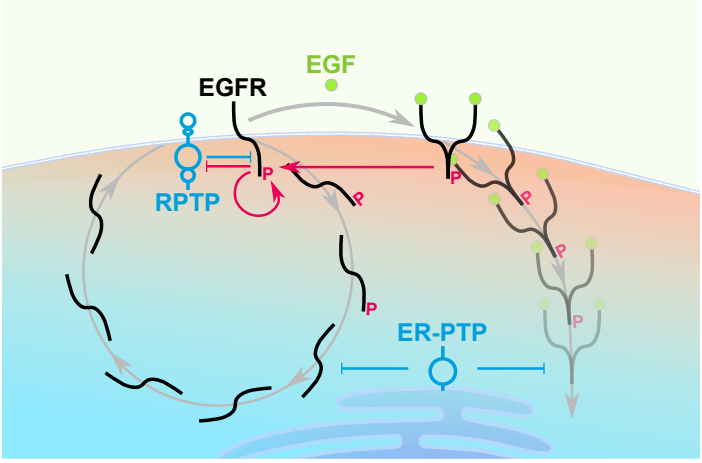

Figure 4.1 Spatial unification of the EGFR-PTP network motifs determines growth factor sensing. Monomeric EGFR (left) is converted to dimeric one (right) upon binding to EGF and undertakes the unidirectional route towards perinuclear degradation. The RPTPs at the plasma membrane are coupled to the autocatalytic EGFR monomers in a double-negative-feedback fashion to set a switch-like amplified activation. Constitutive recycling unifies these interactions to the ones with the ER-bound PTPs to reset the phosphorylation state of EGFR and enhance the sensing capabilities of the system.

maintaining the plasma membrane abundance of the monomers via vesicular trafficking is therefore crucial feature of the time-varying growth factor sensing system.

4.3 The operation regime of the unified EGFR-PTP network depends on its positioning in parameter space

The EGFR-PTPRG interaction motif was revealed as the central unit that dictates the ultra-sensitivity and reversibility of the response to EGF. Crucially, they are determined by the presence of bistability, which is conditioned on the existence of non-linearities of both - the autocatalytic activation as well as the inhibition via double-negative feedback (Fig. 3.25a). The other PTPs modulate the extent of the bistability region, shifting the response away from irreversibility (Figs. 3.25b and 3.25d). Therefore, how EGFR will respond to EGF stimuli depends on the PTPRG/EGFR abundance ratio at the plasma membrane, i.e. the operation regime of the system depends on its positioning in parameter space (Fig. 3.24). High EGFR- or low PTPRG-abundance set the system in a preactivation regime in the extreme case, or a bistable regime where a switch-like, but irreversible activation can take place. This makes EGFR unresponsive to the subsequent changes in EGF concentration, thus the sensitivity of the system is greatly diminished while the phosphorylation is sustained (Fig. 3.26a). On

the other end of the PTPRG/EGFR ratio, low EGFR- or high PTPRG-abundance maintain reversibility with reduced autocatalytic amplification (Fig. 3.26c). However, optimal growth factor sensing of non-stationary signals must combine the essential features of the responses presented at both ends: switch-like amplified activation and reversibility (Fig. 3.26b). We identified that this is achieved on the interface between the two regions, close to the saddle-node bifurcation point that marks the transition from bistability to monostability.

4.3.1 Growth factor signal processing is optimal at criticality

State space and bifurcation analysis revealed that the processing of time-varying input at this criticality point operates via different topological transitions in state space (Fig. 3.30). In the absence of stimulus the system is monostable, with the low EGFR phosphorylation being the single stable steady state. Being just outside of the bistability region in parameter space places the nullclines close to each other at the high EGFR phosphorylation end of the state space. When suprathreshold input is attained the topology of the state space contains only the single active stable steady state, and thus the system trajectory converges there. Removal of the input reverts the topology of the state space through bistability, back at monostability with low EGFR phosphorylation, in the vicinity of the saddle-node bifurcation. The closeness of the nullclines at the high EGFR phosphorylation end of the state space established a 'ghost' attractor where a transient memory of the stimulus was retained that was manifested with prolonged but reversible phosphorylation (Fig. 3.26b). This implies that the cells do not operate using only the stable attractors to encode information about the extracellular state, but rather that they can process and integrate time-varying signals with the state space trajectories using metastable states. The dynamics of these trajectories are translated into temporal phosphorylation responses, as showcased in Fig. 3.30. Therefore, for signalling networks that are organised at criticality it is necessary to consider how the metastable states affect the state space trajectories that guide the temporal phosphorylation response, rather than only consider the positions of the stable attractors.

We showed that the phosphorylation response amplitude of the unliganded EGFR was maximal near the saddle-node bifurcation (Fig. 3.31). Increase of the PTPRG/EGFR ratio moves the system fully into the monostable regime where the autocatalytic activation is reduced and the response amplitude is diminished, while decrease of PTPRG/EGFR diminishes the response amplitude upon subsequent stimuli. In this thesis it was demonstrated experimentally that the EGFR-PTP system operates close to criticality, by stimulating the cells with train of EGF pulses (Fig. 3.27b). The response showed prolonged and reversible EGFR phosphorylation dynamics, matching the theoretical results obtained in Fig. 3.26b. The transient memory duration was observed at about 20–30 min upon 5 min EGF stimulation.

Processing of time-varying signals with a metastable state equips the system with unique features. Temporal dependencies are inherent properties of time-varying signals, and having a sensing system with short-term memory, while still maintaining responsiveness provides plasticity in the processing dynamics. Hence, while on one hand, the metastable state allows the cell to temporarily maintain the signalling state from the past, a topological change in state space arising from a signal change will still induce a proper response (Fig. 3.32). As EGFR activation by EGF leads to PI3K- and Rac1-mediated activation of the Rho-GTPases and coupling to the cell motility machinery [24, 25], one could imagine that directed cell motion in a complex spatial-temporal pattern of a growth factor signal is indeed guided by such transient memory in receptor phosphorylation and cell polarity.

4.3.2 Dynamical organisation of EGFR abundance at the PM is critical for the phosphorylation response

Administering of periodic EGF pulses in time interval of 30 min resulted in reducing response amplitude over time (Fig. 3.27b). This follows from the periodic internalisation of the ligand-bound receptors when EGF is present in the environment (Fig. 4.1). As they are redirected to the lysosome, thus effectively removed from the sensing system, the total EGFR abundance at the plasma membrane is decreased (Fig. 3.28). This depletion effectively pushes the system towards higher PTPRG/EGFR parameter values, which causes shift to the monostable operation regime with lower response amplitude (Fig. 3.24b).

Thus, to sustain optimal information processing capabilities, the system must maintain organisation at the critical transition between the two opposed regimes. The PTPRG/EGFR ratio must be kept in a defined interval near the saddle-node bifurcation. The unidirectional removal of EGFR upon ligand binding disrupts the PTPRG/EGFR abundance at the plasma membrane, which weakens the sensing capabilities. The optimal ratio can be restored by protein synthesis in the long term, which imposes a refractory period for the cell. However, to ensure rapid recovery to the optimal functioning of the network after growth factor stimulation, the PTPRG/EGFR parameter organisation must be dynamically maintained via vesicular trafficking. It is possible to envision that such feedback regulation can be implemented through a fluctuation sensing mechanism, since the fluctuation frequency around the basal EGFR phosphorylation state depends on the positioning of the system in parameter space and can therefore be employed as a readout for deviation from the criticality point. When moving away from the saddle-node bifurcation point, the low-frequency fluctuations could activate a downstream effector (Akt is one such candidate) using a low-pass filter, that in turn promotes EGFR recycling, thereby maintaining EGFR concentration

at the plasma membrane such that the system remains close to criticality. However, this will likely function only up to a certain amplitude or frequency of stimulation, as observed from the weakening response in the cells from the control case (Fig. 3.27b), after which it must rely on expression-dependent replenishing of plasma membrane EGFR.

Growth factor sensing and responding of the EGFR-PTP network can be influenced in multiple ways in aberrant and normal signalling. Mutations that affect the activity of EGFR can increase its signalling and proliferation in tumours, such as the L834R/T766M mutation in lung cancer [154]. Apart from affecting the biochemical properties of the molecules, the network can be regulated by changing the abundances of the proteins as well, as argumented above. High EGFR concentrations has been shown to result in aberrant signalling in the absence of stimulus [46]. Similarly, we showed here that siRNA-mediated knock-down of the tumour suppressor PTPRG [155] affected strongly the sensing capabilities of the system, as the exposure to periodic pulses of EGF resulted in sustained activity of EGFR (Fig. 3.27a). On the other hand, decreasing the plasma membrane abundance of EGFR, by blocking the exit of the EGFR monomers from the recycling endosome with the dominant negative $\text{Rab11}^{\text{S25N}}$ mutant, resulted in diminished phosphorylation response to the periodic EGF stimulation (Fig. 3.27c). Changes of PTPRG/EGFR plasma membrane abundance via vesicular trafficking is thus an important mechanism through which context-dependent regulation of the network can be dynamically manipulated. It has been shown for example that environmental inputs, such as cell-cell contact, can affect the rate of recycling and thus influence the cellular response to EGF stimulation, generating contextual plasticity in growth factor signalling [156]. Eph-induced Akt activation by ephrin, normally present on a neighbouring cell surface, decreases the recycling rate [156], which lowers the EGFR concentration on the plasma membrane, as well as the strength of the negative feedback from PTPN2. This has implications in collective dynamics of cells, such as in wound healing [19] and collective cell migration [157, 158], where cells exhibit more protrusive behaviour in absence of cell-cell contact, while they are less migratory otherwise.

In summary, growth factor receptors are the ‘sensory units’ of the cell that perceive changes in extracellular growth factor stimuli, leading to a variety of cellular responses. In this thesis it was studied how the growth factor sensing properties arise from the dynamics of the network in which EGFR is embedded, and to an extent how the cells generate versatility in their responses using networks with small number of components. We identified how the coupling interactions with the major dephosphorylating PTP activities shape the phosphorylation response of EGFR to EGF, and how the vesicular trafficking unifies them spatially to establish the sensing network architecture. Furthermore, the unique properties and implications of the sensing and responding dynamics of the network were established.

By doing so we gained understanding of the interplay and dependency between the multiple levels, starting from the individual protein interactions, through the dynamics of the unified network, to the sensing system's function and operation.

Bibliography

[1] Ralph A Bradshaw and Edward A Dennis. Cell signaling: Yesterday, today, and tomorrow. In *Handbook of Cell Signaling (Second Edition)*, pages 1–4. Elsevier, 2009.

[2] Hiroaki Kitano. Systems biology: toward system-level understanding of biological systems. *Foundations of systems biology*, pages 1–36, 2001.

[3] David Marr and Tomaso Poggio. From understanding computation to understanding neural circuitry. 1976.

[4] David Marr. *Vision: A Computational Investigation Into*. WH Freeman, 1982.

[5] Boris N Kholodenko, John F Hancock, and Walter Kolch. Signalling ballet in space and time. *Nature reviews Molecular cell biology*, 11(6):414, 2010.

[6] CJ Marshall. Specificity of receptor tyrosine kinase signaling: transient versus sustained extracellular signal-regulated kinase activation. *Cell*, 80(2):179–185, 1995.

[7] Silvia DM Santos, Peter J Verveer, and Philippe IH Bastiaens. Growth factor-induced mapk network topology shapes Erk response determining PC-12 cell fate. *Nature cell biology*, 9(3):324, 2007.

[8] Martin Baumdick, Yannick Brüggemann, Malte Schmick, Georgia Xouri, Ola Sabet, Lloyd Davis, Jason W Chin, and Philippe IH Bastiaens. EGF-dependent re-routing of vesicular recycling switches spontaneous phosphorylation suppression to EGFR signaling. *Elife*, 4, 2015.

[9] Alan Mathison Turing. The chemical basis of morphogenesis. *Philosophical Transactions of the Royal Society of London. Series B, Biological Sciences*, 237(641):37–72, 1952.

[10] Howard C Berg and Edward M Purcell. Physics of chemoreception. *Biophysical journal*, 20(2):193–219, 1977.

[11] Christopher C Govern and Pieter Rein ten Wolde. Optimal resource allocation in cellular sensing systems. *Proceedings of the National Academy of Sciences*, 111(49):17486–17491, 2014.

[12] Kai Wang, Wouter-Jan Rappel, Rex Kerr, and Herbert Levine. Quantifying noise levels of intercellular signals. *Physical Review E*, 75(6):061905, 2007.

[13] Thierry Mora and Ned S Wingreen. Limits of sensing temporal concentration changes by single cells. *Physical review letters*, 104(24):248101, 2010.

[14] Christopher C Govern and Pieter Rein ten Wolde. Fundamental limits on sensing chemical concentrations with linear biochemical networks. *Physical review letters*, 109(21):218103, 2012.

[15] Dan R Robinson, Yi-Mi Wu, and Su-Fang Lin. The protein tyrosine kinase family of the human genome. *Oncogene*, 19(49):5548, 2000.

[16] Mark A Lemmon and Joseph Schlessinger. Cell signaling by receptor tyrosine kinases. *Cell*, 141(7):1117–1134, 2010.

[17] Melany J Wagner, Melissa M Stacey, Bernard A Liu, and Tony Pawson. Molecular mechanisms of SH2-and PTB-domain-containing proteins in receptor tyrosine kinase signaling. *Cold Spring Harbor perspectives in biology*, 5(12):a008987, 2013.

[18] Maria Sibilia, Renate Kroismayr, Beate M Lichtenberger, Anuradha Natarajan, Manfred Hecking, and Martin Holcmann. The epidermal growth factor receptor: from development to tumorigenesis. *Differentiation*, 75(9):770–787, 2007.

[19] X Yu Fu-Shin, Jia Yin, Keping Xu, and Jenny Huang. Growth factors and corneal epithelial wound healing. *Brain research bulletin*, 81(2-3):229–235, 2010.

[20] Maria Sibilia and Erwin F Wagner. Strain-dependent epithelial defects in mice lacking the EGF receptor. *Science*, 269(5221):234–238, 1995.

[21] Päivi J Miettinen, Joel E Berger, Juanito Meneses, Yume Phung, Roger A Pedersen, Zena Werb, and Rik Derynck. Epithelial immaturity and multiorgan failure in mice lacking epidermal growth factor receptor. *Nature*, 376(6538):337, 1995.

[22] Stanley Cohen, G Carpenter, and L King. Epidermal growth factor-receptor-protein kinase interactions. co-purification of receptor and epidermal growth factor-enhanced phosphorylation activity. *Journal of Biological Chemistry*, 255(10):4834–4842, 1980.

[23] Roy S Herbst. Review of epidermal growth factor receptor biology. *International Journal of Radiation Oncology• Biology• Physics*, 59(2):S21–S26, 2004.

[24] Reina E Itoh, Etsuko Kiyokawa, Kazuhiro Aoki, Teruko Nishioka, Tetsu Akiyama, and Michiyuki Matsuda. Phosphorylation and activation of the Rac1 and Cdc42 GEF Asef in A431 cells stimulated by EGF. *Journal of cell science*, 121(16):2635–2642, 2008.

[25] Samer Hanna and Mirvat El-Sibai. Signaling networks of Rho GTPases in cell motility. *Cellular signalling*, 25(10):1955–1961, 2013.

[26] Harley I Kornblum, Raymond Hussain, Jane Wiesen, Paivi Miettinen, Shelley D Zurcher, Kit Chow, Rik Derynck, and Zena Werb. Abnormal astrocyte development and neuronal death in mice lacking the epidermal growth factor receptor. *Journal of neuroscience research*, 53(6):697–717, 1998.

[27] Maria Sibilia, Joachim P Steinbach, Laura Stingl, Adriano Aguzzi, and Erwin F Wagner. A strain-independent postnatal neurodegeneration in mice lacking the EGF receptor. *The EMBO journal*, 17(3):719–731, 1998.

[28] Maria Sibilia, Bettina Wagner, Astrid Hoebertz, Candace Elliott, Silvia Marino, Wolfram Jochum, and Erwin F Wagner. Mice humanised for the EGF receptor display hypomorphic phenotypes in skin, bone and heart. *Development*, 130(19):4515–4525, 2003.

[29] Ke Wang, Hiroaki Yamamoto, Jennie R Chin, Zena Werb, and Thiennu H Vu. Epidermal growth factor receptor-deficient mice have delayed primary endochondral ossification because of defective osteoclast recruitment. *Journal of Biological Chemistry*, 279(51):53848–53856, 2004.

[30] Ryo Iwamoto, Satoru Yamazaki, Masanori Asakura, Seiji Takashima, Hidetoshi Hasuwa, Kenji Miyado, Satoshi Adachi, Masafumi Kitakaze, Koji Hashimoto, Gerhard Raab, et al. Heparin-binding EGF-like growth factor and erbB signaling is essential for heart function. *Proceedings of the National Academy of Sciences*, 100(6):3221–3226, 2003.

[31] Bianca S Verbeek, Sabrina S Adriaansen-Slot, Thea M Vroom, Thomas Beckers, and Gert Rijksen. Overexpression of EGFR and c-erbB2 causes enhanced cell migration in human breast cancer cells and NIH3T3 fibroblasts. *FEBS letters*, 425(1):145–150, 1998.

[32] Aline Appert-Collin, Pierre Hubert, Gérard Crémel, and Amar Bennasroune. Role of ErbB receptors in cancer cell migration and invasion. *Frontiers in pharmacology*, 6:283, 2015.

[33] Axel Ullrich, Lisa Coussens, Joel S Hayflick, Thomas J Dull, Alane Gray, AW Tam, J Lee, Y Yarden, Towia A Libermann, Joseph Schlessinger, et al. Human epidermal growth factor receptor cDNA sequence and aberrant expression of the amplified gene in A431 epidermoid carcinoma cells. *Nature*, 309(5967):418, 1984.

[34] Thomas J Lynch, Daphne W Bell, Raffaella Sordella, Sarada Gurubhagavatula, Ross A Okimoto, Brian W Brannigan, Patricia L Harris, Sara M Haserlat, Jeffrey G Supko, Frank G Haluska, et al. Activating mutations in the epidermal growth factor receptor underlying responsiveness of non–small-cell lung cancer to gefitinib. *New England Journal of Medicine*, 350(21):2129–2139, 2004.

[35] Nicola Normanno, Antonella De Luca, Caterina Bianco, Luigi Strizzi, Mario Mancino, Monica R Maiello, Adele Carotenuto, Gianfranco De Feo, Francesco Caponigro, and David S Salomon. Epidermal growth factor receptor (EGFR) signaling in cancer. *Gene*, 366(1):2–16, 2006.

[36] Roel GW Verhaak, Katherine A Hoadley, Elizabeth Purdom, Victoria Wang, Yuan Qi, Matthew D Wilkerson, C Ryan Miller, Li Ding, Todd Golub, Jill P Mesirov, et al. Integrated genomic analysis identifies clinically relevant subtypes of glioblastoma characterized by abnormalities in PDGFRA, IDH1, EGFR, and NF1. *Cancer cell*, 17(1):98–110, 2010.

[37] Jaime Acquaviva, Hyun Jung Jun, Julie Lessard, Rolando Ruiz, Haihao Zhu, Melissa Donovan, Steve Woolfenden, Abraham Boskovitz, Ami Raval, Roderick T Bronson, et al. Chronic activation of wild-type epidermal growth factor receptor and loss of

Cdkn2a cause mouse glioblastoma formation. *Cancer research*, 71(23):7198–7206, 2011.

[38] John Mendelsohn. Targeting the epidermal growth factor receptor for cancer therapy. *Journal of clinical oncology*, 20(18s):1s–13s, 2002.

[39] Erez M Bublil and Yosef Yarden. The EGF receptor family: spearheading a merger of signaling and therapeutics. *Current opinion in cell biology*, 19(2):124–134, 2007.

[40] Yosef Yarden and Gur Pines. The ERBB network: at last, cancer therapy meets systems biology. *Nature reviews Cancer*, 12(8):553, 2012.

[41] Kathryn M Ferguson, Mitchell B Berger, Jeannine M Mendrola, Hyun-Soo Cho, Daniel J Leahy, and Mark A Lemmon. EGF activates its receptor by removing interactions that autoinhibit ectodomain dimerization. *Molecular cell*, 11(2):507–517, 2003.

[42] Jessica P Dawson, Mitchell B Berger, Chun-Chi Lin, Joseph Schlessinger, Mark A Lemmon, and Kathryn M Ferguson. Epidermal growth factor receptor dimerization and activation require ligand-induced conformational changes in the dimer interface. *Molecular and cellular biology*, 25(17):7734–7742, 2005.

[43] Yongjian Huang, Shashank Bharill, Deepti Karandur, Sean M Peterson, Morgan Marita, Xiaojun Shi, Megan J Kaliszewski, Adam W Smith, Ehud Y Isacoff, and John Kuriyan. Molecular basis for multimerization in the activation of the epidermal growth factor receptor. *Elife*, 5, 2016.

[44] Xuewu Zhang, Jodi Gureasko, Kui Shen, Philip A Cole, and John Kuriyan. An allosteric mechanism for activation of the kinase domain of epidermal growth factor receptor. *Cell*, 125(6):1137–1149, 2006.

[45] Gil Levkowitz, Hadassa Waterman, Eli Zamir, Zvi Kam, Shlomo Oved, Wallace Y Langdon, Laura Beguinot, Benjamin Geiger, and Yosef Yarden. c-Cbl/Sli-1 regulates endocytic sorting and ubiquitination of the epidermal growth factor receptor. *Genes & development*, 12(23):3663–3674, 1998.

[46] Eric K Rowinsky. The erbB family: targets for therapeutic development against cancer and therapeutic strategies using monoclonal antibodies and tyrosine kinase inhibitors. *Annu. Rev. Med.*, 55:433–457, 2004.

[47] Yibing Shan, Michael P Eastwood, Xuewu Zhang, Eric T Kim, Anton Arkhipov, Ron O Dror, John Jumper, John Kuriyan, and David E Shaw. Oncogenic mutations counteract intrinsic disorder in the EGFR kinase and promote receptor dimerization. *Cell*, 149(4):860–870, 2012.

[48] Peter J Verveer, Fred S Wouters, Andrew R Reynolds, and Philippe IH Bastiaens. Quantitative imaging of lateral ErbB1 receptor signal propagation in the plasma membrane. *Science*, 290(5496):1567–1570, 2000.

[49] Tetsuo Yamazaki, Kristien Zaal, Dale Hailey, John Presley, Jennifer Lippincott-Schwartz, and Lawrence E Samelson. Role of Grb2 in EGF-stimulated EGFR internalization. *Journal of cell science*, 115(9):1791–1802, 2002.

[50] Joshua Z Rappoport and Sanford M Simon. Endocytic trafficking of activated EGFR is AP-2 dependent and occurs through preformed clathrin spots. *J Cell Sci*, 122(9):1301–1305, 2009.

[51] Lai Kuan Goh, Fangtian Huang, Woong Kim, Steven Gygi, and Alexander Sorkin. Multiple mechanisms collectively regulate clathrin-mediated endocytosis of the epidermal growth factor receptor. *The Journal of cell biology*, 189(5):871–883, 2010.

[52] Sara Sigismund, Elisabetta Argenzio, Daniela Tosoni, Elena Cavallaro, Simona Polo, and Pier Paolo Di Fiore. Clathrin-mediated internalization is essential for sustained EGFR signaling but dispensable for degradation. *Developmental cell*, 15(2):209–219, 2008.

[53] Wendy S Garrett, Li-Mei Chen, Ruth Kroschewski, Melanie Ebersold, Shannon Turley, Sergio Trombetta, Jorge E Galán, and Ira Mellman. Developmental control of endocytosis in dendritic cells by Cdc42. *Cell*, 102(3):325–334, 2000.

[54] Sara Sigismund, Veronica Algisi, Gilda Nappo, Alexia Conte, Roberta Pascolutti, Alessandro Cuomo, Tiziana Bonaldi, Elisabetta Argenzio, Lisette GGC Verhoef, Elena Maspero, et al. Threshold-controlled ubiquitination of the EGFR directs receptor fate. *The EMBO journal*, 32(15):2140–2157, 2013.

[55] Fangtian Huang, Donald Kirkpatrick, Xuejun Jiang, Steven Gygi, and Alexander Sorkin. Differential regulation of EGF receptor internalization and degradation by multiubiquitination within the kinase domain. *Molecular cell*, 21(6):737–748, 2006.

[56] Bruce Alberts, Alexander Johnson, Julian Lewis, Martin Raff, Keith Roberts, and Peter Walter. *Molecular biology or the cell. Sixth edition*. Garland Science: New York and Abingdon, UK, 2014.

[57] Marko Jovic, Mahak Sharma, Juliati Rahajeng, and Steve Caplan. The early endosome: a busy sorting station for proteins at the crossroads. *Histology and histopathology*, 25(1):99, 2010.

[58] Roberto Villaseñor, Yannis Kalaidzidis, and Marino Zerial. Signal processing by the endosomal system. *Current opinion in cell biology*, 39:53–60, 2016.

[59] Jean Gruenberg. The endocytic pathway: a mosaic of domains. *Nature reviews Molecular cell biology*, 2(10):721, 2001.

[60] Frederick R Maxfield and Timothy E McGraw. Endocytic recycling. *Nature reviews Molecular cell biology*, 5(2):121, 2004.

[61] Ira Mellman. Endocytosis and molecular sorting. *Annual review of cell and developmental biology*, 12(1):575–625, 1996.

[62] Kristi G Bache, Camilla Raiborg, Anja Mehlum, and Harald Stenmark. STAM and Hrs are subunits of a multivalent ubiquitin-binding complex on early endosomes. *Journal of Biological Chemistry*, 278(14):12513–12521, 2003.

[63] Harald Stenmark and Vesa M Olkkonen. The Rab GTPase family. *Genome biology*, 2(5):reviews3007–1, 2001.

[64] Fawaz G Haj, Peter J Verveer, Anthony Squire, Benjamin G Neel, and Philippe IH Bastiaens. Imaging sites of receptor dephosphorylation by PTP1B on the surface of the endoplasmic reticulum. *Science*, 295(5560):1708–1711, 2002.

[65] Ola Sabet, Rabea Stockert, Georgia Xouri, Yannick Brüggemann, Angel Stanoev, and Philippe IH Bastiaens. Ubiquitination switches EphA2 vesicular traffic from a continuous safeguard to a finite signalling mode. *Nature communications*, 6:8047, 2015.

[66] Elaine M Khan, Roni Lanir, Aaron R Danielson, and Tzipora Goldkorn. Epidermal growth factor receptor exposed to cigarette smoke is aberrantly activated and undergoes perinuclear trafficking. *The FASEB Journal*, 22(3):910–917, 2008.

[67] Alexander Sorkin and Mark von Zastrow. Signal transduction and endocytosis: close encounters of many kinds. *Nature reviews Molecular cell biology*, 3(8):600, 2002.

[68] Simona Polo and Pier Paolo Di Fiore. Endocytosis conducts the cell signaling orchestra. *cell*, 124(5):897–900, 2006.

[69] GM Di Guglielmo, PC Baass, WJ Ou, BI Posner, and JJ Bergeron. Compartmentalization of SHC, GRB2 and mSOS, and hyperphosphorylation of Raf-1 by EGF but not insulin in liver parenchyma. *The EMBO journal*, 13(18):4269–4277, 1994.

[70] David Teis, Nicole Taub, Robert Kurzbauer, Diana Hilber, Mariana E de Araujo, Miriam Erlacher, Martin Offterdinger, Andreas Villunger, Stephan Geley, Georg Bohn, et al. p14–MP1-MEK1 signaling regulates endosomal traffic and cellular proliferation during tissue homeostasis. *J Cell Biol*, 175(6):861–868, 2006.

[71] Arola Fortian and Alexander Sorkin. Live-cell fluorescence imaging reveals high stoichiometry of Grb2 binding to the EGF receptor sustained during endocytosis. *J Cell Sci*, 127(2):432–444, 2014.

[72] Roberto Villaseñor, Hidenori Nonaka, Perla Del Conte-Zerial, Yannis Kalaidzidis, and Marino Zerial. Regulation of EGFR signal transduction by analogue-to-digital conversion in endosomes. *Elife*, 4, 2015.

[73] Yukio Nishimura, Soichi Takiguchi, Shigeru Ito, and Kazuyuki Itoh. EGF-stimulated akt activation is mediated by EGFR recycling via an early endocytic pathway in a gefitinib-resistant human lung cancer cell line. *International journal of oncology*, 46(4):1721–1729, 2015.

[74] Ira Mellman and Yosef Yarden. Endocytosis and cancer. *Cold Spring Harbor perspectives in biology*, 5(12):a016949, 2013.

[75] Wendell A Lim and Tony Pawson. Phosphotyrosine signaling: evolving a new cellular communication system. *Cell*, 142(5):661–667, 2010.

[76] Andrew R Reynolds, Christian Tischer, Peter J Verveer, Oliver Rocks, and Philippe IH Bastiaens. EGFR activation coupled to inhibition of tyrosine phosphatases causes lateral signal propagation. *Nature cell biology*, 5(5):447, 2003.

[77] Christian Tischer and Philippe IH Bastiaens. Lateral phosphorylation propagation: an aspect of feedback signalling? *Nature Reviews Molecular Cell Biology*, 4(12):971, 2003.

[78] Aneta Koseska and Philippe IH Bastiaens. Cell signaling as a cognitive process. *The EMBO Journal*, page e201695383, 2017.

[79] Hernán E Grecco, Malte Schmick, and Philippe IH Bastiaens. Signaling from the living plasma membrane. *Cell*, 144(6):897–909, 2011.

[80] John J Tyson, Katherine C Chen, and Bela Novak. Sniffers, buzzers, toggles and blinkers: dynamics of regulatory and signaling pathways in the cell. *Current opinion in cell biology*, 15(2):221–231, 2003.

[81] Nicholas K Tonks. Protein tyrosine phosphatases: from genes, to function, to disease. *Nature reviews Molecular cell biology*, 7(11):833, 2006.

[82] Jannik N Andersen, Peter G Jansen, Søren M Echwald, Ole H Mortensen, Toshiyuki Fukada, Robert Del Vecchio, Nicholas K Tonks, and Niels Peter H Møller. A genomic perspective on protein tyrosine phosphatases: gene structure, pseudogenes, and genetic disease linkage. *The FASEB Journal*, 18(1):8–30, 2004.

[83] Jackie Felberg and Pauline Johnson. Characterization of recombinant CD45 cytoplasmic domain proteins evidence for intramolecular and intermolecular interactions. *Journal of Biological Chemistry*, 273(28):17839–17845, 1998.

[84] Guoqiang Jiang, Jeroen den Hertog, and Tony Hunter. Receptor-like protein tyrosine phosphatase α homodimerizes on the cell surface. *Molecular and cellular biology*, 20(16):5917–5929, 2000.

[85] Christophe Blanchetot, Leon G Tertoolen, John Overvoorde, and Jeroen den Hertog. Intra-and intermolecular interactions between intracellular domains of receptor protein-tyrosine phosphatases. *Journal of Biological Chemistry*, 277(49):47263–47269, 2002.

[86] Jie Sun, Shaoying Lu, Mingxing Ouyang, Li-Jung Lin, Yue Zhuo, Bo Liu, Shu Chien, Benjamin G Neel, and Yingxiao Wang. Antagonism between binding site affinity and conformational dynamics tunes alternative cis-interactions within Shp2. *Nature communications*, 4:2037, 2013.

[87] John V Frangioni, Pamela H Beahm, Victor Shifrin, Christine A Jost, and Benjamin G Neel. The nontransmembrane tyrosine phosphatase PTP-1B localizes to the endoplasmic reticulum via its 35 amino acid C-terminal sequence. *Cell*, 68(3):545–560, 1992.

[88] Deborah E Cool, Nicholas K Tonks, Harry Charbonneau, Kenneth A Walsh, Edmond H Fischer, and Edwin G Krebs. cDNA isolated from a human T-cell library encodes a member of the protein-tyrosine-phosphatase family. *Proceedings of the National Academy of Sciences*, 86(14):5257–5261, 1989.

[89] Joshua M Kruger, Takayasu Fukushima, Vera Cherepanov, Niels Borregaard, Carola Loeve, Christina Shek, Kalpana Sharma, A Keith Tanswell, Chung-Wai Chow, and Gregory P Downey. Protein-tyrosine phosphatase MEG2 is expressed by human neutrophils localization to the phagosome and activation by polyphosphoinositides. *Journal of Biological Chemistry*, 277(4):2620–2628, 2002.

[90] Annalisa Carlucci, Chiara Gedressi, Luca Lignitto, Luigi Nezi, Emma Villa-Moruzzi, Enrico V Avvedimento, Max Gottesman, Corrado Garbi, and Antonio Feliciello. Protein-tyrosine phosphatase PTPD1 regulates focal adhesion kinase autophosphorylation and cell migration. *Journal of Biological Chemistry*, 283(16):10919–10929, 2008.

[91] Annalisa Carlucci, Monia Porpora, Corrado Garbi, Mario Galgani, Margherita Santoriello, Massimo Mascolo, Domenico di Lorenzo, Vincenzo Altieri, Maria Quarto, Luigi Terracciano, et al. PTPD1 supports receptor stability and mitogenic signaling in bladder cancer cells. *Journal of biological chemistry*, 285(50):39260–39270, 2010.

[92] Pedro Roda-Navarro and Philippe I Bastiaens. Dynamic recruitment of protein tyrosine phosphatase ptpd1 to EGF stimulation sites potentiates EGFR activation. *PloS one*, 9(7):e103203, 2014.

[93] Leila Belle, Naveid Ali, Ana Lonic, Xiaochun Li, James L Paltridge, Suraya Roslan, David Herrmann, James RW Conway, Freya K Gehling, Andrew G Bert, et al. The tyrosine phosphatase PTPN14 (Pez) inhibits metastasis by altering protein trafficking. *Sci. Signal.*, 8(364):ra18–ra18, 2015.

[94] Tasneem Motiwala and Samson T Jacob. Role of protein tyrosine phosphatases in cancer. *Progress in nucleic acid research and molecular biology*, 81:297–329, 2006.

[95] Suling Liu, Yasuro Sugimoto, Claudio Sorio, Cristina Tecchio, and Young C Lin. Function analysis of estrogenically regulated protein tyrosine phosphatase γ (PTPγ) in human breast cancer cell line MCF-7. *Oncogene*, 23(6):1256, 2004.

[96] Claudia AL Ruivenkamp, Tom van Wezel, Carlo Zanon, Alphons PM Stassen, Cestmir Vlcek, Tamás Csikós, Anita M Klous, Nikos Tripodis, Anastassis Perrakis, Lucie Boerrigter, et al. Ptprj is a candidate for the mouse colon-cancer susceptibility locus Scc1 and is frequently deleted in human cancers. *Nature genetics*, 31(3):295, 2002.

[97] Marco Tartaglia and Bruce D Gelb. Germ-line and somatic PTPN11 mutations in human disease. *European journal of medical genetics*, 48(2):81–96, 2005.

[98] Rongzhen Xu, Yingzi Yu, Shu Zheng, Xiaoying Zhao, Qinghua Dong, Zhiwen He, Yun Liang, Qinghua Lu, Yongmin Fang, Xiaoxian Gan, et al. Overexpression of Shp2 tyrosine phosphatase is implicated in leukemogenesis in adult human leukemia. *Blood*, 106(9):3142–3149, 2005.

[99] Karin Kolmodin and Johan Åqvist. The catalytic mechanism of protein tyrosine phosphatases revisited. *FEBS letters*, 498(2-3):208–213, 2001.

[100] Sue Goo Rhee, Yun Soo Bae, Seung-Rock Lee, and Jaeyul Kwon. Hydrogen peroxide: a key messenger that modulates protein phosphorylation through cysteine oxidation. *Science Signaling*, 2000(53):pe1–pe1, 2000.

[101] Benoît D'Autréaux and Michel B Toledano. ROS as signalling molecules: mechanisms that generate specificity in ROS homeostasis. *Nature reviews Molecular cell biology*, 8(10):813, 2007.

[102] Zhiyou Cai and Liang-Jun Yan. Protein oxidative modifications: beneficial roles in disease and health. *Journal of biochemical and pharmacological research*, 1(1):15, 2013.

[103] Yvonne MW Janssen-Heininger, Brooke T Mossman, Nicholas H Heintz, Henry J Forman, Balaraman Kalyanaraman, Toren Finkel, Jonathan S Stamler, Sue Goo Rhee, and Albert van der Vliet. Redox-based regulation of signal transduction: principles, pitfalls, and promises. *Free Radical Biology and Medicine*, 45(1):1–17, 2008.

[104] Gregory Huyer, Susana Liu, John Kelly, Jason Moffat, Paul Payette, Brian Kennedy, George Tsaprailis, Michael J Gresser, and Chidambaram Ramachandran. Mechanism of inhibition of protein-tyrosine phosphatases by vanadate and pervanadate. *Journal of Biological Chemistry*, 272(2):843–851, 1997.

[105] Seung-Rock Lee, Ki-Sun Kwon, Seung-Ryul Kim, and Sue Goo Rhee. Reversible inactivation of protein-tyrosine phosphatase 1B in A431 cells stimulated with epidermal growth factor. *Journal of Biological Chemistry*, 273(25):15366–15372, 1998.

[106] Kalyankar Mahadev, Assaf Zilbering, Li Zhu, and Barry J Goldstein. Insulin-stimulated hydrogen peroxide reversibly inhibits protein-tyrosine phosphatase 1b in vivo and enhances the early insulin action cascade. *Journal of Biological Chemistry*, 276(24):21938–21942, 2001.

[107] Tzu-Ching Meng, Deirdre A Buckley, Sandra Galic, Tony Tiganis, and Nicholas K Tonks. Regulation of insulin signaling through reversible oxidation of the protein-tyrosine phosphatases TC45 and PTP1B. *Journal of Biological Chemistry*, 279(36):37716–37725, 2004.

[108] Tzu-Ching Meng, Toshiyuki Fukada, and Nicholas K Tonks. Reversible oxidation and inactivation of protein tyrosine phosphatases in vivo. *Molecular cell*, 9(2):387–399, 2002.

[109] Ryouhei Tsutsumi, Jana Harizanova, Rabea Stockert, Katrin Schröder, Philippe IH Bastiaens, and Benjamin G Neel. Assay to visualize specific protein oxidation reveals spatio-temporal regulation of SHP2. *Nature communications*, 8(1):466, 2017.

[110] Christophe Blanchetot, Leon GJ Tertoolen, and Jeroen den Hertog. Regulation of receptor protein-tyrosine phosphatase α by oxidative stress. *The EMBO journal*, 21(4):493–503, 2002.

[111] Erica Novo and Maurizio Parola. Redox mechanisms in hepatic chronic wound healing and fibrogenesis. *Fibrogenesis & tissue repair*, 1(1):5, 2008.

[112] David I Brown and Kathy K Griendling. Nox proteins in signal transduction. *Free Radical Biology and Medicine*, 47(9):1239–1253, 2009.

[113] JD van Buul, M Fernandez-Borja, EC Anthony, and PL Hordijk. Expression and localization of NOX2 and NOX4 in primary human endothelial cells. *Antioxidants & redox signaling*, 7(3-4):308–317, 2005.

[114] Bryan C Dickinson and Christopher J Chang. Chemistry and biology of reactive oxygen species in signaling or stress responses. *Nature chemical biology*, 7(8):504, 2011.

[115] J David Lambeth. NOX enzymes and the biology of reactive oxygen. *Nature Reviews Immunology*, 4(3):181, 2004.

[116] Candice E Paulsen, Thu H Truong, Francisco J Garcia, Arne Homann, Vinayak Gupta, Stephen E Leonard, and Kate S Carroll. Peroxide-dependent sulfenylation of the EGFR catalytic site enhances kinase activity. *Nature chemical biology*, 8(1):57, 2012.

[117] Alastair J Barr, Emilie Ugochukwu, Wen Hwa Lee, Oliver NF King, Panagis Filippakopoulos, Ivan Alfano, Pavel Savitsky, Nicola A Burgess-Brown, Susanne Müller, and Stefan Knapp. Large-scale structural analysis of the classical human protein tyrosine phosphatome. *Cell*, 136(2):352–363, 2009.

[118] Zhong Yao, Katelyn Darowski, Nicole St-Denis, Victoria Wong, Fabian Offensperger, Annabel Villedieu, Shahreen Amin, Ramy Malty, Hiroyuki Aoki, Hongbo Guo, et al. A global analysis of the receptor tyrosine kinase-protein phosphatase interactome. *Molecular cell*, 65(2):347–360, 2017.

[119] Gabi Tarcic, Shlomit K Boguslavsky, Jean Wakim, Tai Kiuchi, Angela Liu, Felicia Reinitz, David Nathanson, Takamune Takahashi, Paul S Mischel, Tony Ng, et al. An unbiased screen identifies DEP-1 tumor suppressor as a phosphatase controlling EGFR endocytosis. *Current Biology*, 19(21):1788–1798, 2009.

[120] Feng Liu and Jonathan Chernoff. Protein tyrosine phosphatase 1B interacts with and is tyrosine phosphorylated by the epidermal growth factor receptor. *Biochemical Journal*, 327(Pt 1):139, 1997.

[121] Tony Tiganis, Anton M Bennett, Kodimangalam S Ravichandran, and Nicholas K Tonks. Epidermal growth factor receptor and the adaptor protein p52Shc are specific substrates of T-cell protein tyrosine phosphatase. *Molecular and cellular biology*, 18(3):1622–1634, 1998.

[122] Taichang Yuan, Yongping Wang, Zhizhuang J Zhao, and Haihua Gu. Protein-tyrosine phosphatase PTPN9 negatively regulates ErbB2 and epidermal growth factor receptor signaling in breast cancer cells. *Journal of Biological Chemistry*, 285(20):14861–14870, 2010.

[123] Angel Stanoev, Amit Mhamane, Klaus C Schuermann, Hernan E Grecco, Wayne Stallaert, Martin Baumdick, Yannick Brueggemann, Maitreyi S Joshi, Pedro Roda-Navarro, Sven Fengler, et al. Interdependence of EGFR with PTPs on juxtaposed membranes generates a growth factor sensing and responding network. *bioRxiv*, page 309781, 2018.

[124] Hernán E Grecco, Pedro Roda-Navarro, Andreas Girod, Jian Hou, Thomas Frahm, Dina C Truxius, Rainer Pepperkok, Anthony Squire, and Philippe IH Bastiaens. In situ analysis of tyrosine phosphorylation networks by FLIM on cell arrays. *Nature methods*, 7(6):467, 2010.

[125] François Jacob. Evolution and tinkering. *Science*, 196(4295):1161–1166, 1977.

[126] Uri Alon. *An introduction to systems biology: design principles of biological circuits*. CRC press, 2006.

[127] Boris N Kholodenko, Anatoly Kiyatkin, Frank J Bruggeman, Eduardo Sontag, Hans V Westerhoff, and Jan B Hoek. Untangling the wires: a strategy to trace functional interactions in signaling and gene networks. *Proceedings of the National Academy of Sciences*, 99(20):12841–12846, 2002.

[128] Sabrina Hempel, Aneta Koseska, Zoran Nikoloski, and Jürgen Kurths. Unraveling gene regulatory networks from time-resolved gene expression data–a measures comparison study. *BMC bioinformatics*, 12(1):292, 2011.

[129] Karen Sachs, Omar Perez, Dana Pe'er, Douglas A Lauffenburger, and Garry P Nolan. Causal protein-signaling networks derived from multiparameter single-cell data. *Science*, 308(5721):523–529, 2005.

[130] Smita Krishnaswamy, Matthew H Spitzer, Michael Mingueneau, Sean C Bendall, Oren Litvin, Erica Stone, Dana Pe'er, and Garry P Nolan. Conditional density-based analysis of T cell signaling in single-cell data. *Science*, 346(6213):1250689, 2014.

[131] J.R. Lakowicz. *Principles of Fluorescence Spectroscopy. Third edition*. New York: Springer, 2006.

[132] Michael H Sonntag, Jenny Ibach, Lidia Nieto, Peter J Verveer, and Luc Brunsveld. Site-specific protection and dual labeling of human epidermal growth factor (hEGF) for targeting, imaging, and cargo delivery. *Chemistry-a European Journal*, 20(20):6019–6026, 2014.

[133] Martin E Masip, Jan Huebinger, Jens Christmann, Ola Sabet, Frank Wehner, Antonios Konitsiotis, Günther R Fuhr, and Philippe IH Bastiaens. Reversible cryo-arrest for imaging molecules in living cells at high spatial resolution. *Nature methods*, 13(8):665, 2016.

[134] Nobuyuki Otsu. A threshold selection method from gray-level histograms. *IEEE transactions on systems, man, and cybernetics*, 9(1):62–66, 1979.

[135] Siddhartha Chib and Edward Greenberg. Understanding the metropolis-hastings algorithm. *The american statistician*, 49(4):327–335, 1995.

[136] Jeffrey S Rosenthal et al. Optimal proposal distributions and adaptive mcmc. *Handbook of Markov Chain Monte Carlo*, 4, 2011.

[137] Anton Arkhipov, Yibing Shan, Rahul Das, Nicholas F Endres, Michael P Eastwood, David E Wemmer, John Kuriyan, and David E Shaw. Architecture and membrane interactions of the EGF receptor. *Cell*, 152(3):557–569, 2013.

[138] Nicholas F Endres, Rahul Das, Adam W Smith, Anton Arkhipov, Erika Kovacs, Yongjian Huang, Jeffrey G Pelton, Yibing Shan, David E Shaw, David E Wemmer, et al. Conformational coupling across the plasma membrane in activation of the EGF receptor. *Cell*, 152(3):543–556, 2013.

[139] Natalia Jura, Yibing Shan, Xiaoxian Cao, David E Shaw, and John Kuriyan. Structural analysis of the catalytically inactive kinase domain of the human EGF receptor 3. *Proceedings of the National Academy of Sciences*, 106(51):21608–21613, 2009.

[140] E Charafe-Jauffret, C Ginestier, F Monville, P Finetti, J Adelaide, N Cervera, S Fekairi, Luc Xerri, J Jacquemier, D Birnbaum, et al. Gene expression profiling of breast cell lines identifies potential new basal markers. *Oncogene*, 25(15):2273, 2006.

[141] Martin Offterdinger, Virginie Georget, Andreas Girod, and Philippe IH Bastiaens. Imaging phosphorylation dynamics of the epidermal growth factor receptor. *Journal of Biological Chemistry*, 279(35):36972–36981, 2004.

[142] Douglas A Lauffenburger and Jennifer J Linderman. *Receptors: models for binding, trafficking, and signaling*. Oxford University Press on Demand, 1996.

[143] Hanna Björkelund, Lars Gedda, and Karl Andersson. Comparing the epidermal growth factor interaction with four different cell lines: intriguing effects imply strong dependency of cellular context. *PloS one*, 6(1):e16536, 2011.

[144] Tobias Welz, Joel Wellbourne-Wood, and Eugen Kerkhoff. Orchestration of cell surface proteins by Rab11. *Trends in cell biology*, 24(7):407–415, 2014.

[145] Senye Takahashi, Keiji Kubo, Satoshi Waguri, Atsuko Yabashi, Hye-Won Shin, Yohei Katoh, and Kazuhisa Nakayama. Rab11 regulates exocytosis of recycling vesicles at the plasma membrane. *J Cell Sci*, 125(17):4049–4057, 2012.

[146] Antonios D Konitsiotis, Lisaweta Roßmannek, Angel Stanoev, Malte Schmick, and Philippe IH Bastiaens. Spatial cycles mediated by UNC119 solubilisation maintain Src family kinases plasma membrane localisation. *Nature communications*, 8(1):114, 2017.

[147] K Hipel. Geophysical model discrimination using the Akaike information criterion. *IEEE Transactions on Automatic Control*, 26(2):358–378, 1981.

[148] Steven H Strogatz. *Nonlinear dynamics and chaos: with applications to physics, biology, chemistry, and engineering*. CRC Press, 2018.

[149] Sudin Bhattacharya, Qiang Zhang, and Melvin E Andersen. A deterministic map of Waddington's epigenetic landscape for cell fate specification. *BMC systems biology*, 5(1):85, 2011.

[150] James E Ferrell Jr and Sang Hoon Ha. Ultrasensitivity part III: cascades, bistable switches, and oscillators. *Trends in biochemical sciences*, 39(12):612–618, 2014.

[151] Ken-Iichi Sato, Ayako Sato, Mamoru Aoto, and Yasuo Fukami. c-Src phosphorylates epidermal growth factor receptor on tyrosine 845. *Biochemical and biophysical research communications*, 215(3):1078–1087, 1995.

[152] Nir Osherov and Alexander Levitzki. Epidermal-Growth-Factor-dependent activation of the Src-family kinases. *The FEBS Journal*, 225(3):1047–1053, 1994.

[153] Martin Baumdick, Marton Gelleri, Chayasith Uttamapinant, Vaclav Beranek, Jason W Chin, and Philippe Bastiaens. A conformational sensor based on genetic code expansion reveals an autocatalytic component in EGFR activation. *bioRxiv*, page 314682, 2018.

[154] Monica Red Brewer, Cai-Hong Yun, Darson Lai, Mark A Lemmon, Michael J Eck, and William Pao. Mechanism for activation of mutated epidermal growth factor receptors in lung cancer. *Proceedings of the National Academy of Sciences*, 110(38):E3595–E3604, 2013.

[155] Arthur Kwok Leung Cheung, Joseph Chok Yan Ip, Adrian Chi Hang Chu, Yue Cheng, Merrin Man Long Leong, Josephine Mun Yee Ko, Wai Ho Shuen, Hong Lok Lung, and Maria Li Lung. PTPRG suppresses tumor growth and invasion via inhibition of Akt signaling in nasopharyngeal carcinoma. *Oncotarget*, 6(15):13434, 2015.

[156] Wayne Stallaert, Ola Sabet, Yannick Bruggemann, Lisa Baak, and Philippe Bastiaens. Contact inhibitory Eph signalling decouples EGFR activity from vesicular recycling to generate contextual plasticity. *bioRxiv*, page 202705, 2017.

[157] Danfeng Cai, Shann-Ching Chen, Mohit Prasad, Li He, Xiaobo Wang, Valerie Choesmel-Cadamuro, Jessica K Sawyer, Gaudenz Danuser, and Denise J Montell. Mechanical feedback through E-cadherin promotes direction sensing during collective cell migration. *Cell*, 157(5):1146–1159, 2014.

[158] Roberto Mayor and Sandrine Etienne-Manneville. The front and rear of collective cell migration. *Nature reviews Molecular cell biology*, 17(2):97, 2016.

Acknowledgements

It has been more than four years since I decided to embark on this special PhD journey, and I am looking back on it now with gratification. There were a lot of good and challenging times, during which I discovered many things that redefined me. I was fortunate enough to have shared my time and space with some great people that have made this journey unforgettable.

My foremost thanks go to my supervisor, Aneta Koseska. I am very lucky to have had a talented mentor like you, to whom I can turn for advice and help at any moment and be sure to get support. The passion for science, fresh ideas, and sharp focus for approaching problems are some of the values I hope I can adopt somehow.

Another big thank you goes to Philippe Bastiaens for the strong support and many prolific discussions. I am happy to have joined this great lab with a unique culture at a crucial point in my life.

Next to thank are the PTP people with whom we had millions of meetings, Amit, Wayne, Rabea, Klaus, Mai, Yannick, Martin, I have gained a great deal of knowledge working with you. It took a great team effort during the challenging times, and I am happy we were in it together.

Thank you to all of the people that make the lab tick smoothly - Astrid, Tanja, thanks for the management; Sven, Michael, Manu, Kirsten, Lisaweta, Michelle, Svenja, Jutta, Hendrike, the rest, thanks for all the help.

Thank you Lucia, Christa and the IMPRS faculty members and students, being part of the school was an honour and an enjoyable experience.

To all the people in the department, I enjoyed interacting with every single one of you, within the lab and outside of it. Thank you for making this time much more relaxing and memorable. I came here a clueless computer scientist, and now I am a little less clueless one, because of your open-mindedness and everyday scientific discussions.

Special thanks goes to my support network, Ola and Amit, you were like a family away from home. To the Hombruch boys, Farid, Wayne, Amit, Dhruv, Andrej, thank you for the countless fun times we had. For our little Balkan clique, Marija and Antonio, thanks for being fun, kind and supportive friends. My current and past office mates, Akhilesh, Sarah,

Mai, Hui, Martin, Aneta, Klaus, Andrej, Malte, thanks for all the goofy breaks in every day. Thanks Bruno for the cool discussions. The SynBio people, Johanna, Hans, Mike, Ilaria, and especially Konstantin, thanks for putting up with my ignorance around the lab. I will also happily remember the interactions with Marina, Marton, Jan, Jana, Martin, Björn, Sven, Johann, Lisa, Azra, Lena, Julia, Peter, Christian, Leif, Frank, Holger, Jens, Justine, Zeta, Eli, Maja, and all the other people that made MPI Dortmund such a great place.

I have to send my special thanks to my family and friends at home. Especially thanks to my parents, Svetlana and Ilija, who have made sacrifices and were always there for me and supporting me. My sister Emilija, with our newest family addition Mihail, thanks for being the best sister anyone can ask for.

My final thank you goes to Rosana, who has always been a great and encouraging partner, in spite of the long distance. Thank you for all the love and support, it means the world to me.

Angel Stanoev, June 2018